1-1-2015

Biomechanical And Biological Evaluation Of A Model Of Post-Traumatic Osteoarthritis Following Noninvasive, Traumatic Rupture Of The Anterior Cruciate Ligament

Tristan Maerz
Wayne State University,

BIOMECHANICAL AND BIOLOGICAL EVALUATION OF A MODEL OF POST-TRAUMATIC OSTEOARTHRITIS FOLLOWING NONINVASIVE, TRAUMATIC RUPTURE OF THE ANTERIOR CRUCIATE LIGAMENT

by

TRISTAN MAERZ

DISSERTATION

Submitted to the Graduate School

of Wayne State University

Detroit, Michigan

in partial fulfillment of the requirements

for the degree of

DOCTOR OF PHILOSOPHY

2015

MAJOR: BIOMEDICAL ENGINEERING

Approved By:

_____

Advisor Date

_____

_____

_____

DEDICATION

To my parents, Birgit and Dietrich Maerz.

ACKNOWLEDGEMENTS

This work could not have been possible without the support of a large number of people. First, I'd like to thank my advisor, Dr. Howard Matthew, for his mentorship and support. I thank my committee members, Dr. Michele Grimm, Dr. Weiping Ren, and Dr. David Marcantonio, for their guidance and time. I'd like to acknowledge all mentors and professors from Lawrence Tech and Wayne State that have supported and encouraged me during my education. I thank all my coworkers and lab mates at Beaumont for their help, either directly or indirectly, with experiments part of my dissertation or by unloading me on other projects. Most notably, Kevin Baker, Michael Kurdziel, Michael Newton, Abigail Davidson, Perry Altman for their support and assistance in dissertation experiments, and Denise Koueiter for proofreading and editing. I want to thank all my friends, both in the U.S. and in Germany, my sisters, Julia and Jennifer, my grandparents, Eva and Willy Hummel, and my late grandmother Christel Maerz for their support during the recent busy years. I thank my girlfriend Basma for her calm guidance and thoughtfulness, and especially for her understanding of a busy schedule. Lastly, and most importantly, I thank my parents, Birgit and Dietrich Maerz, for everything they have done and sacrificed for myself and my sisters. This work is entirely because of them, and, therefore, for them.

TABLE OF CONTENTS

LIST OF TABLES

LIST OF FIGURES

CHAPTER 1: INTRODUCTION

Osteoarthritis (OA) remains one of the most prevalent medical conditions in the world. Though the exact worldwide incidence of OA is difficult to calculate, the World Health Organization (WHO) estimates that worldwide, 9.6% of men and 18.0% of women are affected by OA.(Woolf and Pfleger, 2003) Based on 2008 studies by Helmick(Helmick et al., 2008) and Lawrence(Lawrence et al., 2008), the Center for Disease Control (CDC) estimates that in the U.S., ~13.9% of adults 25 years of age and older, and ~33.6% of adults older than 65 years are affected by OA. Other studies have reported much higher incidences, and this variability has been attributed to extensive variability in symptoms and their associated severities.(Haugen et al., 2011) In addition to causing pain, disorder, and dysfunction, it is also one of the highest global causes of economic loss.(Brown et al., 2006)

The exact pathogenesis of OA remains unknown. While it is documented that age, gender, obesity, diabetes, and other musculoskeletal injuries or conditions are associated with the progression of OA, precise trigger mechanisms and their temporal relationships to OA have yet to be elucidated. To date, the only property of OA that is truly understood is its perpetuity and seemingly self-accelerating nature. This was recognized as early as 1743, when Dr. William Hunter, a Scottish surgeon and anatomist, stated that “ulcerated cartilage is a troublesome thing and that, once destroyed, is not repaired.”(Hunter, 1995)

Post-traumatic osteoarthritis (PTOA) is the onset and progression of OA-like symptoms following trauma due to sporting injury, motor vehicle accidents, or other injurious events. It has been estimated that PTOA constitutes ~12% of all OA cases, (Brown et al., 2006) and there is a 20 – 50% risk of developing PTOA following any joint injury.(Dirschl et al., 2004) The severity

and rate of onset is directly related to the severity of trauma, and few interventional clinical treatments have shown repeatable success. PTOA is most prevalent in the tibiofemoral and tibiotalar joints, and intraarticular fractures with displacement of cartilage fragments cause a more rapid onset and, ultimately, more severe PTOA than destabilization of the joints due to capsule, tendon, ligament, and/or meniscus damage.(Brown et al., 2006)

Rupture of the Anterior Cruciate Ligament (ACL) is a well-described injury leading to the onset of PTOA. As the major stabilizer of anterior translation of the tibiofemoral joint, the ACL is critical in maintaining knee stability during sporting activities. High-magnitude and high-rate anterior translation and/or rotation of the tibia with respect to the femur cause ACL sprains or ruptures. Excessive inflammation due to damage to ligament, cartilage, meniscus, and synovium tissue in addition to adverse biomechanical loading of these tissues following destabilization of the knee are postulated factors contributing to the onset of PTOA (Anderson et al., 2011; Buckwalter and Brown, 2004; Mankin et al., 2007). Though the gold-standard treatment of ACL ruptures is ACL reconstruction in efforts to remove damaged tissues and restabilize tibiofemoral articulation, PTOA following ACL rupture is reported to be as high as 90% . (Gillquist and Messner, 1999; Lohmander et al., 2004; Myklebust and Bahr, 2005; Roos et al., 1995; Von Porat et al., 2004)

Stem and progenitor cells are critical components of tissue homeostasis, metabolism , turnover, repair, and immunomodulation.(Singer and Caplan, 2011) During neonatal development, mesenchymal stem cells (MSCs) are responsible for the formation of mesenchymal tissues, including articular cartilage, bone, tendons, ligaments, meniscus, and the connective tissue component of the synovium. Following severe bodily injury such as myocardial infarction, stroke, multi-trauma, or whole-body irradiation, MSCs and hematopoietic stem cells (HSCs) are

known to be mobilized out of the bone marrow or perivascular niche to be involved in tissue regeneration and immunomodulation. However, to date, little is known regarding the systemic and local response of stem or progenitor cells in the setting of ACL rupture. It is unknown whether ACL rupture causes bone marrow-derived MSCs to be mobilized into peripheral blood and homed to the knee joint to participate in repair or immunomodulation. It is, thus, postulated that the onset of PTOA following ACL rupture is, in part, due to the incomplete MSC response and, consequently, an incomplete regenerative capacity.

Animal models of PTOA following ACL injury rely, to date, on surgical transection of the ACL to simulate the anterior instability of the knee present following rupture. However, surgical transection may fail to accurately represent the biological response due to high-magnitude tibiofemoral loading and subsequent ACL injury. In the rat, ACL transection to study PTOA is widespread (Guilak et al., 1994a; Hashimoto et al., 2002a; Jansen et al., 2011; Jansen et al., 2012; Martin and Buckwalter, 2006a; Ruan et al., 2013a)**,** but very little research has investigated noninvasive ACL rupture and the associated biological phenomena related to MSC mobilization, migration, and homing in a setting more representative of human injury. The purpose of this proposal is to (1) mechanically characterize a noninvasive model of rat ACL rupture using an applied axial tibial force; (2) compare the onset of PTOA in this noninvasive model to the onset of PTOA after surgical transection; and (3) study the acute biological response following noninvasive ACL rupture as it relates to MSC mobilization and the expression of cartilage-related biomarkers.

CHAPTER 2: BACKGROUND

2.1 - The Form and Function of Articular Cartilage:

Articular cartilage (AC) covers the surfaces of interfacing bones in most diarthrodial joints in the mammalian body.(Mankin et al., 2007) It is viscoelastic and provides lubrication for efficient motion of a joint while absorbing various loading types to prevent injury to surrounding tissues. Although often described as inert, AC is a highly dynamic tissue with complex interactions between chondrocytes, the only cell type of this tissue, solid tissue matrix macromolecules, and interstitial fluid.

Biochemical Composition of Articular Cartilage

AC is most commonly described as a biphasic material: it consists solid matrix phase (ca. 20% of total wet tissue mass by weight) and an interstitial fluid phase (ca. 80% of total wet tissue mass by weight). Biomechanically speaking, it is often described as triphasic – the third phase being fixed charge density (FCD) – and this will be covered in later sections. AC contains four main tissue layers or zones – the superficial or tangential zone (10%-20% of total thickness), the transitional or middle zone (40% - 60%), the radial or deep zone (30%-38%), and the calcified cartilage zone (<2%) (Figure 2.1.1). A “tidemark” delineates the interface between the calcified cartilage zone and subchondral bone, but this interface is not always distinct, and as such, the calcified cartilage zone is described as a hybrid between cartilage and bone.(Mankin et al., 2007)

Collagens contribute nearly 60% of the dry weight of AC, proteoglycans contribute 25%-35%, and noncollagenous proteins and glycoproteins contribute 15%-20%.(Mankin et al., 2007) The collagen network has a distinct orientation throughout the entire thickness of AC, often described as a series of arches. Collagen fibers are oriented nearly parallel to the joint surface in

the superficial layer, 30° - 60° to the joint surface in the middle layer, and perpendicular to the joint surface in the deep layer (Figure 2.1.1B), as first described by Benninghoff in 1925.(Benninghoff, 1925) This configuration allows for the effective absorption and transmission of compressive, shear, and tensile loading. Like most collagenous tissues, AC contains a large variety of collagen types. The most common collagens are types II, VI, IX, X, and XI, and the relative proportions of these do not change drastically from layer to layer in adult cartilage. During skeletal development, a larger proportion of collagen IX (~10%) and collagen XI (~10%) exist relative to collagen II (~80%), and these proportions diminish during maturation (collagen IX: ~1%, collagen XI: ~3%, collagen II: >90%).(Eyre and Wu, 1987) These three collagen polymers are able to form a highly crosslinked collagen II:IX:XI heteropolymer, which is highly resistive to tensile loading and biochemical digestion, making it an important macromolecule of the cartilage matrix.(Hagg et al., 1998)

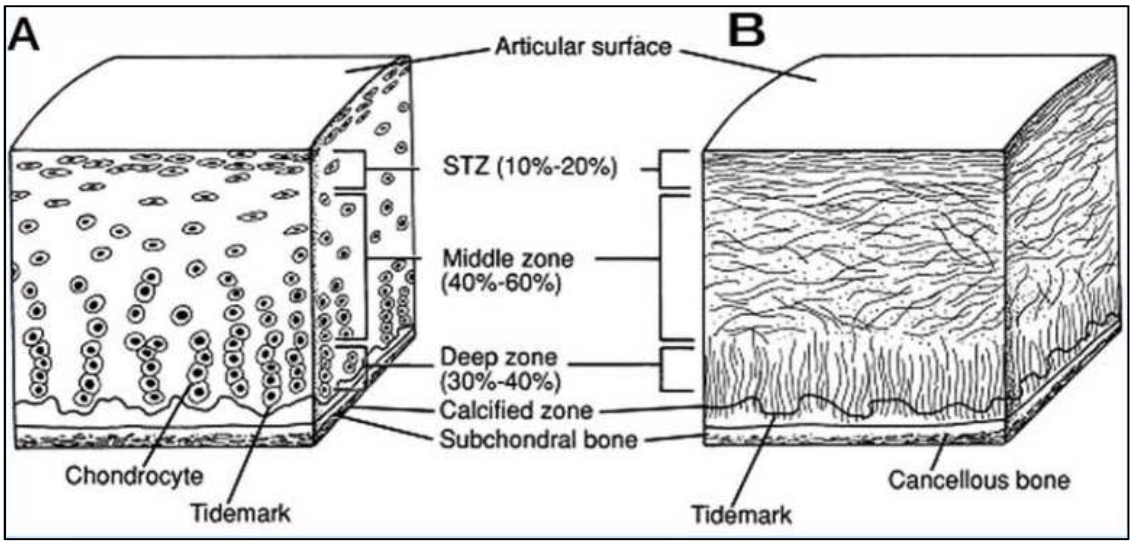

Figure 2.1.1 – *Schematic representation of the layers of articular cartilage, chondrocyte orientation, and collagen fiber orientation. Figure reproduced from Fox.(Fox et al., 2009)*

Proteoglycans (PG), the second major macromolecules type in AC, are made up of a protein core and one or numerous glycosaminoglycan (GAG) chains, and they account for 10%-15% of the wet weight of AC. The concentration of PGs increases with cartilage depth, with very little PGs in the superficial layer and a high concentration in the deep layer. GAGs are long unbranched polysaccharide chains made up of repeating disaccharides that contain an amino sugar.(Bayliss et al., 1983) GAG chains, often made up of up to 100 monosaccharides, extend from the protein core and repel one another due to their similar charge but attract cations, giving rise to the fixed charge density of AC (Figure 2.1.2). The most common GAGs found in AC are hyaluronic acid, chondroitin sulfate, keratan sulfate, and dermatan sulfate,(Mankin et al., 2007) and their relative proportion and size varies with both age, injury, and disease. Proteoglycans within AC can be split up into two major classes: large aggregating macromolecules termed "aggrecans", making up nearly 90% of all PGs in AC, and the smaller proteoglycans, making up ~10% of PGs in AC. Examples or smaller proteoglycans are decorin, biglycan, and fibromodulin. Aggrecans possess a large number of both chondroitin sulfate and keratan sulfate chains, whereas smaller PGs can have only one or two chains. The majority of aggrecans noncovalently bind with hyaluronic acid (HA), and GAG chains interact with the central core via link proteins (Figure 2.1.2). The length of the central HA molecule can vary between 100-10,000 nm, and aggregate size has been shown to diminish with both age and disease (Roughley and White, 1980), correlating with the age-related decrease in hydration and biomechanical integrity of AC. Smaller PGs have much shorter protein cores and, rather than contributing to hydration or biomechanical properties of AC like aggrecans do, have been attributed to modulating cell function, cell-cell, cell-matrix, and matrix-matrix behavior(Fox et al., 2009). For example,

fibromodulin and decorin both bind to type II collagen fibrils and have been attributed to stabilizing the collagen network(Bayliss et al., 1983).

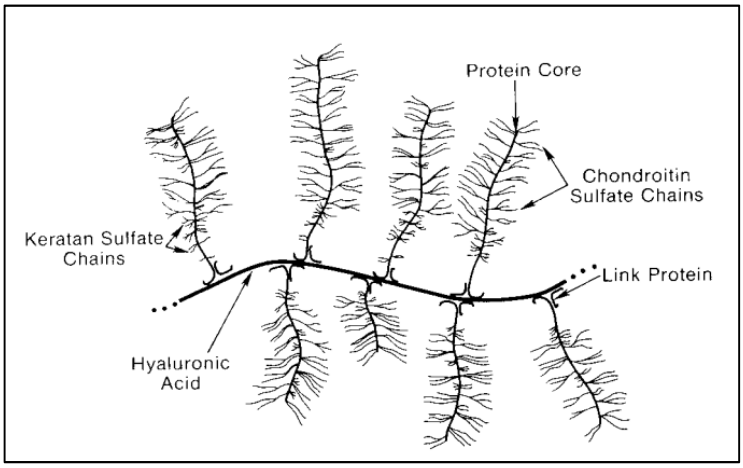

Figure 2.1.2 *– Schematic Representation of an Aggrecan Proteoglycan. A central protein "backbone", here hyaluronic acid, is bound to a large number (up to 100) glycosaminoglycan(GAG) side chains, most commonly chondroitin sulfate, keratan sulfate, or dermatan sulfate, via link proteins. GAGs repel each other due to similar charge and attract cations from the AC matrix. Aggregate size is directly proportional to the compressive properties of AC and has been shown to diminish with age and disease. Figure reproduced from Newman.(Newman, 1998)*

Noncollagenous proteins and glycoproteins make up the smallest proportion of the solid phase of AC. While they are the least studied and understood constituent of AC, they are mainly involved in cell-matrix interactions. For example, anchorin CII is a collagen-binding protein found to bind to the surface of chondrocytes to facilitate "anchoring" of cells to type II collagen.(Mollenhauer et al., 1984) Other common molecules are vitronectin, fibronectin, and cartilage oligomeric protein (COMP).

The proportion of interstitial fluid within the AC matrix is a critical component of AC as it relates directly to the tissue's ability to absorb and distribute loads without transferring adverse forces to chondrocytes. Water contributes ~80% of the wet weight of AC, and the interaction of water with macromolecules, namely aggrecans, is the primary source of the high compressive

properties of AC. Fluid movement in and out, and within, the AC matrix is dependent upon loading magnitude and speed in addition to aggrecan density. Aggrecans possess a large number of negative charges that attract cations and repel anions, which increases the concentrations of important cations such as sodium and decrease the concentration of anions such as chloride. This regulation of tissue osmolarity gives rise to the fixed charge density of AC, which is heavily dependent upon water content. Furthermore, due to the inherently low vascularity of AC, fluid movement due to cyclic loading during normal daily activity is thought to be the primary source of nutrient delivery within the AC.(Fox et al., 2009) Thus, decreased fluid content can be attributed to decreased nutrient transport and, ultimately, degeneration. As a highly viscoelastic tissue, cartilage mechanics are dependent upon the movement of fluid within the matrix, and the delicate balance between fluid content and macromolecule concentration is an important physiologic phenomenon.

Chondrocytes

Mature AC contains only a single cell type – the articular chondrocyte.(Dell'Accio et al., 2003) In comparison to tissue such as skin, muscle, liver, or kidney, AC has a very low concentration of cells – chondrocytes make up less than 1% - 2% of the total tissue volume of AC. Although the AC chondrocyte is a highly specialized, terminally differentiated cell, it varies distinctly in shape, size, and phenotype from AC zone to zone. Chondrocytes in the superficial zone are flattened and oriented along the tangential collagen fibers. As the inherent biochemical composition of the superficial zone suggests, chondrocytes in the superficial zone exhibit high expression of collagen genes and low expression of proteoglycans.(Coates and Fisher, 2010)

2.2 - Pathophysiology of Post-Traumatic Osteoarthritis

Although the exact pathophysiologic mechanism of PTOA remains to be fully defined, it is understood that numerous types of events can lead to PTOA. The sudden application of a mechanical force to the joint is generally defined as the initiating event of PTOA.(Anderson et al., 2011) Acute damage to AC is caused either directly during the force application or immediately following the destabilization of the joint, leading to nonanatomic articulation and/or subluxation. In the former, the magnitude and frequency of loading determines the degree of injury to AC. Low-energy loading can cause damage to cells and/or extracellular matrix (ECM) macromolecules without macrophysical damage to the AC tissue (i.e. a tear, rupture). High-energy may cause complete disruption of the ECM, causing macroscopic tears or cracks in addition to damage to cells, and very high-energy force application is able to completely displace articular cartilage fragments.(Buckwalter, 2002; Buckwalter and Brown, 2004) Acute damage caused due to subluxation and nonanatomic articulation following immediately after the force application, oftentimes still within the same gait or loading cycle, is less common but potentially equally damaging. (Buckwalter and Brown, 2004)

Chronic damage to AC leading to PTOA can also be caused by joint destabilization following ligamentous or tendinous injury. Tear or complete rupture of a supporting ligament, meniscus, or tendon responsible for facilitating anatomic articulation can lead to adverse, nonanatomic stress distributions within the joint, leading to focal regions of high-magnitude loading. For example, rupture of the medial collateral ligament (MCL) of the knee causes medial instability, which can result in increased lateral loading and medial subluxation due to the lack of the primary medial support the MCL provides.(Gardiner and Weiss, 2003)

Following joint trauma, a seemingly unstoppable cascade of biologic events take place. Anderson *et al* have created a schematic diagram illustrating the variety of events both acutely and chronically following joint injury(Anderson et al., 2011) (Figure 2.2.1). The timeline demonstrates the catabolic processes such as cell and tissue necrosis, apoptosis, matrix degradation, and tissue inflammation present after injury. Anabolic processes become restored in the intermediate phase and begin to predominate in the late phase, where tissue remodeling occurs.

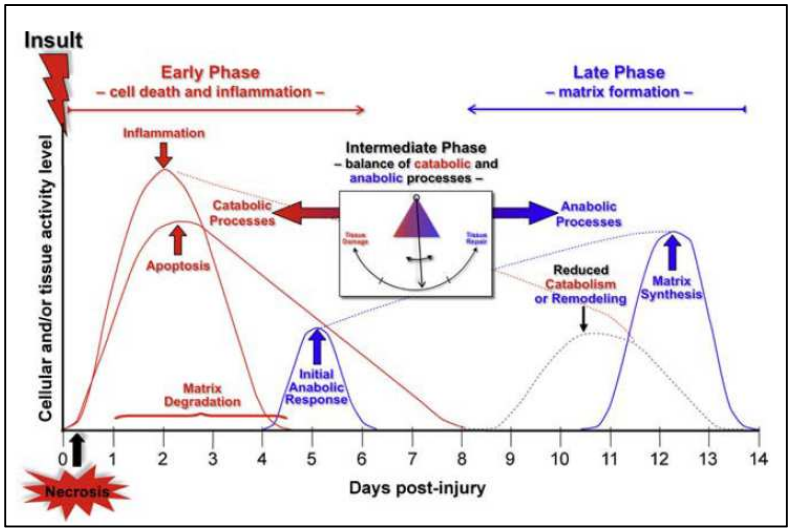

Figure 2.2.1 – *Schematic timeline of biologic events following joint trauma. Catabolic processes such as cell and tissue necrosis, apoptosis, matrix degradation, and tissue inflammation predominate in the early phase. In the intermediate phase, balance between catabolism and anabolism is slowly restored. In the late phase, matrix synthesis is upregulated to remodel injured tissue. Figure reproduced from Anderson(Anderson et al., 2011).*

Numerous biologic moieties are released into synovial fluid following joint injury. Proinflammatory cytokines such as members of the Interleukin family, namely IL-1β, IL-6, IL-8, tumor necrosis factor alpha (TNF-α), in addition to nitric oxide and matrix metalloproteinases (MMP-1, -2, -3, -8, -9, -13) are well-documented to be released after injury.(Green et al., 2006; Lohmander et al., 2003; Martin and Buckwalter, 2006a; Schaible et al., 2010; Tchetverikov et

al., 2005) Though the exact temporal and spatial relationships of these molecules and, importantly, their tissue of origin, has yet to be outlined, it has been shown that nearly every tissue in the joint is able to contribute to this molecular release. In addition to the aforementioned molecules, recent studies have demonstrated that reactive oxygen species (i.e. oxygen free radicals) are released from AC chondrocytes, a feed-forward loop of chondrocyte apoptosis and matrix degradation.(Goodwin et al., 2010; Martin et al., 2009) Tenascin-C, a glycoprotein found mainly in tendons and ligaments, has recently been shown to be released into synovial fluid following ACL rupture in humans.(Chockalingam et al., 2012)

The chronic pathophysiology of PTOA are less well understood, mainly due to the lack of representative animal models and corresponding time scales able to mimic the chronic stages of PTOA. It is, however, known that progressive ECM loss, most notably PGs, as well as cellular apoptosis and phenotypic shifts are present in advanced PTOA.(Anderson et al., 2011; Mankin et al., 2007) Loss of water content, most likely due to changes in electrostatic interactions concurrent with sGAG loss, in addition to cartilage thinning are also commonly cited symptoms. It can, thus, be understood how PTOA, or any OA for that matter, is inherently self-accelerating: loss of water content and mechanical properties leads to adverse loading of chondrocytes and ECM molecules, which leads to further loss of mechanical properties.

2.3 - Anterior Cruciate Ligament Anatomy and its Injury as a Cause for Post-Traumatic Osteoarthritis

As one of the most common sporting injuries worldwide(Jones and Rocha, 2012), anterior cruciate ligament (ACL) rupture or tear also represents a major mechanism by which PTOA can develop.(Feller, 2004) The incidence of ACL rupture is not well described and varies as a function of age, but studies have reported 30-81 per 100,000 (Ferry et al., 2013; Frobell et al., 2007; Gianotti et al., 2009) , 4.8% among ambulatory patients aged 50 – 90 years(Englund et al., 2006), and 3.6% of patients aged ~25 years.(Shelbourne et al., 1998)

Anterior Cruciate Ligament Anatomy

The ACL is the major anterior stabilizer of the tibiofemoral joint, resisting anterior translation of the tibia with respect to the femur. It connects to the femur in the intercondylar notch/fossa at the medial surface of the lateral femoral condyle and to the tibia at the anterocentrally (Figure 2.3.1)

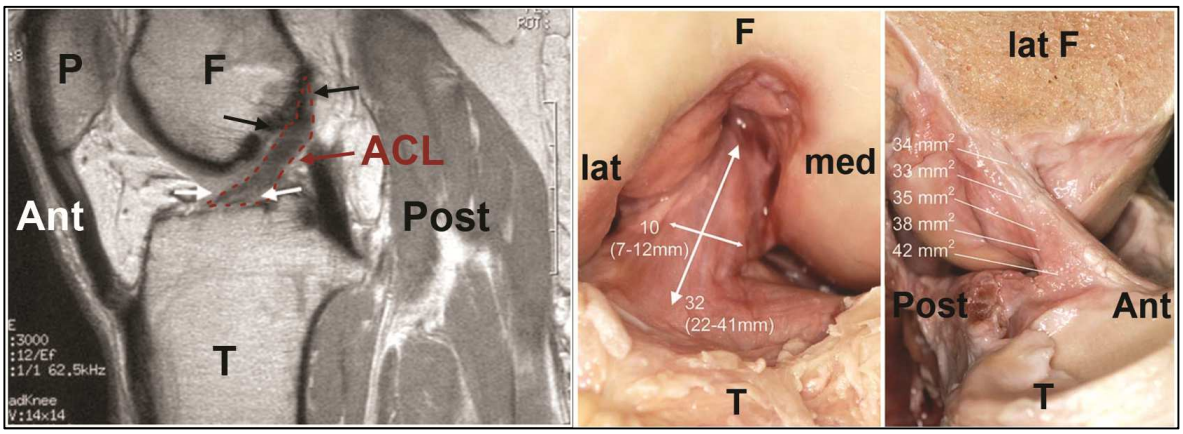

Figure 2.3.1 – *Anatomy of the Intact Anterior Cruciate Ligament (ACL). On sagittal proton density-weighted MRI (left image), the ACL appears as a dark band (red outline, red arrow) connecting the anterior tibia (white arrows) to the posterolateral femoral condyle within the intercondylar fossa (black arrows).Macroscopically, the ACL is visualized from the anterior knee (middle image) as a ~32 mm long, ~10mm wide ligament. A sagittal cross section (right image) shows that the ACL is thickest at the tibial insertion. P=patella; F=femur; T=tibia;*

Ant=anterior; Post=posterior; lat=lateral; med=medial. Left image reproduced from Craig et al(Craig et al., 2005). Middle and right image reproduced from Duthon et al.(Duthon et al., 2006)

The cross-sectional shape of the ACL is irregular along its length and varies during flexion-extension, but its tibial insertion is generally described as larger and wider in the medial-lateral direction.(Amis and Dawkins, 1991) The ACL is made up of two distinct bundles: the anteromedial bundle (AMB) and posterolateral bundle (PLB) (Figure 2.3.2). The AMB connects to the anterior – cranial aspect of the femoral ACL attachment and attaches to the anteromedial aspect of the tibial attachment. The PLB connects to the posterior – caudal aspect of the femoral attachment and to the posterolateral aspect of the tibial attachment.(Amis and Dawkins, 1991) Due to non-concentric articulation of the femoral condyles on the menisci, the two bundles are not isometric and are strained in varying magnitudes along the flexion-extension spectrum: the AMB lengthens and tightens in flexion whereas the PLB shortens and becomes lax. In extension, the PLB tightens slightly and the AMB relaxes but never becomes as lax as the PLB.(Hollis et al., 1991) As such, the two bundles provide complementary stabilization along the flexion-extension spectrum, giving rise to the continuous anterior stability.

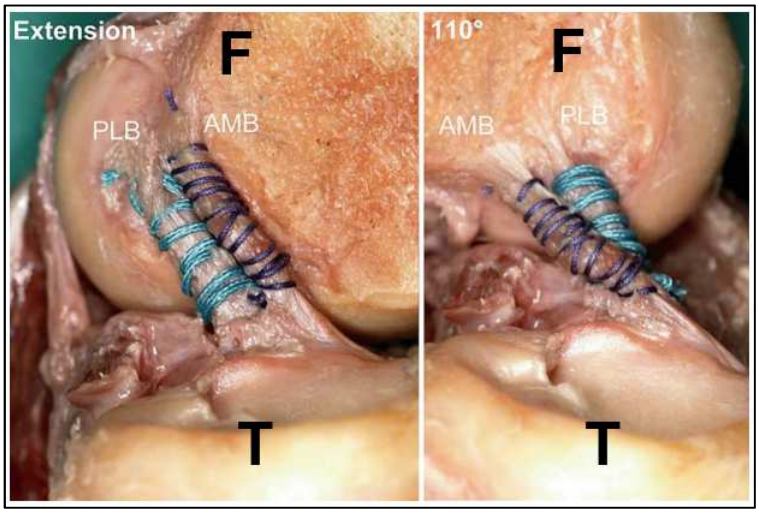

Figure 2.3.2 – *The two bundles of the ACL. The posterolateral bundle (PLB) is taught in extension (left image, blue suture) but shortens and becomes slack in flexion (right image, blue suture). The anteromedial bundle (AMB) lengthens and tightens in flexion (right image, purple suture) and shortens slightly in extension (right image, purple suture). F = femur; T=tibia. Image reproduced from Duthon et al.(Duthon et al., 2006)*

Anterior Cruciate Ligament Rupture

ACL rupture can occur in a variety of loading scenarios. Rupture mechanisms are generally divided into two categories: noncontact and contact injuries. One mechanism of contact injury is the application of a valgus force to the knee, causing the ACL to rupture due to extensive strain caused by valgus deformation.(Boden et al., 2000a). The valgus force is sometimes coupled with rotation and/or flexion, and injury mechanisms are therefore not purely valgus. Furthermore, contact ACL rupture can also occur due to an excessive posterior force on the distal femur with a static, or "planted" foot, causing rapid posterior motion of the femur with respect to the tibia and, ultimately, ACL rupture. It is important to note that a contact force may be combined with a noncontact initiating motion, thus compounding, for example, torsional and translational forces.

A large variety of noncontact ACL injury mechanisms have been proposed in the literature,(Yu and Garrett, 2007) and large prospective clinical studies have sought to investigate

risk factors associated with noncontact ACL rupture.(Uhorchak et al., 2003) Amongst proposed noncontact injury mechanisms are sudden and high-magnitude quadriceps contraction at 20° of flexion analogous to sudden deceleration from sprinting(DeMorat et al., 2004), high-magnitude joint loading during valgus deformation and slight flexion, analogous to landing from a jump with a valgus knee(Krosshaug et al., 2007), high-speed direction change, causing extreme tibial rotation and translation such as during "cutting" while sprinting (Krosshaug et al., 2007; Meyer and Haut, 2008), high-magnitude compressive loading at 30° of flexion(Meyer and Haut, 2008), and others.

Numerous injuries concomitant to ACL rupture have been described, and it is generally understood that multiple injuries (i.e. multi trauma) leads to lower clinical outcomes.(Levy et al., 2009) Among the most common injuries present after ACL rupture are MCL injury, PCL injury, LCL injury, meniscus injury, posterolateral corner injury, and gross articular cartilage injury.(Bin and Nam, 2007; Lohmander et al., 2007; Strobel et al., 2006; Widuchowski et al., 2007) Bone bruising is a common symptom following ACL rupture and has been shown to vary with the mechanism of injury.(Viskontas et al., 2008)

Post-Traumatic Osteoarthritis following Anterior Cruciate Ligament Rupture

The onset and progression of PTOA following ACL rupture is well-documented. The incidence of PTOA in the tibiofemoral compartment following ACL rupture with or without reconstruction vary from 10 % - 100% at 10 to 30 years following injury, depending on patient factors, injury severity, and reconstruction. (Ait Si Selmi et al., 2006; Gillquist and Messner, 1999; Lohmander et al., 2004; Myklebust and Bahr, 2005; Nebelung and Wuschech, 2005; Roos et al., 1995; Von Porat et al., 2004) Less data exists regarding PTOA in the patellofemoral

compartment, with numbers ranging from 16 - 75%.(Cohen et al., 2007; Järvelä et al., 2001; Neuman et al., 2009)

Clinical data pertaining to OA following ACL rupture is highly variable, and Lohmander *et al* used a systematic review to compile the incidence of radiographically-diagnosed OA and a knee-specific subjective outcomes score, the Knee Injury and Osteoarthritis score (KOOS), as a function of years after ACL injury and subsequent reconstruction (Figure 2.3.3).(Lohmander et al., 2007)

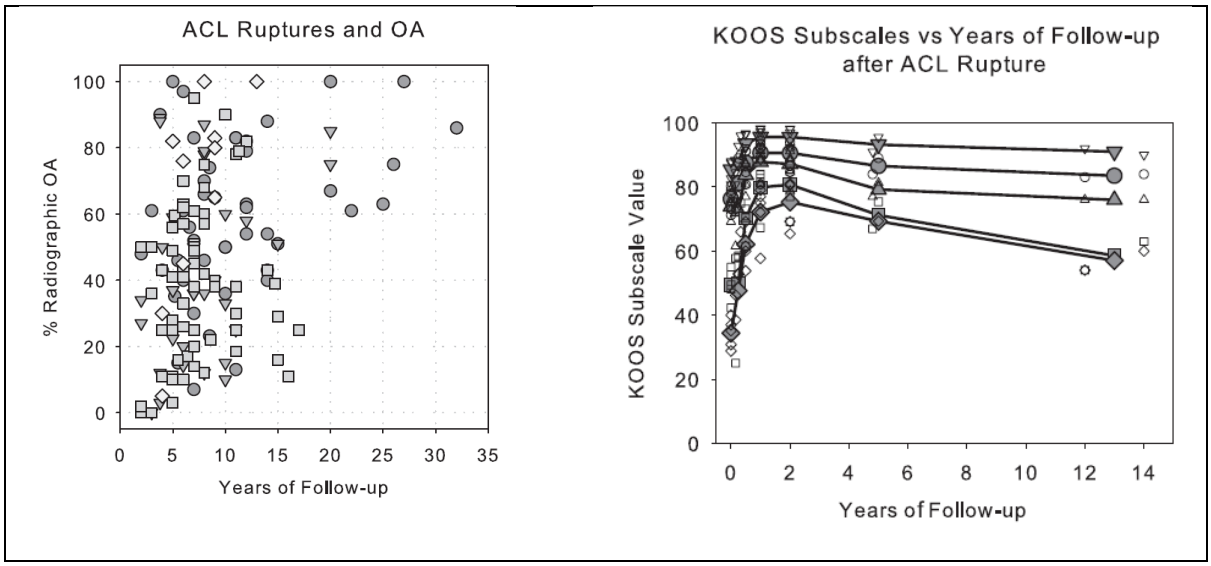

Figure 2.3.3 – *A scatterplot of radiographically-diagnosed OA as a function of years of follow-up after ACL injury and/or reconstruction (Left). A knee-specific subjective clinical outcomes measure (KOOS) as a function of years of follow-up after ACL injury and subsequent reconstruction (right). Figures reproduced from Lohmander.(Lohmander et al., 2007)*

The plots demonstrate that there is extensive variability in the incidence of OA following ACL injury but that the high incidence of OA does not necessarily result in lower outcomes as a function of time after injury and/or reconstruction. Clinical outcomes do, however, seem to deteriorate slowly after 2-4 years of follow-up regardless of OA status. Interestingly, these graphs also do not directly support that ACL reconstruction provides long-term protection

against progressive PTOA. On the contrary, the literature seems to show that even if ACL reconstruction is performed quickly after injury, PTOA is nearly inevitable.

There are a variety of direct and indirect risk factors associated with the development of PTOA following ACL rupture.(Louboutin et al., 2009) In addition to concomitant injuries at the time of the index injury, obesity, female gender, age, meniscectomy as part of surgical treatment, high native anterior tibial translation, genu recurvatum, genu varum, and intensity of physical exercise are among known risk factors for the development of PTOA.

Molecular and Cellular Mechanisms following ACL Rupture

It is unclear whether the onset of PTOA following ACL rupture is mainly due to the initial joint trauma at the time of injury or due to the alteration of native joint kinematics after rupture. Although ACL reconstruction does not fully restore tibiofemoral articulation to that of its healthy state, the literature clearly demonstrates that ACL reconstruction restores joint stability by reducing anterior tibial translation(Gao and Zheng, 2010). However, as previously stated, the incidence of PTOA does not seem to vary between surgically and nonsurgically treated patients.(Lohmander et al., 2007) It can, thus, be reasoned that the onset of PTOA is initiated at the time of injury and is largely due to the excessive biomechanical loads and catabolic moieties released within the joint after injury occurs.

To date, most research has focused on catabolic and proinflammatory proteins and cytokines along with their inhibitors after ACL rupture, and it is widely documented that synovial fluid-borne levels of these factors are elevated after ACL rupture.(Higuchi et al., 2006; Lohmander et al., 2003; Lohmander et al., 1994; Tang et al., 2009c) A paucity of data exists regarding the cellular response, both locally and systemically, following ACL rupture. Though it

is known that injured tissues undergo necrosis and apoptosis, little research has been done to determine whether stem and/or progenitor cells are involved in events following ACL rupture in the context of PTOA. Mesenchymal stem cells (MSCs) are present in the synovium(Sakaguchi et al., 2005; Yoshimura et al., 2007), in the ACL itself(Nohmi et al., 2012; Steinert et al., 2011), and in very small quantities in the other tissues of the joint.(da Silva Meirelles et al., 2006) Furthermore, MSCs can be found in vascular structures as perivascular MSCs, sometimes termed pericytes,(Crisan et al., 2008) though it is not known in what concentration, if any, MSCs reside in the intraarticular vasculature. In addition to their potent regenerative capacity, MSC**s** serve as immunomodulatory cells and may, therefore, play an integral role in the modulation of post-injury inflammation.(Chen and Tuan, 2008)

Nohmi and coworkers have shown that MSCs isolated from ruptured ACLs have a diminishing capacity to form colonies and differentiate as time from rupture increases.(Nohmi et al., 2012) Morito *et al* have shown that synovial fluid-level MSC concentrations are increased after ACL rupture compared to healthy patients.(Morito et al., 2008) The study demonstrated that, in addition to increased MSC levels in injured patients, MSC levels continued to increase after reconstructive surgery and that these MSCs were more similar to synovium-derived MSCs than bone marrow-derived MSCs, as analyzed by GeneChip. Lastly, in a rabbit model, they showed that intraarticularly injected MSCs adhered preferentially to the injured ligament rather than other tissues, an indicator that the injured tissue was signaling for homing, migration, and adhesion. Sekiya *et al* have shown that MSC concentration in synovial fluid increases with increasing OA grade(Sekiya et al., 2012), and this group also demonstrated that these circulating MSCs were more similar to synovium-derived MSCs than bone marrow-derived MSCs. Jones

and coworkers showed increased synovial fluid levels of MSCs in early OA patients while confirming that these cells are distinct from bone marrow (BM) cells.(Jones et al., 2008)

Homing of injected MSCs to injured tissues within the knee joint has been shown by only a few studies. Agung *et al* created surgical injury to the ACL, medial meniscus, and the femoral condyles and subsequently injected green fluorescent protein (GFP)-positive bone marrow-derived MSCs. *(Agung et al., 2006)* When 10^6 MSCs were injected, GFP-positive cells were observed only in the ACL at 8 weeks. When 10^7 cells were injected, GFP-positive cells were observed in the ACL, the meniscus, and the cartilage. These cells were surrounded by positive collagen staining, indicating their roles in tissue repair. This study highlights the homing capacity of injured tissues but also the need for high MSC concentrations. In a similar experiment, Horie *et al* showed that synovium-derived MSCs injected into the joint homed to massive meniscal defects and participated in regeneration.(Horie et al., 2009)

Some circulating, serum-level and synovial-level biomarkers for PTOA have been identified following ACL rupture. Catterall *et al* collected serum and synovial fluid from patients immediately following ACL rupture (~15 days after injury) and at the follow-up visit prior to reconstructive surgery (~48 days after injury).(Catterall et al., 2010) They analyzed 21 biomarkers by ELISA and assessed sGAG content in synovial fluid by Alcian Blue staining. The study did not have data from healthy patients to establish baseline biomarker concentrations. Their results show that in synovial fluid, C-Reactive protein (CRP), lubricin, and proteoglycan markers had significant decreases between the time of injury and the time of surgery. Interestingly, collagen biomarkers increased after time of injury. Pruksakorn *et al* showed that chondroitin sulfate epitope (WF6) and hyaluronic acid are present in increased concentrations in patients after ACL rupture, but had limited patient numbers.(Pruksakorn et al., 2009) Svoboda *et*

al used ELISA to measure levels of 4 biomarkers of cartilage turnover before and after ACL injury in 45 patients and used 45 healthy patients as matched controls.(Svoboda et al., 2013) They analyzed the two markers for cartilage synthesis: procollagen II carboxy propeptide (CPII) and aggrecan chondroitin sulfate 846 epitope (CS846); and two markers for cartilage degradation, type I and II degradation Col2 3/4 short assay (C1,2C) and collagen type II cleavage (C2C). They found significant differences in the change in concentration in 3 of the 4 biomarkers between injury and control patients and showed no pre-injury differences. Future work is necessary to determine the exact temporal patterns of these cartilage turnover markers. Tourville and coworkers measured biomarkers of collagen turnover and correlated those to clinical outcomes and joint space width in healthy patients and patients following ACL injury.(Tourville et al., 2013) They found increased ratios of collagen cleavage-to-synthesis ratios (type I and II cleavage product (uC1,2C) to procollagen II C-propeptide (sCPII)) in the serum of injured patients compared to controls both at 1 and 4 year follow-up. Also, the study found that increased type II cleavage-to-synthesis ratios (i.e. uCTX-II/sCPII ratio) were found in patients with abnormal joint space width at 4 year follow-up. Recently, Zhang *et al* showed that serum-level small non-coding RNA (snoRNA) U38 and U48 were significantly higher in the serum of patients with progression PTOA following ACL injury.(Zhang et al., 2012) No study has performed a high throughput proteome-wide investigation of serum-level or synovial fluid-level biomarkers following ACL rupture, and future work is warranted in this area to potentially identify more biomarkers indicative of PTOA after ACL injury.

To date, no study has shown whether ACL rupture induces systemic mobilization of stem cells and how the concentration of serum-level biomarkers of cartilage turnover and homing factors change in conjunction to MSC mobilization. While serious bodily injury such as

myocardial infarction(Zohlnhöfer et al., 2006) or stroke(Sprigg et al., 2006) induces systemic mobilization of BM-derived MSCs due to high secretion of the potent MSC-homing factor Stromal Cell Derived Factor -1 (SDF-1), no group has elucidated whether orthopaedic soft tissue injuries induce mobilization of BM-derived MSCs into the peripheral vascular system. As the BM represents the largest depot of MSCs, a possible explanation for incomplete healing of intraarticular injuries is the lack of MSC mobilization. Although synovium-derived MSCs are known to be increased in synovial fluid following injury, it is not known whether these cells alone are sufficient in providing an immunomodulatory and regenerative response. To this end, the onset of PTOA following intraarticular injury, namely ACL rupture, may therefore be, in part, due to the insufficient MSC response immediately after injury. Future research is necessary to elucidate the systemic mobilization of MSCs following ACL rupture to determine their potential role as mediators of PTOA. Additionally, proteome-wide analyses of cartilage biomarkers and stem cell homing factors in peripheral blood after ACL rupture can provide treatment targets for inhibition of cartilage degradation and/or increased stem cell mobilization acutely after rupture.

2.4 - Animal Models of Post-Traumatic Osteoarthritis

To accurately study PTOA, a variety of animal models have been developed and subsequently employed. Aside from PTOA due to ligamentous injury, other models have used intra-articular fracture(Furman et al., 2007), high impact- joint loading(Borrelli et al., 2009), or meniscectomy(Ashraf et al., 2011; Lindhorst et al., 2000). Animals most commonly utilized are the mouse(Furman et al., 2007; Ruan et al., 2013a), rat(Ashraf et al., 2011; Guilak et al., 1994a; Hashimoto et al., 2002a; Jansen et al., 2011; Jansen et al., 2012; Martin and Buckwalter, 2006a; Ruan et al., 2013a), rabbit(Borrelli et al., 2009; Guilak et al., 1994a), and dog(Lindhorst et al., 2000). A variety of ligamentous injury-induced PTOA models, sometimes termed joint instability-induced PTOA models, have been published, and these include ACL transection(Guilak et al., 1994a; Hashimoto et al., 2002a; Jansen et al., 2011; Jansen et al., 2012; Martin and Buckwalter, 2006a; Ruan et al., 2013a), combined meniscectomy and ACL transection(Appleton et al., 2007; Hayami et al., 2006), noninvasive injury via biomechanical loading (Christiansen et al., 2012b; Onur et al., 2013; Tang et al., 2009b; Tang et al., 2009c), or knee triad injury (MCL transection, medial meniscus, ACL transection) (Jones et al., 2010).

The most widely published model of PTOA following ligamentous injury is ACL transection.(Guilak et al., 1994a; Hashimoto et al., 2002a; Jansen et al., 2011; Jansen et al., 2012; Martin and Buckwalter, 2006a; Ruan et al., 2013a) ACL transection causes joint instability, leading to adverse compressive and shear forces on articular cartilage during tibiofemoral articulation. This model of PTOA has been well characterized, and numerous studies have shown that long-term findings are representative of OA: loss of proteoglycan content(Altman et al., 1984b; Guilak et al., 1994b), osteophyte formation(Hashimoto et al., 2002b), altered biomechanical properties of articular cartilage(Altman et al., 1984b), loss/thinning of articular

cartilage(Guilak et al., 1994b), and chondrocyte death(Martin and Buckwalter, 2006b). Ruan *et al* used an ACL transection model in mice and demonstrated increased Col10a1 and MMP13 gene expression, decreased cartilage volume, along with decreased motor and sensory reactions two months following transection. (Ruan et al., 2013b) Altman *et al* studied ACL transection in a canine model and showed decreased water content, increased joint swelling, decreased proteoglycan content, and increased cartilage stiffness. (Altman et al., 1984b) Hayami *et al* examined multiple time points post-ACL transection in a rat (1,2,4,6,10 weeks) and found detectable cartilage surface damage and proteoglycan loss as early as one week. (Hayami et al., 2006)

Only a few groups have used noninvasive, traumatic ACL rupture by mechanical loading in efforts to induce PTOA. Onur *et al* applied a 12 N compressive load at 5 mm/s for 230 cycles or until ACL rupture in a 90° flexed knee joint in mice. (Onur et al., 2013) After 1 and 8 weeks they saw a significant increase in OA score and osteophyte formation in the group that received cyclic cartilage compression with ACL rupture. Christiansen and coworkers also used a mouse model in which they applied tibal compression via the paw, keeping the ankle flexed at 30° . Each leg was subjected to a compressive load of 12 N, causing transient anterior subluxation of the tibia relative to the femur and ultimate rupture of the ACL. (Christiansen et al., 2012b) PTOA was characterized with micro-computed tomography (μCT) and Safranin-O histology. They demonstrated loss of trabecular bone volume, proteoglycan loss, chondrocyte atrophy, loss of the superficial zone of cartilage by 56 days. Interestingly, this study also demonstrated extensive heterotopic ossification, likely a byproduct of the high displacement induced during loading. A later paper published by the same group examined loading rate-dependent injury modes in the same mechanical loading protocol in mice and found that low loading rates caused

bony avulsion at the ACL insertion whereas high loading rates caused midsubstance rupture of the ACL (Lockwood et al., 2013). Tang *et al* used a rotational mechanical load in a rat to show increased levels of IL-1β, IL-6, TNF-α, and MMP-2 levels in explanted ACL, PCL, synovium, cartilage, and meniscal tissue. (Tang et al., 2009b) A follow-up study by the same group showed temporal shifts in MMP and tissue inhibitor of matrix metalloproteinase (TIMP) levels following noninvasive, rotational ACL rupture.(Xue et al., 2009) A lack of data exists regarding the molecular and cellular events following noninvasive ACL rupture of the rat in the context of PTOA. Future studies utilizing biomechanical loading to induce an isolated, noninvasive ACL rupture are necessary.

CHAPTER 3: STATEMENT OF PROBLEM

While the animal model of surgical ACL transection is widely utilized in rats, it fails to properly represent a clinically-relevant ACL injury as it occurs in humans. In addition to the absence of high-magnitude biomechanical loading of knee tissues, surgical transection induces confounding biological phenomena within the joint due to surgical cutting of the skin, synovium, and ACL, and, thus, does not provide an appropriate research platform with which to study the acute biologic mechanisms associated with ACL injury that may be initiators of the post-traumatic osteoarthritis (PTOA) cascade. Anterior cruciate ligament (ACL) rupture has been shown to be a major initiator of PTOA, and even ACL reconstruction fails to thwart the progression of PTOA. While it is known that the concentration of synovium-derived mesenchymal stem cells (MSCs) within the synovial fluid increases after ACL rupture, no study has elucidated whether ACL rupture induces systemic mobilization of bone marrow-derived MSCs into the peripheral vascular system to allow for homing and migration of these cells to the injured tissue. Furthermore, analyses of cartilage biomarkers and stem cell mobilization factors in peripheral blood following ACL rupture are, to date, lacking. A need exists for a repeatable, noninvasive ACL rupture model representative of human ACL injury with which to study the aforementioned mechanisms following injury in order to elucidate the etiology of PTOA.

CHAPTER 4: RESEARCH HYPOTHESIS

It is hypothesized that the rapid application of an axial tibial force in a flexed rat knee causes noninvasive, isolated rupture of the anterior cruciate ligament. Furthermore, it is hypothesized that this rupture leads to the onset and progression of PTOA, and that this will occur in a manner more representative of the process in humans. Lastly, it is hypothesized that mesenchymal stem cells are not mobilized into peripheral blood following ACL rupture but several serum-level biomarkers indicative of joint injury can be identified as potential targets for PTOA regulation.

CHAPTER 5: SPECIFIC AIMS

1). **Develop and Biomechanically Characterize a Model of Noninvasive Rupture of the Anterior Cruciate Ligament of the Rat**

- Methods: Axial tibial force in 100° of flexion; varying endpoint displacement and displacement rate; quantitative motion capture; quantitative joint laxity assessment; injury assessment using μCT, and dissection.

2). **Compare and Contrast the Onset and Progression of Post-Traumatic Osteoarthritis Following Noninvasive Rupture of the ACL to Surgical Transection of the ACL**

- Methods: Noninvasive ACL rupture using developed protocol, surgical transection using established protocol, 4 and 10-week endpoint, quantitative μCT, histology, cartilage biomarker assays.

3). **Analyze and Compare the Acute Biological Response Following both Noninvasive ACL Rupture and Surgical ACL Transection**

- Methods: Noninvasive ACL rupture, acute stem cell mobilization using flow cytometry, serum-level biomarkers, synovial fluid-level SDF-1.

CHAPTER 6: AIM # 1 - DEVELOP AND BIOMECHANICALLY CHARACTERIZE A MODEL OF NONINVASIVE RUPTURE OF THE ANTERIOR CRUCIATE LIGAMENT OF THE RAT

6.1 - Introduction

The pathomechanisms, kinetics, and potential treatment strategies of PTOA are commonly investigated using small-animal models. The most common model of PTOA following ACL injury is surgical ACL transection(Guilak et al., 1994a; Hashimoto et al., 2002a; Jansen et al., 2011; Jansen et al., 2012; Martin and Buckwalter, 2006a; Ruan et al., 2013a), which causes acute joint destabilization and, consequently, adverse joint kinematics and inflammation, leading to the onset of OA-like symptoms such as the loss of proteoglycan content(Altman et al., 1984a; Guilak et al., 1994a), osteophyte formation(Hashimoto et al., 2002a), altered biomechanical properties of articular cartilage(Altman et al., 1984a), loss/thinning of articular cartilage(Guilak et al., 1994a), and chondrocyte death(Martin and Buckwalter, 2006a). Due to the invasive nature of surgically-induced ACL injury, the ACL transection model may not accurately mimic the native biological response present in humans following ACL injury. The lack of high-magnitude tibiofemoral loading and tensile failure of the ACL represents a short-coming of the ACL transection model, and, furthermore, surgical cutting and suturing of the skin and joint capsule may induce confounding biological phenomena not present in human tissues after ACL injury.

Noninvasive loading protocols to induce ACL injury in small animals have been employed by only a few studies. Onur *et al* applied a cyclic compressive load to the distal femur of the flexed knee joint in mice until ACL rupture occurred, which induced OA-like degenerative changes at 8 weeks.(Onur et al., 2014) Tang *et al* used a rotational mechanical load in a rat to

characterize pro-inflammatory cytokine and proteinase expression following noninvasive ACL rupture.(Tang et al., 2009a; Wu et al., 2009) Christiansen and coworkers used a mouse model in which they applied tibial compression via the paw with the knee flexed at ~90°. Each leg was subjected to a compressive load of 12 N, causing transient anterior subluxation of the tibia relative to the femur and ultimate failure of the ACL.(Christiansen et al., 2012a) They demonstrated a loss of trabecular bone volume, proteoglycan loss, chondrocyte atrophy, and loss of the superficial zone of cartilage by 56 days. Another study by the same group examined loading rate-dependent injury modes in the same mechanical loading protocol in mice and found that low loading rates caused bony avulsion at the ACL insertion whereas high loading rates caused midsubstance rupture of the ACL.(Lockwood et al., 2014)

To date, the tibial compression ACL injury model has not been employed in the rat, and no group has characterized joint biomechanics and/or laxity during and after injury. As the rat is a common model for PTOA as well as ACL reconstruction(Brophy et al., 2011; Kadonishi et al., 2012; Mifune et al., 2013), a clinically-relevant model of ACL injury in the rat can be of significant use for future studies. To this end, the purpose of this study was to biomechanically characterize a noninvasive ACL injury in the rat using a tibial compression protocol. Specifically, we sought to investigate the repeatability of four loading protocols at varying speed and endpoint displacement, perform motion capture to quantity joint motion during loading, and quantify post-loading laxity. We hypothesized that both high displacement and high speed are necessary to induce complete ACL injury and that complete ACL injury results in increases in anterior-posterior laxity but not varus or valgus laxity.

6.2 – Methods

This work has been recently accepted for publication(Maerz et al., 2015) and has been closely replicated in the following sections.

Specimen Preparation

Adult, female Lewis rats (200-250 grams) (n=9 per group) were euthanized by CO_2 asphyxiation under an Institutional Animal Care and Use Committee (IACUC)-approved protocol. Immediately after euthanasia, both hind limbs were dissected to remove the skin, and small incisions were made over the lateral aspect of the femoral metaphysis and the lateral aspect of the tibial tuberosity using a No. 15 scalpel. A 1.00 mm Kirschner wire (K-Wire) was used to drill a hole into the femoral metaphysis and tibial tuberosity, and a 1.00 mm pin attached to a 4.00 mm hemispherical retroreflective motion-tracking marker was rigidly inserted into each hole. One additional reference marker was drilled into the greater trochanter of the femur, and another reference marker was attached to the testing fixture holding the animal's paw.

Mechanical Loading Protocol

The fixture and testing protocol utilized in this study are modified from a previously-published tibial compression knee injury model in mice.(Christiansen et al., 2012a) A custom fixture was rigidly mounted onto the stage of an electromechanical materials testing system (MTS Insight 5, Eden Prairie, MN, USA). The bottom fixture supports the animal in a prone position, and a knee stage with an 8.5 mm wide, 25 mm long, and 3.5 mm deep trough is positioned at the center of the actuator. The knee stage limits medial-lateral motion while providing room for anterior subluxation of the tibia relative to the femur. The top fixture was mounted at the center of the actuator, and it rigidly supports the rat's hind paw in 30° of dorsiflexion without allowing medial or lateral motion. Resultant knee flexion after positioning

of the animal is ~100° (Figure 6.2.1A). Four displacement-controlled loading protocols were employed to induce tibial-compression knee injury and/or anterior cruciate ligament injury. A 3 N preload was held for 10 seconds, followed by 10 preconditioning cycles of 1 – 5 N at 0.5 Hz. A 15 N preload ramp at 0.1 mm/s was then applied, and immediately after reaching a 15 N load, a displacement-controlled ramp using one of four testing conditions is applied: high and low speed (8 mm/s and 1 mm/s, respectively), and high and low endpoint displacement (3 mm and 2 mm, respectively). The four resultant testing groups were: high-speed, high-displacement (HSHD); high-speed, low-displacement (HSLD); low-speed, low-displacement (LSLD), and low-speed, high-displacement (LSHD). These loading parameters were chosen based on preliminary tests performed at varying speeds and endpoint displacement. These preliminary experiments demonstrated that displacements higher than 3 mm increased the incidence of fracture while 2 mm was found to be the minimum displacement necessary to induce ACL injury. Load, displacement, and time data was sampled at 200 Hz during each test.

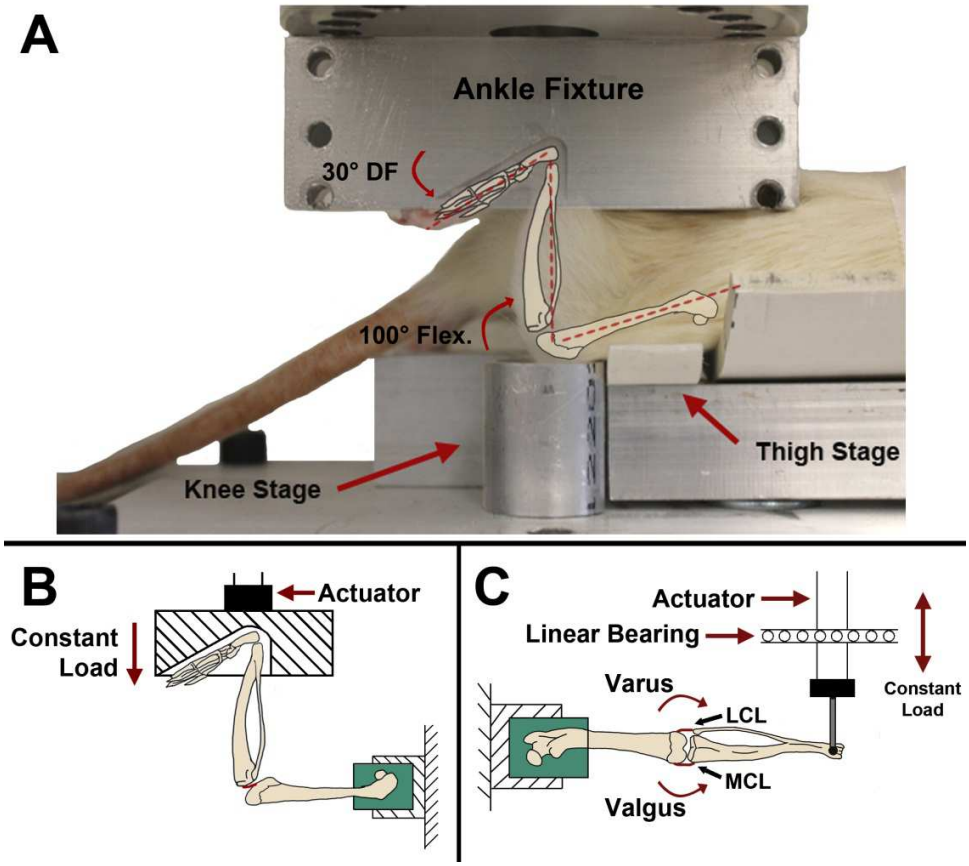

Figure 6.2.1 – *Mechanical Loading and Laxity testing fixtures. (A) To induce ACL injury, a compressive displacement is applied to the tibia with the knee flexed to ~100°. Medial-lateral motion of the knee is constrained with a trough in the knee stage, and the paw is fully constrained and flexed to 30° of dorsiflexion. (B) Following injury loading, Anterior-Posterior (AP) laxity was quantified with a subluxation test by the application of a constant tibial compressive load. (C) Varus and valgus laxity are assessed by the application of a constant load applied at the distal tibia to induce either varus or valgus joint stress.*

Motion Tracking and Analysis

During the duration of each mechanical test, motion of each reflective marker was tracked using a four-camera, 5 megapixel motion capture system (Oqus 5, Qualisys, Göteborg, Sweden). Data was collected continuously at a 179 Hz and analysis was performed using both the Qualisys Track Manager software and Matlab (v2013a, Mathworks, Natick, MA). Experiments performed to determine the resolution of this system using the same reflective

markers, the same camera-to-object distance, and displacement speeds of both 1 mm/s and 8 mm/s found that the system has a resolution of 279 µm with a 98.07% accuracy at 8 mm/s, and a 49.02 µm resolution with 99.31% accuracy at 1 mm/s. The motion-capture system was synchronized to the materials testing system using an external circuit to capture time-synchronized data between the two systems. Following acquisition, data was converted into a calibrated coordinate system where the z direction constitutes the vertical axis of the actuator (i.e. the direction of the applied load along the tibia), the x axis constitutes the medial-lateral direction with respect to the animal, and the y axis constitutes the cranial-caudal direction with respect to the animal. To analyze the motion of the tibia relative to the femur, the position of the proximal tibial marker was normalized to the position of the distal femoral marker at each data point. Relative tibiofemoral motion was analyzed in all three 2D anatomical planes (transverse, coronal, and sagittal) as well as in 3D. Motion was analyzed at the point of peak load, which constituted either ACL injury or the highest load when injury was not successfully induced, as well as motion between the point of peak load and maximum 3D joint displacement, which represented joint motion after ACL injury when injury was successful. Motion was also analyzed as total motion (i.e. total distance traveled by the tibia relative to the femur) as well as net motion.

Quantitative Joint Laxity Testing

Following mechanical loading, limbs were disarticulated at the hip joint, and approximately 1 cm of the proximal femur was exposed to facilitate clamping. Anterior-Posterior (AP) laxity was assessed using a subluxation test in which the femur was rigidly clamped, the knee was flexed to 90°, and the paw was fixed in a clamp in 30° of dorsiflexion.(Figure 6.2.1B) AP Laxity testing was performed with a 10 second 0.3 N preload, 10 preconditioning cycles

between 0.1 and 0.5 N at a rate of 0.25 Hz, another 10 second 0.3N preload, and a ramp to 2 N at 0.25 mm/s, which was held for 10 seconds. AP laxity was expressed as net displacement due to the applied 2N load as well as compliance during the applied load, expressed in mm/N. After AP laxity testing, the paw was disarticulated at the ankle joint, and a 1mm pinhole was drilled anterior-to-posterior in the distal tibia. The femur was rigidly mounted in the clamp, and the distal tibia was attached to a linear bearing with a 0.8 mm stainless steel pin via the drilled pin hole. The linear bearing was attached to the actuator, which applied a downward load to assess varus laxity and an upward load to assess valgus laxity (Figure 6.2.1C). The linear bearing ensured that linear actuator motion resulted in arc motion of the tibia in order to eliminate joint distraction, which would skew load-controlled testing. Varus and valgus laxity testing was performed with a 10 second 0.3 N preload, 10 preconditioning cycles between 0.1 and 0.5 N at a rate of 0.25 Hz, another 10 second 0.3N preload, and a ramp to 1 N at 0.25 mm/s, which was held for 10 seconds. Varus and valgus laxity were expressed as net displacement due to the applied 2N load in the respective directions as well as compliance during the applied load. Healthy, non-loaded specimens were used as laxity controls.

Micro Computed Tomography and Gross Dissection

Following mechanical loading and assessment of joint laxity, limbs were imaged using micro computed tomography (µCT) at 70 kVp, 114 µA at an isotropic voxel size of 36 µm (µCT40, Scanco Medical, Brüttisellen, Switzerland). A blinded investigator assessed each image set for gross fractures of the tibia or femur, and bony avulsions of the ACL were identified by small bone pieces in the center of the joint near the femoral notch.

Following imaging, each sample was dissected to confirm ACL injury, to identify and confirm potential fractures, ruptures, or avulsions, and to characterize the location and/or type of injury.

Data Analysis and Statistical Comparison

Statistical analysis was performed in SPSS (v22, IBM, Armonk, NY). The normality and equal variance assumptions were assessed using the Shapiro-Wilk test and Levene's test, respectively. Differences in independent normally distributed and non-normally distributed variables were compared between groups using one-way analysis of variance (ANOVA) and Kruskal-Wallis tests, respectively. Multiple comparisons were performed with a Sidak *P*-value correction at α = 95%. Differences in independent, normally distributed and non-normally distributed variables between two groups (e.g. injured vs non-injured specimens) were compared using *t*-tests and Mann Whitney U tests, respectively. The association between complete ACL injury and testing speed and displacement was assessed using χ^2 tests. *P* values lower than 0.05 were considered significant.

6.3 - Results

Complete Injury and Fracture Incidence

Complete ACL injury occurred in 100% of rats in HSHD, 33.33% (3/9) in HSLD, 55.56% (5/9) in LSHD, and 0% in LSLD. Injury was significantly associated with higher testing speed (χ^2 = 5.46, P = 0.019) and higher endpoint displacement (χ^2 = 13.48, P < 0.001). No bony metaphyseal fractures occurred during loading, and no fractures involving the pin hole were identified on µCT images. However, a distal femoral physeal fracture/slip occurred in one specimen in each of HSLD, LSHD, and LSLD during mechanical loading. These fractures were

confirmed on µCT images, indicating separation of the distal femoral physis with a concomitant coronally-oriented bony fracture of the distal femoral epiphysis (Figure 6.3.1A). All three of these fractures were several millimeters away from the pinholes drilled for retroreflective marker placement, and µCT images did not indicate fracture propagation to the pinholes.

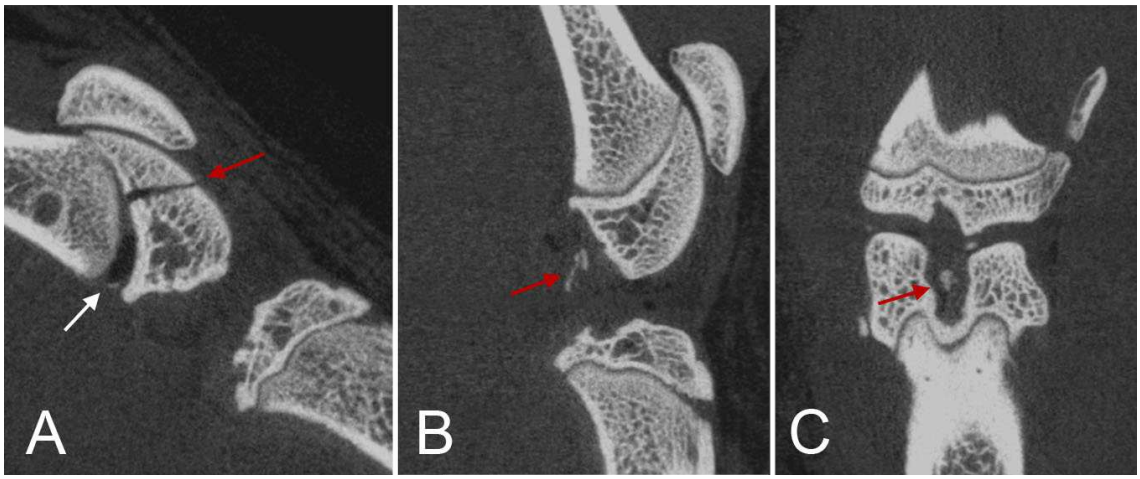

Figure 6.3.1 – *µCT imaging following loading. Three specimens exhibited physeal displacement (A, white arrow) with a concomitant distal femoral epiphyseal fracture (A, red arrow). Avulsions were noted by small pieces of bone in the joint space, apparent near the femoral footprint on both sagittal (B, red arrow) and coronal slices (C, red arrow).*

Loading-dependent Injury Types

ACL injury was confirmed with gross observation of the dissected joint (Figure 6.3.2). Of the 17 specimens that experienced complete ACL injury, three major injury types were observed: a true midsubstance rupture with ligamentous tissue fully attached to both the femoral and tibial footprints, where the rupture was found to be closer to the femoral footprint in all specimens. The second injury type was a combination avulsion and midsubstance rupture where one bundle of the ACL avulsed from the femoral footprint and the other bundle exhibited a midsubstance rupture . The third injury type was a full avulsion of the femoral attachment where both bundles

remained attached to bone, and the avulsion footprint could be visualized on the femur. Of the 9 injured specimens in HSHD, 2 specimens exhibited midsubstance rupture of the ACL, 4 specimens in HSHD exhibited the combination rupture-avulsion injury, and 3 specimens exhibited full avulsions. In two of the combination injury specimens, we were able to confirm that the anteromedial bundle was the avulsed bundle, and the posterolateral bundle was ruptured. Of the 3 injured specimens in HSLD, 2 exhibited the combination avulsion-rupture injury and 1 exhibited a midsubstance rupture. All 5 of the 5 injured specimens in LSHD were full avulsions. µCT data confirmed avulsion injuries by the appearance of a small bony piece in the femoral notch (Figure 6.3.1B,C), whereas no bone pieces were visualized in the joint in specimens that experienced midsubstance rupture.

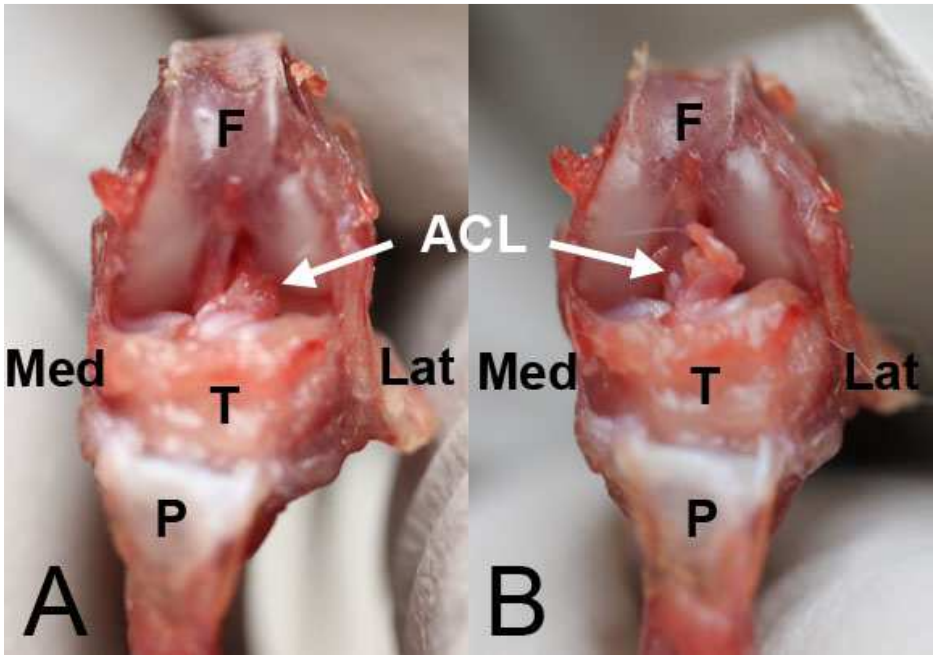

Figure 6.3.2 – *Complete ACL injury was confirmed in dissected joints. The intact ACL spans the joint from the anterior tibia to the medial wall of the lateral femoral condyle (A). Complete injury of the ACL (B) occurred by either midsubstance rupture, bony avulsion from the femoral footprint, or a combination injury where one bundle of the ACL was avulsed and the other bundle exhibited a midsubstance rupture. F = femur; T = tibia; P = patellar tendon. Med = medial; Lat = lateral.*

Joint Motion During Tibial Compression Loading

Relative tibiofemoral joint motion of all tested specimens is summarized in Table 6.3.1. In general, the motion in the transverse plane was most pronounced. HSHD exhibited significantly higher total coronal motion and transverse motion after peak load compared to HSLD. LSHD had significantly higher total sagittal motion compared to HSLD. HSHD had the highest 3D motion compared to other groups, but these differences were not significant due to the relatively large standard deviations when grouping both complete-injury and uninjured specimens. When comparing only specimens that exhibited complete ACL injury, more pronounced differences in relative tibiofemoral joint motion are observed between groups (Table 6.3.2). HSHD exhibited significantly higher total coronal motion, higher total 3D motion, and higher transverse motion after peak load compared to HSLD. LSHD had significantly higher total sagittal motion compared to HSLD.

Table 6.3.1 – *Relative Tibiofemoral Joint Motion during Injury Loading (All Specimens)*

	Coronal Motion (mm ± SD)		**Transverse Motion** (mm ± SD)		**Sagittal Motion** (mm ± SD)		**3D Motion** (mm ± SD)	
	Total	After Peak Load	Total	After Peak Load	Total	After Peak Load	Total	After Peak Load
HSHD	[a]4.98 ± 1.19	3.20 ± 1.47	6.69 ± 1.77	[a]3.40 ± 1.50	5.10 ± 0.83	1.73 ± 0.81	7.25 ± 1.63	3.23 ± 1.26
HSLD	[a]2.96 ± 1.70	1.53 ± 1.01	4.25 ± 2.56	[a]1.37 ± 0.98	[c]3.61 ± 2.05	1.00 ± 0.72	5.00 ± 2.61	1.85 ± 1.08
LSHD	4.28 ± 0.77	2.05 ± 1.34	6.44 ± 0.70	1.62 ± 1.37	[c]5.93 ± 0.85	1.76 ± 1.49	7.07 ± 0.78	2.34 ± 1.88
LSLD	3.49 ± 2.00	1.33 ± 1.15	4.57 ± 2.18	1.04 ± 0.81	3.82 ± 1.61	0.91 ± 1.04	5.38 ± 2.34	1.55 ± 1.35

[a] HSHD and HSLD differ; [b] HSHD and LSHD differ; [c] HSLD and LSHD differ. SD = standard deviation.

Table 6.3.2 – *Relative Tibiofemoral Joint Motion during Rupture Loading (Complete-Injury Specimens Only)*

	Coronal Motion (mm ± SD)		**Transverse Motion** (mm ± SD)		**Sagittal Motion** (mm ± SD)		**3D Motion** (mm ± SD)	
	Total	After Peak Load	Total	After Peak Load	Total	After Peak Load	Total	After Peak Load
HSHD	[a]4.98 ± 1.19	3.20 ± 1.47	6.69 ± 1.77	[a]3.40 ± 1.50	5.10 ± 0.83	1.73 ± 0.81	[a]7.25 ± 1.63	3.23 ± 1.26
HSLD	[a]2.80 ± 0.75	1.48 ± 1.07	3.91 ± 1.49	[a]1.21 ± 1.02	[c]3.44 ± 1.17	1.01 ± 0.82	[a]4.41 ± 1.48	1.65 ± 1.15
LSHD	4.40 ± 0.30	2.04 ± 1.03	6.39 ± 1.80	1.75 ± 1.45	[c]5.73 ± 0.98	1.42 ± 1.30	7.01 ± 0.87	1.99 ± 1.60
LSLD	N/A	N/A	N/A	N/A	N/A	N/A	N/A	N/A

[a] HSHD and HSLD differ; [b] HSHD and LSHD differ; [c] HSLD and LSHD differ. SD = standard deviation.
Note: N/A in LSLD because no specimens ruptured in LSLD.

Complete-injury specimens had significantly higher total motion after peak load in the transverse plane (2.58 mm ± 1.65) compared to specimens that did exhibit complete injury(1.25 mm ± 0.97, P = 0.031). There was significantly higher net displacement in the coronal plane in injured specimens (2.15 mm ± 0.87) compared to non-injured specimens (1.45 mm ± 0.69, P = 0.034). Joint motion plots indicate that complete-injury specimens exhibited tibial internal rotation up to the point of ACL failure, and after failure, the tibia displaced caudally, anteriorly and exhibited external rotation (Figure 6.3.3A, 4B), indicating tibial subluxation over the femoral condyles with a rotational component. Specimens that did not exhibit complete injury, however, exhibited only tibial internal rotation with less pronounced tibial subluxation (Figure 6.3.3C, D). Motion after the point of peak loading is markedly lower in specimens that did not exhibit ACL failure, most notably in the medial-lateral direction, and no external rotation past the point of the start of loading is noted.

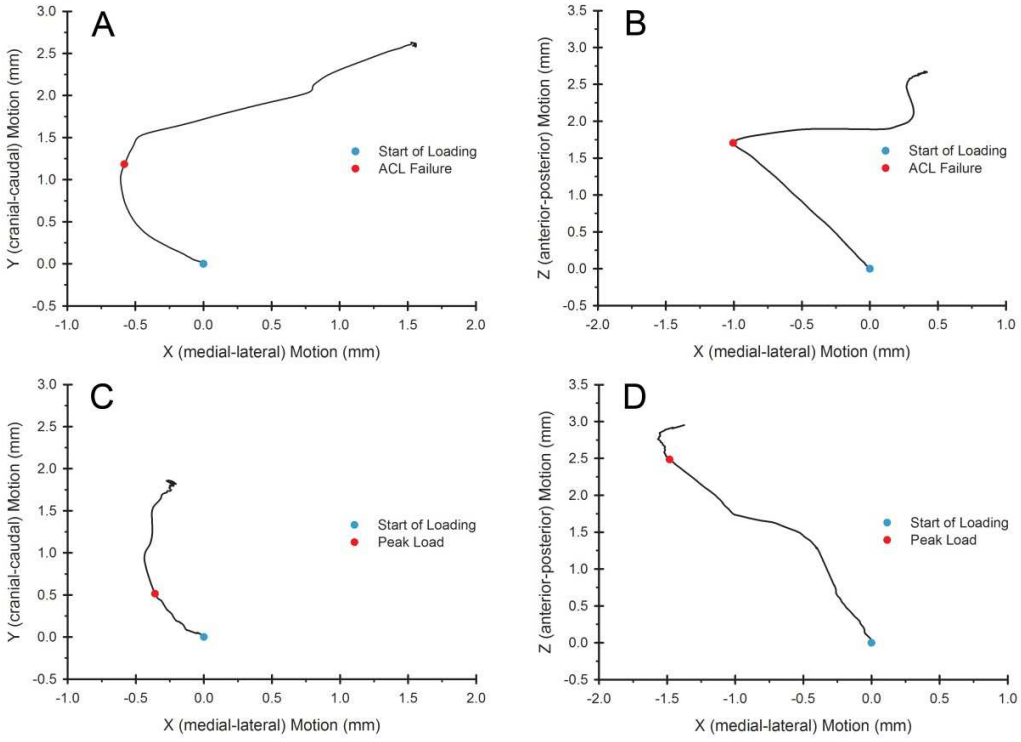

Figure 6.3.3 - *Joint motion in the coronal plane (A,C) and transverse plane (B,D) in specimens that exhibited complete ACL injury (A,B) and specimens that did not exhibit complete injury (C, D). The tibia internally rotates up to the point of peak load or ACL failure, but tibial external rotation with pronounced anterior and caudal subluxation is noted only in specimens that exhibited ACL failure and complete injury.*

The most profound differences in relative tibiofemoral joint motion were observed when grouping high displacement groups (HSHD, LSHD) and low displacement groups (HSLD, LSLD). There was a significant difference in total 3D motion (high-displacement: 7.17 mm ± 1.29; low-displacement: 5.19 mm ± 2.38, P = 0.008), 3D motion after peak load (high-displacement: 2.84 mm ± 1.57; low-displacement: 1.70 mm ± 1.19, P = 0.036), motion after peak load in the transverse plane (high-displacement: 2.69 mm ± 1.66; low-displacement: 1.22 mm ± 0.88, P = 0.014), total motion in the transverse plane (high-displacement: 6.58 mm ± 1.37; low-displacement: 4.41 mm ± 2.27, P = 0.004), motion after peak load in the coronal plane (high-displacement: 2.74 mm ± 1.49; low-displacement: 1.43 mm ± 1.04, P = 0.016), total motion in the coronal plane (high-displacement: 4.70 mm ± 1.07; low-displacement: 3.20 mm ± 1.76, P = 0.013), total motion in the sagittal plane (high-displacement: 5.46 mm ± 0.92; low-displacement: 3.72 mm ± 1.76, P = 0.002), and motion after peak load in the sagittal plane (High-displacement: 1.75 mm ± 1.11; Low-displacement: 0.95 mm ± 0.85; *P* = 0.037). Differences between grouped high and low speed groups were less pronounced, and the only difference was observed in transverse motion after peak load (high speed: 2.59 mm ± 1.64; low speed: 1.35 mm ± 1.13, *P* = 0.043).

Joint Laxity

Quantitative joint laxity testing results of all specimens are summarized in Table 6.3.3. When all specimens are analyzed, only HSHD exhibited a significant increase in AP and varus

displacements compared to uninjured limbs, with corresponding decreases in respective compliance. There were no significant differences in valgus laxity between any groups. When comparing only specimens that exhibited complete ACL injury, HSHD, HSLD, and LSHD all had significant increases in AP net displacement, AP compliance, varus displacement, and varus compliance compared to unloaded controls. (Table 6.3.4) No group exhibited significant increases in valgus displacement or valgus compliance. There were no differences in any laxity variable between groups when comparing only specimens that exhibited complete injury.

Table 6.3.3 – *Laxity Testing Results*

	Anterior-Posterior Laxity		Varus Laxity		Valgus Laxity	
	Net Displ. (mm ± SD)	Compliance (mm/N ± SD)	Net Displ. (mm ± SD)	Compliance (mm/N ± SD)	Net Displ. (mm ± SD)	Compliance (mm/N ± SD)
Control	0.350 ± 0.12	0.162 ± .05	2.20 ± 0.27	3.15 ± 0.59	2.50 ± 0.39	3.98 ± 0.98
HSHD	*1.07 ± 0.27	*0.566 ± 0.13	*3.53 ± 0.98	*5.26 ± 1.33	2.58 ± 0.34	3.74 ± 0.53
HSLD	0.648 ± 0.53	0.313 ± 0.23	2.94 ± 0.97	4.57 ± 2.00	2.60 ± 0.35	3.55 ± 0.56
LSHD	0.900 ± 0.73	0.335 ± 0.20	3.02 ± 0.85	4.63 ± 1.48	2.61 ± 0.66	3.86 ± 1.29
LSLD	0.239 ± 0.10	0.120 ± 0.05	2.16 ± 0.98	3.09 ± 1.14	3.12 ± 0.99	4.54 ± 1.30

* indicates significant difference to Control. Displ = displacement. SD = standard deviation.

Table 6.3.4 – *Laxity Testing Results (Complete-Injury Specimens Only)*

	Anterior-Posterior Laxity		Varus Laxity		Valgus Laxity	
	Net Displ. (mm ± SD)	Compliance (mm/N ± SD)	Net Displ. (mm ± SD)	Compliance (mm/N ± SD)	Net Displ. (mm ± SD)	Compliance (mm/N ± SD)
Control	0.350 ± 0.12	0.162 ± .05	2.20 ± 0.27	3.15 ± 0.59	2.50 ± 0.39	3.98 ± 0.98
HSHD	*1.07 ± 0.27	*0.566 ± 0.13	*3.53 ± 0.98	*5.26 ± 1.33	2.58 ± 0.34	3.74 ± 0.53
HSLD	*1.20 ± 0.48	*0.578 ± 0.12	*4.07 ± 0.33	*6.72 ± 1.66	2.81 ± 0.17	3.63 ± 0.25
LSHD	*1.31 ± 0.60	*0.472 ± 0.07	*3.55 ± 0.53	*5.57 ± 0.81	2.50 ± 0.21	3.52 ± 0.26
LSLD	N/A	N/A	N/A	N/A	N/A	N/A

* indicates significant difference to Controls. Displ = displacement. SD = standard deviation.
Note: N/A in LSLD because no specimens ruptured in LSLD.

Specimens that exhibited complete injury had significantly higher AP displacement (Injured: 1.16 mm ± 0.4; Non-injured: 0.257 mm ± 0.11, $P < 0.001$) and AP compliance (Injured: 0.541 mm/N ± 0.12; Non-injured: 0.128 mm/N ± 0.06, $P < 0.001$) compared to non-injured

specimens. Specimens that had complete injury had significantly higher varus displacement (Injury: 3.64 mm ± 0.78; Non-injury: 2.18 mm ± 0.69, $P < 0.001$) and varus compliance (Injury: 5.61 mm/N ± 1.30; Non-injury: 3.86 mm/N ± 1.51, $P < 0.001$) compared to non-injured specimens. There was no difference in valgus displacement or valgus compliance between injured and non-injured specimens.

There were marked differences in AP and varus laxity when comparing high and low displacement groups. High-displacement had significantly larger AP displacement (High-displacement: 0.991 mm ± 0.53; Low-displacement: 0.444 mm ± 4.3, $P = 0.003$), AP compliance (High-displacement: 0.457 mm/N ± 0.20; Low-displacement: 0.217 mm/N ± 0.19, $P = 0.006$), varus displacement (high-displacement: 3.29 mm ± 0.93; low-displacement: 2.55 mm ± 1.03, $P = 0.031$), and varus compliance (high-displacement: 4.96 mm/N ± 1.39; low-displacement: 3.83 mm/N ± 1.75, $P = 0.021$). Valgus displacement or compliance did not vary as a function of displacement. When comparing high and low speed groups, there were significant differences in AP displacement (high-speed: 0.873 mm ± 0.45; low-speed: 0.569 mm ± 0.61, $P = 0.026$) and AP compliance (high-speed: 0.447 mm/N ± 0.22; low-speed: 0.228 mm/N ± 0.18, $P = 0.004$), but no difference was found in varus displacement, varus compliance, valgus displacement, or valgus displacement.

6.4 - Discussion

Animal models accurately reproducing the biologic cascades after joint injury are important research tools, but the most prevalent model for PTOA in the rat is surgical ACL transection, which could introduce confounding biological variables due to its surgical nature. To date, models of noninvasive ACL injury in the rat are sparse, and, to this end, the purpose of this study was to biomechanically characterize the tibial compression model in the rat. We

hypothesized that both high speed and high displacement are necessary to induce complete ACL injury. This hypothesis was confirmed, but high displacement was more highly associated with complete injury than high speed. We found that complete ACL injury can be repeatedly induced with a 3 mm compressive displacement of the tibia at 8 mm/s when the knee is flexed to 100°. We also hypothesized that complete ACL injury would induce A-P laxity but not varus or valgus laxity. This hypothesis was only partially confirmed: ACL injury causes marked increases in anterior-posterior and varus laxity, and joint displacement in the transverse and coronal planes was the most contributory to ACL injury in our model.

Only a few studies have utilized noninvasive joint loading to induce ACL rupture in the rat, and no study has utilized the tibial compression model in the rat. Tang *et al* utilized a rotational model to study post-injury protein expression. (Tang et al., 2009a) In this model, ACL injury was induced by rotating the tibia and femur in opposite directions in 120° of joint extension**.** No characterization of the injury or post-injury joint mechanics was performed, and it is difficult to determine how injury induced by their loading protocol compares to injuries observed in the present study. The tibial compression model has been previously employed in the mouse. Christiansen *et al* applied a 12 N tibial compressive load to induce a noninvasive ACL injury(Christiansen et al., 2012a), which induced OA-like changes such as cartilage degeneration and subchondral bone changes. The load was applied at 1 mm/s and the authors stated that bony avulsion of the ACL occurred in all specimens. A follow-up study by that group indicated that true ACL rupture was achieved at higher speed (500 mm/s) whereas lower speed injury (1 mm/s) caused a “disruption of the ACL with an avulsion fracture from the posterior femur.”(Lockwood et al., 2014) Interestingly, histologic evidence of articular cartilage degeneration did not vary between injury mode (i.e. avulsion vs. mid-substance rupture, and only acute trabecular bone

changes were impacted by injury mode). Our data corroborates that loading rate determines injury type. We also observed ACL avulsion at 1 mm/s, but since the 8 mm/s loading rate in our "high speed" group was markedly lower than the 500 mm/s "high speed" group used by Christiansen *et al* , we observed avulsion, midsubstance rupture, and a combination avulsion-rupture injury in our high speed group. Although differences in joint biomechanics between the mouse and rat may cause some discrepancies in injury type, this finding likely indicates that 8 mm/s represents the lower end of the loading rate range necessary to induce true ACL rupture, and future studies are necessary to determine which loading rate repeatedly induces ACL rupture in the rat.

ACL rupture in humans occurs most prevalently in non-contact scenarios during rapid deceleration or change of direction(Boden et al., 2000b; Boden et al., 2010), and several biomechanical motions have been shown to induce ACL rupture, including anterior tibial translation due to high-magnitude tibiofemoral compression (Meyer and Haut, 2005)**,** internal tibial rotation(Meyer and Haut, 2008)**,** and combined tibial rotation and valgus joint stress.(Boden et al., 2010; Meyer and Haut, 2008) Meyer *et al* have shown that tibial compression causes transient anterior subluxation of the tibia relative to the femur.(Meyer and Haut, 2008) In their study, internal tibial rotation was noted to occur during pre-failure compressive loading, and following ACL rupture, the tibia rotated externally. In our study, we observed that joint motion in the transverse and coronal planes was markedly higher in specimens that exhibited complete ACL injury compared to specimens that did not exhibit injury. The medial-lateral motion component of these planes was most pronounced, and motion plots indicate that this is tibial rotation and/or translation. Due to anatomic size restrictions, it was only possible to place one marker in each bone, and we, therefore, cannot definitively

conclude whether rotation or translation predominated. However, our results of motion in the medial-lateral direction after rupture are consistent with Meyer's biomechanics study of human ACL rupture, indicating that not only vertical and anterior tibial displacement occurs during and after ACL rupture. We observed that only specimens that experienced ACL injury exhibited increased LCL laxity, a concomitant joint injury also observed in humans following ACL rupture, although rarer than MCL injury.(Lee et al., 1988; Levine et al., 2013) Since total motion after peak load in the transverse plane as well as net displacement in the coronal plane was significantly higher in injured specimens, we conclude that these motions cause LCL injury, and tibial external rotation immediately after ACL failure is the most likely cause. Meyer *et al* did not investigate LCL injury following ACL rupture, nor were joint laxity tests performed, and we cannot conclude whether our proposed mechanism of LCL injury is fully representative of concomitant LCL injury in humans. Future studies assessing the exact pathomechanism of LCL injury in both our models and human injury are necessary.

We did not measure any increases in valgus laxity due to ACL injury. Medial collateral ligament (MCL) injury is a common concomitant injury during ACL rupture in humans(Sankar et al., 2006; Yoon et al., 2011), notably during the common "valgus collapse" mechanism of ACL injury.(Boden et al., 2010; Koga et al., 2010; Quatman and Hewett, 2009) In a biomechanics study assessing relative ACL and MCL strain during simulated landing-induced ACL rupture in human cadaveric specimens, Quatman *et al* found that MCL strain is most pronounced in multiplanar tibiofemoral loading, which includes anterior shear, abduction, and internal tibial rotation.(Quatman et al., 2013) They stated that the MCL strain observed in their study is not sufficient to induce MCL injury, but a valgus and internal rotation moment are necessary to strain the MCL. Their simulated landing model allowed unconstrained tibial

rotation and varus-valgus joint deformation at 25° of flexion. Our loading protocol rigidly fixed the paw at 100° of knee flexion, which inherently constrains tibial internal rotation and valgus deformation (i.e. tibial abduction). Other studies have indicated that concomitant MCL injury during ACL rupture is induced by valgus loading (Mazzocca et al., 2003; Shin et al., 2009), and we, therefore, conclude that valgus injury was not induced in our model due to the lack of valgus loading and fully unconstrained tibial internal rotation.

This study has several limitations. Our motion capture data is inherently limited by the system's resolution at a given speed. At a capture rate of 179 Hz and with 4 mm retroreflective markers, our resolution was 279 µm with a 98.07% accuracy at 8 mm/s, and a 49.02 µm resolution with 99.31% accuracy at 1 mm/s. Inherently higher error at the higher loading rate could not be avoided, and high-speed groups may therefore have higher error. Secondly, we utilized µCT imaging at a resolution of 36 µm to assess specimens for fractures and bony avulsions, but we cannot exclude the possibility of missing microfractures or very small avulsions given the µCT imaging parameters. Due to size restrictions and the risk of fracture, we were only able to place one retroreflective marker in the tibia and femur, which limited the information able to be ascertained from motion capture data. Lastly, as this is a biomechanics study of cadaveric rats, the biomechanical behavior of live tissue may not be fully represented in our data set, and no information about the actual impact of this ACL injury on PTOA can be gathered. Further studies are underway to assess cartilage degeneration following ACL injury due to tibial compression in the rat.

This study biomechanically characterized the tibial compression model of ACL injury in the rat. A reproducible ACL injury can be induced by the application of a tibial axial displacement of 3 mm at 8 mm/s when the knee is flexed at ~100°, and this injury causes

concomitant LCL injury due to post-failure tibiofemoral motion in the transverse and coronal planes. Motion-capture data indicates that this injury is consistent with human models of ACL injury, and this injury model may be applied in future rat studies of PTOA and/or ACL reconstruction.

CHAPTER 7: AIM # 2 - COMPARE AND CONTRAST THE ONSET AND PROGRESSION OF POST-TRAUMATIC OSTEOARTHRITIS FOLLOWING NONINVASIVE RUPTURE OF THE ACL TO SURGICAL TRANSECTION OF THE ACL

7.1 - Introduction

The biological events leading to PTOA after joint injury have yet to be fully outlined. Animal models of PTOA are widespread, and the most common ACL injury-induced PTOA model is surgical ACL transection. It has been shown to induce the onset of OA-like symptoms such as the loss of proteoglycan content(Altman et al., 1984a; Guilak et al., 1994a), osteophyte formation(Hashimoto et al., 2002a), altered biomechanical properties of articular cartilage(Altman et al., 1984a), loss/thinning of articular cartilage(Guilak et al., 1994a), and chondrocyte death(Martin and Buckwalter, 2006a). However, given the invasive surgical nature of the model, it is unclear whether these changes are representative of human PTOA after traumatic ACL rupture.

Clinical studies have shown that ACL rupture induces acute and chronic changes to articular cartilage morphology(Argentieri et al., 2014; Roemer et al., 2014; Su et al., 2013), the menisci(Roemer et al., 2014; Williams et al., 2012), subchondral bone(Nakamae et al., 2006; Peterfy et al., 2004; Roemer et al., 2014), epiphyseal bone(Nakamae et al., 2006), synovium(Roemer et al., 2014), and ligaments(Roemer et al., 2014) in the knee. It is still unknown whether the acute trauma and inflammation, the joint destabilization, or the chronic change in joint kinematics has the largest impact on the degenerative changes observed in knee tissues after ACL injury, but it is generally understood that the PTOA cascade is self-perpetuating.

As outlined in Section 2.2, the kinetics of PTOA following joint injury can be divided into three main phases: early, intermediate, and late(Anderson et al., 2011). During the early phase, constituting the first several days after injury, catabolic events such as inflammation and cell death predominate. In the following intermediate phase, inflammation begins to subside and anabolic remodeling processes are initiated, though these do not yet outweigh ongoing catabolic cascades. In the late phase, anabolic matrix synthesis predominates to compensate previous events, and tissue remodeling proceeds chronically. All aforementioned knee tissues are influenced by these three phases, and understanding the kinetics of degenerative changes in the context of the anabolic-catabolic balance is critical when investigating interventional or regenerative therapies.

To date, no study has compared the degenerative, PTOA-like changes observed in the rat following surgical ACL transection to a noninvasive, traumatic model of ACL injury. Specifically, it is unknown whether the ACL transection model underestimates the degenerative cascades due to the lack of a traumatic injury or whether the surgical nature of the ACL transection model (i.e. surgical cutting and suturing of the skin and synovium, surgical cutting of the ACL) introduces confounding inflammatory effects that potentially exacerbate and overestimate degenerative changes in the knee. As demonstrated in Section 6 – Aim #1, a noninvasive ACL injury model able to repeatably induce ACL rupture using axial tibial compression has been developed and characterized. The mode of injury and tibiofemoral joint motion during loading are representative of human ACL injury, and it is hypothesized that this injury model will lead to PTOA-like degenerative changes in the rat knee. As such, the purpose of the following aim was to compare and contrast the onset and progression of PTOA following noninvasive ACL rupture to the surgical ACL transection model. We hypothesize that

noninvasive ACL rupture induces more extensive degenerative changes in articular cartilage compared to ACL transection and that these will coincide with increased serum and synovial fluid concentrations of cartilage biomarkers. Furthermore, we hypothesize that bony remodeling will be observed in both groups but the ACL rupture group will exhibit increases in bone mineral density and trabecular thickness due to the traumatic nature of the injury.

7.2 - Methods

Treatment Groups and Procedures

Under an institutional animal care and use committee (IACUC)-approved protocol, thirty-six female Lewis Rats (14 weeks of age) were randomized to one of three treatment groups: Control, Rupture, or Transection (n=12 per group). Animals within each group were then randomized to one of two time-points: 4 weeks or 10 weeks. On the morning of all procedures, animals were administered 5 mg/kg subcutaneous Carprofen, a non-steroidal anti-inflammatory drug. Anesthesia was induced by intraperitoneal 75-100 mg/kg ketamine with 3-5 mg/kg xylazine and maintained using 0.5% - 1.5% isofluorane during the duration of the procedure. Subcutaneous atropine (0.05 mg/kg) was administered immediately after anesthetic induction. Post-operative analgesia was administered with an initial dose of subcutaneous buprenorphine (0.03 mg/kg) following immediately after anesthesia recovery and an additional dose (0.01 mg/kg) 8-12 hours after the initial dose. No animals required additional doses after the second dose.

Animals in the Rupture group were administered a noninvasive anterior cruciate ligament (ACL) rupture using a biomechanical loading protocol with a custom fixture on a materials testing system (Insight, MTS, Eden Prarie, MN, USA), as previously described and characterized

in Section 6 - Aim #1.(Maerz et al., 2015) In brief, the protocol is a variation of the tibial compression model first demonstrated in mice by Christiansen *et al(Christiansen et al., 2012a)*. In the present study, the animal is placed prone on a bed, and the right knee is flexed to 100^0 on a stage with a 3 mm deep trough restricting medial/lateral translation. The paw is rigidly mounted in 30^0 of dorsiflexion in a fixture constraining all motions except flexion/extension (Figure 6.2.1A). Following preload, 10 cycles of preconditioning, and a secondary preload to 15N, a rapid vertical displacement of 3 mm at 8 mm/s was applied to the paw fixture. The rapid axial tibial displacement causes anterior tibial subluxation, tibial internal rotation, failure of the ACL, followed by tibial external rotation, as previously characterized in Section 6 - Aim #1 and by Maerz *et al(Maerz et al., 2015)*. ACL failure occurs at ca. 60 – 70 N of axial force, and in addition to anterior laxity, varus laxity is observed following this injury protocol, as characterized in Section 6 – Aim #1. Complete ACL rupture was confirmed following biomechanical loading using an anterior drawer test, whereby anterior joint laxity is confirmed by the application of an anterior tibial force (Figure 7.2.1).

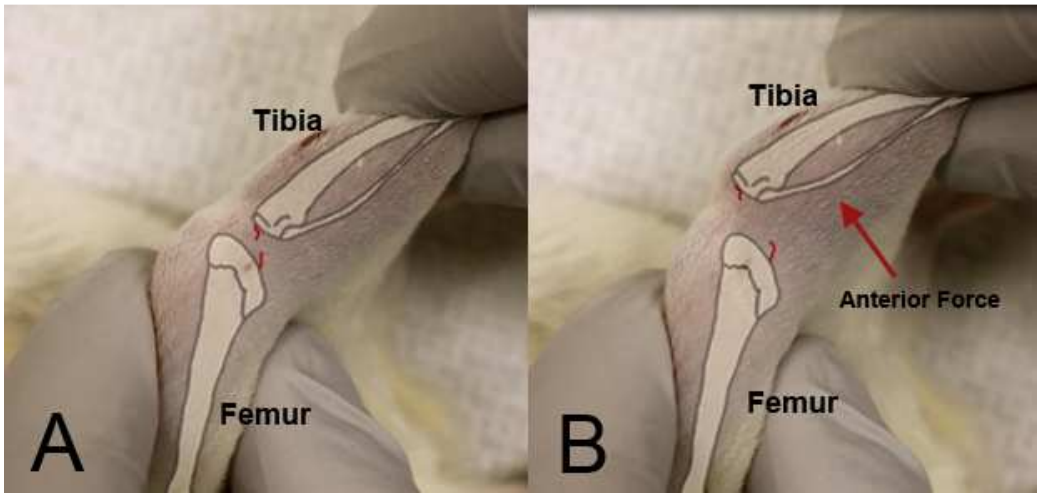

Figure 7.2.1 – *Confirmation of ACL rupture using an anterior drawer test. The reduced knee joint (A) is anteriorly dislocated by the application of an anterior tibial force, causing subluxation of the tibia with respect to the femur (B) due to the loss of anterior stability afforded by the ACL.*

In the Transection group, complete surgical transection of the ACL was performed as previously described(Jansen et al., 2012; Martin and Buckwalter, 2006a; Ruan et al., 2013b). In brief, following anesthetic administration as described above, the right knee was shaved and prepared with betadine and alcohol. The animals were positioned supine on a warm water recirculator to aid in thermoregulation. A midline knee incision was made using a No. 15 scalpel blade. Medial and lateral skin flaps were then developed. A medial parapatellar arthrotomy was made, and the patella was subluxated laterally. The knee was then hyperflexed to aid in visualization of the ACL and to maintain patellar subluxation. The ACL was transected mid-substance using a Size 0 micro scalpel (Biomedical Research Instruments, Silver Spring, Maryland, USA), taking care to avoid contact with any cartilaginous surfaces. Anterior and posterior drawer testing was subsequently performed to confirm complete ACL rupture and PCL integrity, respectively. The knee was lavaged with sterile saline. The arthrotomy was then closed

using 6-0 Prolene (Ethicon 8697G) interrupted sutures and the skin was closed using 5-0 undyed Vicryl (Ethicon J493G) buried interrupted sutures.

Animals in the Control group were administered identical analgesia and anesthesia but received no injury or surgical treatment. All animals were allowed normal diet and *ad libitum* cage activity until sacrifice at either 4 or 10 weeks. Sacrifices were performed by CO_2 asphyxia, and a 5 ml blood draw was immediately performed via cardiac puncture. Blood was allowed to coagulate for 30 mins and centrifuged for 10 mins at 2000 rpm in order to collect serum. All serum was aliquoted into 150 µL volumes and immediately stored at -80^{0}C for future analysis.

Following blood collection, synovial fluid was aspirated from the right knee using a lavage procedure. The posterior joint capsule was carefully exposed but not violated, and a 23-gauge needle was carefully inserted into the center of the knee via the femoral notch in a posterior-to-anterior fashion. A 27-gauge needle was then used to inject 400 µL of PBS using an anteromedial approach immediately lateral to the patellar tendon. Slow injection of the PBS facilitated the collection of ca. 150-200 µL of joint lavage fluid, which was immediately stored at -80^{0}C for future analysis.

Micro computed Tomography (µCT)

Following sacrifice, the right limb was carefully dissected to expose articular cartilage of the femur and tibia. Periarticular soft tissues such as the synovium, meniscus, and ligaments were removed, and the tibia and femur were cut distally and proximally, respectively, to expose the medullary cavity. All specimens were fixed using 10% neutral buffered formalin (NBF) for 48 hours. Specimens were then rinsed five times using distilled water and rehydrated in phosphate-buffered saline (PBS) for 24 hrs. To facilitate contrast-enhanced imaging of articular

cartilage, equilibrium partitioning of an ionic contrast agent (EPIC) - µCT was employed. This previously-described technique contrast enhances articular cartilage by the preferential exclusion of a negatively-charged molecule from sulfated glycosaminoglycan (sGAG)-rich tissues(Kotwal et al., 2012; Palmer et al., 2006; Xie et al., 2010). In addition to enabling accurate segmentation and visualization, this technique also facilitates quantification of differential sGAG distribution within a tissue. Specimens were incubated in 20% ioxaglate (Hexabrix, Guerbet Group, France) pH = 7.2, for 24 hrs. Specimens were then carefully dabbed with a moist towel and mounted rigidly in a humidified µCT specimen holder containing humidifying beads able to maintain an 80% humid atmosphere within the holder. µCT imaging of the distal femur and proximal tibia was performed at 70 kVp, 114 mA with an isotropic voxel resolution of 12 µm and a 250 ms integration time (µCT40, Scanco Medical, Brütissellen, Switzerland). Following imaging, specimens were rinsed in PBS to remove the contrast agent and dehydrated using an ethanol series up to 70% v/v ethanol, in which all specimens were stored until histologic processing.

µCT Segmentation of Articular Cartilage, Subchondral Bone, and Epiphyseal Bone

µCT images were converted to DICOM, filtered using a noise-reducing Gaussian filter (σ = 0.2) , and a custom MATLAB (r2014a, The Mathworks, Nattick, MA, USA) program was employed to segment articular cartilage. In brief, blinded manual outlining of the articular surface of both the tibia and femur was performed on sagittal images. Due to the drastic differences in the attenuation between air (-1000 HU), contrast-enhanced articular cartilage (800 – 2500 HU), and bone (3500 – 6500 HU), outlining around articular cartilage to include both air and subchondral bone allows for accurate segmentation (Figure 7.2.2). A three-dimensional (3D) region-growing algorithm (Christian Wuerslin, University of Tuebingen and University of Stuttgart, Germany. http://www.mathworks.com/matlabcentral/fileexchange/41666-fast-3d-2d-

region-growing--mex-) was employed to segment cartilage voxels. This algorithm requires only a seed point within the 3D structure and a single intensity difference threshold describing the acceptable difference in intensity between the seed point and any other voxel. A difference threshold of 1500 was found to reproducibly segment cartilage without including any bone voxels. Small, malsegmented objects representing subchondral bone marrow were removed using size-exclusion and connectivity algorithms, which dictate that only one large volume (i.e. articular cartilage) can remain following processing.

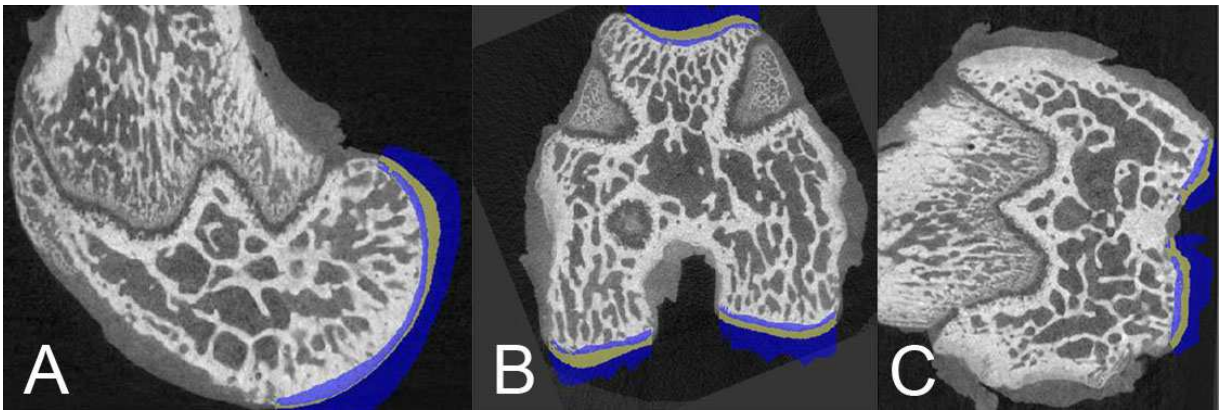

Figure 7.2.2 – *Outlining of Articular Cartilage on Contrast-Enhanced μCT images. Regions-of-interest (ROIs) were manually drawn on sagittal μCT images around articular cartilage, encompassing subchondral bone and air (A). A 3D region-growing algorithm was used to accurately segment only articular cartilage, which could be confirmed and edited on axial (B) and coronal images (C).Tibial cartilage was outlined in an identical manner.*

Subchondral bone was segmented automatically using a custom MATLAB program which employs the already-segmented articular cartilage volume. The program segmented subchondral bone 252 μm (i.e. 21 voxels) deep to any articular cartilage voxel using a binary dilation with a disk-shaped structuring element. Following dilation, a high-pass intensity threshold of 3500 HU removed air, articular cartilage, bone marrow, and other soft tissue to yield only subchondral bone.

Epiphyseal bone was segmented from metaphyseal bone using manual outlining on coronal images along the distal femoral epiphysis and proximal tibial epiphysis. A high-pass intensity threshold of 3500 HU removed air, articular cartilage, bone marrow, and other soft tissue to yield only epiphyseal bone (Figure 7.2.3).

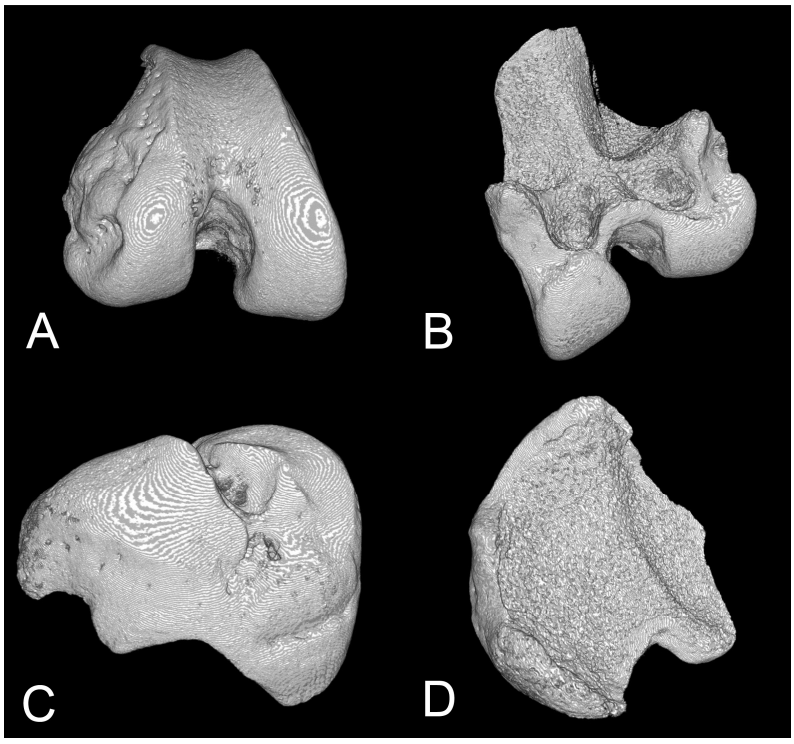

Figure 7.2.3 – *Segmented epiphyseal bone. Manual outlining and a high-pass threshold was used to segment femoral (A,B) and tibial (C,D) epiphyseal bone for densitometric and morphologic analysis.*

μCT Analysis of Articular Cartilage, Subchondral Bone, and Epiphyseal Bone

Segmented 3D articular cartilage volumes were converted to consistent 2D height maps using conformal parameterization, as outlined in detail in Appendix 1. Following segmentation of compartments, parameterization, generation of height maps, and subsequent subcompartmental segmentation, articular cartilage morphology was analyzed by mean height, peak-to-valley distance (P-V), and arithmetic surface roughness S_a.

Subchondral and epiphyseal bone were analyzed using a custom MATLAB algorithm in conjunction with Miji, a Matlab-ImageJ interface(Sage et al., 2012; Schindelin et al., 2012), and the BoneJ plug-in for ImageJ(Doube et al., 2010). Bone volumes were exported to ImageJ, and mean trabecular thickness (Tb.Th. Mean), trabecular thickness standard deviation (Tb. Th. Std), and maximum trabecular thickness (Tb.Th. Max) were quantified using the trabecular thickness script in the BoneJ plugin. Bone volume fraction (BV/TV) was calculated using a bone threshold of 3500 HU. Bone mineral density (BMD) and tissue mineral density (TMD) were calculated using calibration data of a series of hydroxyapatite concentrations. All analyses were performed separately in the medial, lateral, and trochlear compartments of both the femur and tibia as well as the entire tibial and femoral volumes.

Histologic Processing and Analysis

Following fixation in 10% NBF, all samples were decalcified to completion in 10% formic acid and dehydrated in an increasing ethanol series. Both the tibia and femur were bisected sagittally to facilitate separate sectioning of the medial and lateral compartments. Due to the natural taper of the trochlear cartilage with respect to the condylar cartilage, sectioning of the femoral compartments was performed with a 10^0 oblique angle to capture both trochlear and condylar cartilage on all sections. Tibial compartments were sectioned in true sagittal fashion without an oblique angle. Four sections spaced 200 µm from the medial and lateral compartment of the femur and tibia were then stained with both Hematoxylin & Eosin (H&E) as well as Safranin-O/Fast Green (Saf-O). Microscopic imaging was performed at 20x using an automatic slide imaging system (Aperio, Leica Biosystems, Buffalo Grove, IL, USA). Qualitative evaluation of articular cartilage was performed by three blinded investigators using the OARSI Modified Mankin score (Table 7.2.1)(Kraus et al., 2010). Results of all three raters were

averaged to calculate a composite score for each animal, and composite scores of each animal within a group were averaged to obtain a group average at each time point.

Biomarker Quantification in Serum and Synovial Lavage Fluid

Collected serum was thawed at room temperature prior to quantification. Following a 5 min centrifugation at 2,000 rpm to settle particulate, concentrations of six biomarkers of cartilage metabolism and breakdown (Table 7.2.2) were quantified using enzyme-linked immunosorbent assays (ELISAs). Synovial fluid was thawed, centrifuged, and analyzed for cartilage oligomeric matrix protein (COMP) concentration using ELISA.

Table 7.2.1 – *OARSI Modified Mankin Score using for Qualitative Histological Assessment*

Parameter	Grade	Description
Articular Cartilage Structure	0	Normal, smooth, uninterrupted surface
	1	Mild surface irregularities (undulations)
	2	Irregular surface, 1-3 superficial clefts (fissures)
	3	>3 fissures and/or loss of cartilage in the superficial zone
	4	1-3 fissures extending into the middle zone
	5	>3 fissures and/or loss of cartilage extending into the middle zone
	6	1-3 fissures extending into the deep zone
	7	>3 fissures extending into the deep zone and/or loss of cartilage to deep zone
	8	Fissures or loss of cartilage extending to the zone of calcified cartilage
Proteoglycan Content (staining by Safranin-O)	0	Uniform throughout articular cartilage
	1	Decreased in superficial zone only and for < half the length of the condyle or plateau
	2	Decreased in superficial zone for half the length or greater of the condyle or plateau
	3	Decreased in superficial and middle zones for <half the length of the condyle or plateau
	4	Decreased in superficial and middle zones for half the length or greater of the condyle or plateau
	5	Decreased in all 3 zones for <half the length of the condyle or plateau
	6	Decreased in all 3 zones for half the length or greater of the condyle or plateau
Cellularity	0	Normal (1/2 cells/lacuna)
	1	Diffuse/slight hypercellularity
	2	Regions of hypercellularity and clustering
	3	Diffuse hypocellularity
Tidemark Integrity	0	Intact/single tidemark
	1	Crossed by vessels/duplication of tidemark
Osteophytes	0	No osteophyte present
	1	Small osteophyte
	2	Medium-sized osteophyte
	3	Large osteophyte

Table 7.2.2 – *Biomarkers of cartilage metabolism and breakdown analyzed in serum*

Analyte	Analyte Details	Supplier
CS846	Aggrecan Epitope	Ibex, Montreal, Quebec Canada
C2C	Collagenase neoepitope of Collagen II	Ibex, Montreal, Quebec Canada
CTxII	Collagen II turnover	Nordic Bioscience, Herlev, Denmark
CPII	Collagen II synthesis	Ibex, Montreal, Quebec Canada
C1,2C	Type I/II collagen turnover	Ibex, Montreal, Quebec Canada
COMP	Cartilage Oligomeric Matrix Protein	MD Bioproducts, St. Paul, MN, USA

Data Analysis and Statistical Comparison

All statistical analyses were performed in SPSS (v22, IBM, Armonk, NY). The normality and equal variance assumptions were assessed using the Shapiro-Wilk test and Levene's test, respectively. Differences in independent, normally distributed and non-normally distributed variables were compared between groups at each time point using one-way analysis of variance (ANOVA) and Kruskal-Wallis tests, respectively. Differences in independent, normally distributed and non-normally distributed variables between the 4 and 10-week time points were assessed using *t*-tests and Mann Whitney U tests, respectively. Multiple comparisons were performed with a Sidak *P*-value correction at $\alpha = 95\%$. Inter-rater agreement in qualitative assessment of histologic grade was calculated using the intraclass correlation coefficient (ICC). Correlations of continuous, normally-distributed variables were calculated using the Pearson product-moment correlation coefficient. Correlations of ordinal, nonparametric variables were calculated using the Spearman rank-order correlation coefficient. *P* values lower than 0.05 were considered significant.

7.3 - Results

Subchondral Bone Remodeling

Subchondral bone remodeling was observed as a function of both age and injury A comprehensive numerical summary of subchondral bone remodeling data can be found in Appendix 2, Femur: Tables A2.1 and A2.2; Tibia: Tables A2.3 and A2.4. Due to aging, Control animals exhibited significant increases in femoral and tibal bone volume fraction (BV/TV), bone mineral density (BMD), and tissue mineral density (TMD) in all compartments between 4 and 10 weeks. Trabecular thickness mean and trabecular thickness max increased significantly between 4 and 10 weeks in both the femur and in the tibia as a result of aging in the Control group.

Transection induced a loss of femoral subchondral BV/TV at both 4 and 10 weeks (Figure 7.3.1, Figure 7.3.2**)**, whereas Rupture exhibited only slight, non-significant decreases at 4 weeks and significant decreases in the trochlear compartment and whole femur at 10 weeks. Transection had a significantly lower femoral subchondral BV/TV compared to Rupture in all compartments at 4 weeks and in the lateral compartment at 10 weeks (Figure 7.3.2).

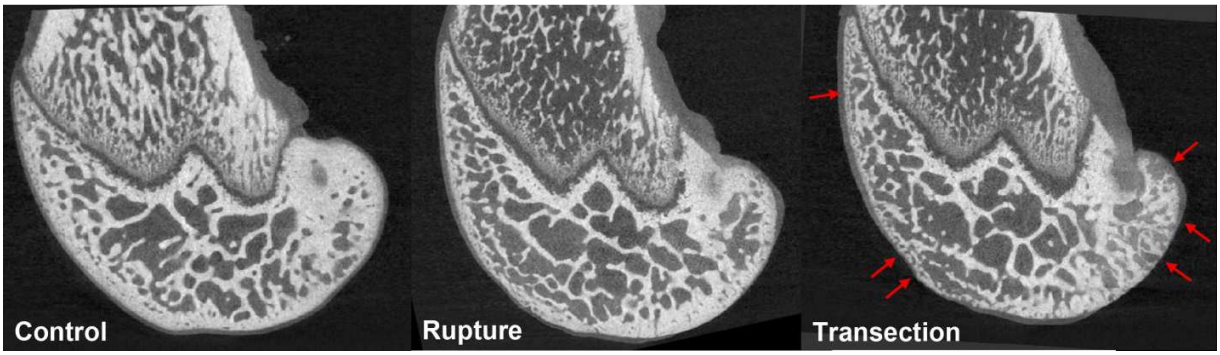

Figure 7.3.1 – *Representative sagittal sections of the medial femoral condyle of Control (left), Rupture (middle), and Transection (right) at 4 weeks. Significant subchondral bone loss was observed in the Transection group (red arrows), with only subtle changes in the Rupture group.*

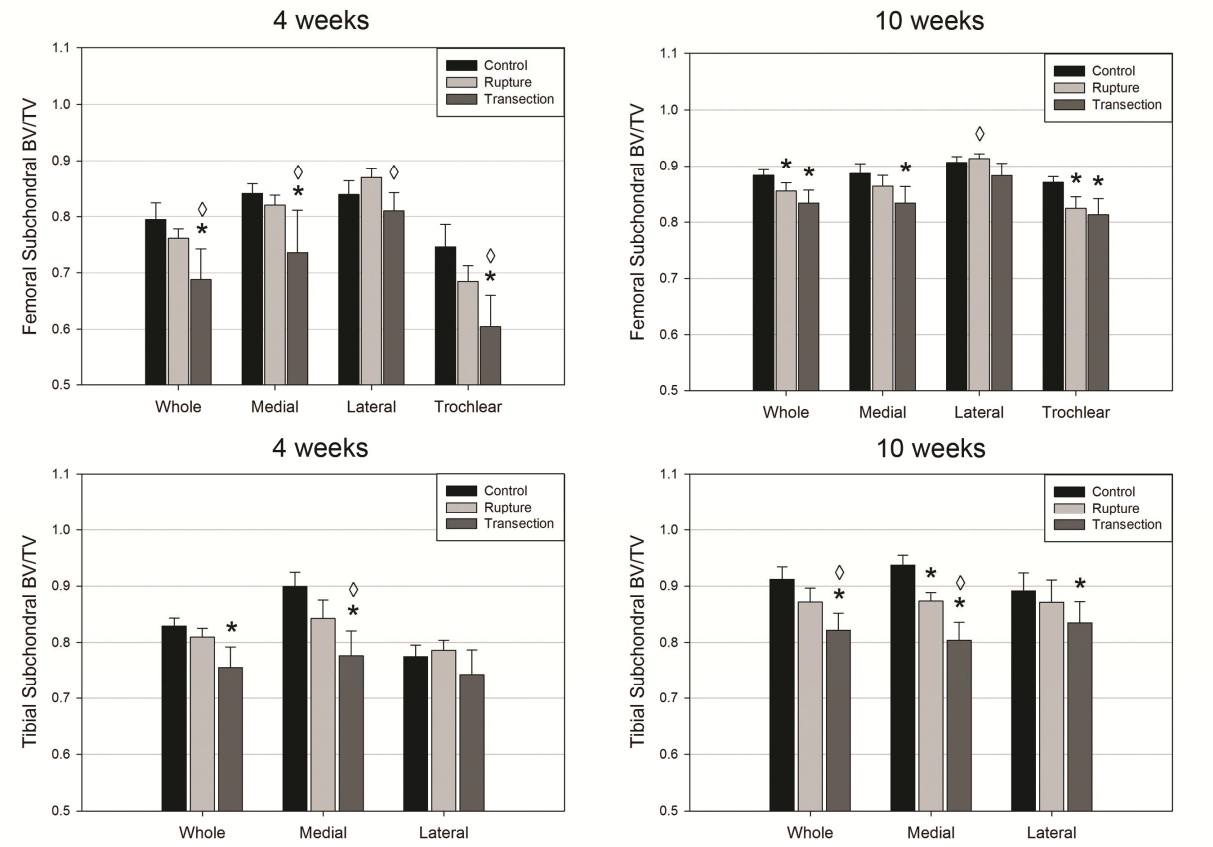

Figure 7.3.2 – *Femoral and Tibial Subchondral Bone Volume Fraction (BV/TV) at 4 weeks and 10 weeks. * denotes significant difference to Control. ◊ denotes significant difference between Rupture and Transection.*

Slight decreases in femoral subchondral BMD and TMD (Figure 7.3.3) were observed in both Rupture and Transection at 4 weeks, and Transection had significantly lower femoral subchondral BMD in the trochlear compartment and significantly lower femoral subchondral TMD in the lateral compartment compared to Rupture at 4 weeks. At 10 weeks, Rupture exhibited globally higher femoral subchondral TMD compared to Control, whereas Transection exhibited globally lower femoral subchondral TMD and BMD. Rupture had significantly higher femoral subchondral BMD in the lateral compartment and whole femur and significantly higher femoral subchondral TMD in the medial and lateral compartments as well as the whole femur compared to Transection (Figure 7.3.3). Only slight changes in femoral subchondral trabecular

morphology were observed. Rupture exhibited significantly higher Tb.Th. Mean in the lateral compartment compared to Transection at 10 weeks, and both Rupture and Transection exhibited significantly lower femoral subchondral Tb. Th. Mean compared to Control at 10 weeks (Figure 7.3.4; Appendix 2, Table A2.2).

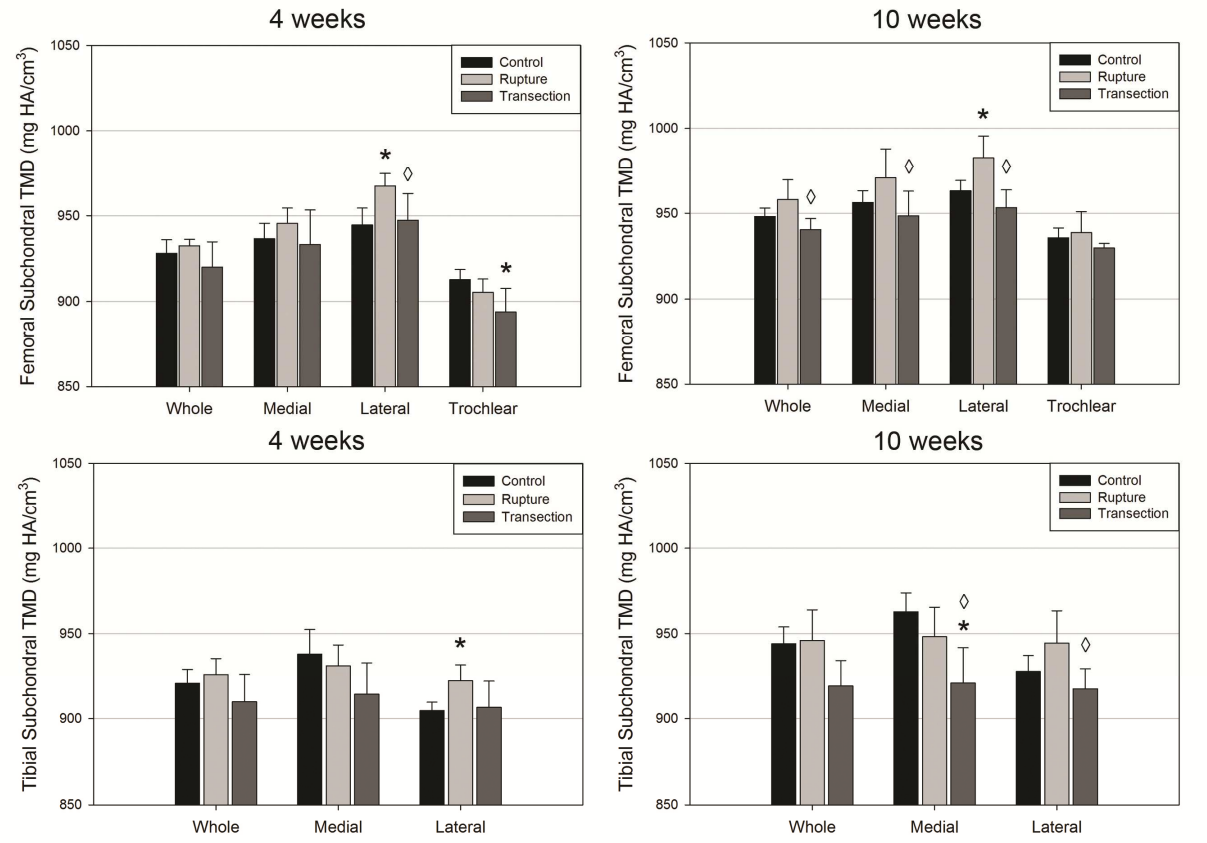

Figure 7.3.3 – *Femoral and Tibial Subchondral Bone Tissue Mineral Density (TMD) at 4 weeks and 10 weeks. * denotes significant difference to Control. ◊ denotes significant difference between Rupture and Transection.*

Less profound changes were observed in the subchondral bone of the tibia. Both Rupture and Transection exhibited significant decreases in tibial subchondral BV/TV in the medial compartment compared to Control at both 4 and 10 weeks, and Transection had significantly lower tibial subchondral BV/TV in the medial compartment compared to Rupture at 4 and 10 weeks (Figure 7.3.2). Rupture had significantly higher tibial subchondral BMD and TMD

compared to Transection at 10 weeks (Figure 7.3.3). No extensive changes in tibial subchondral trabecular morphology were noted (Figure 7.3.4; Appendix 2, Table A2.3, A2.4).

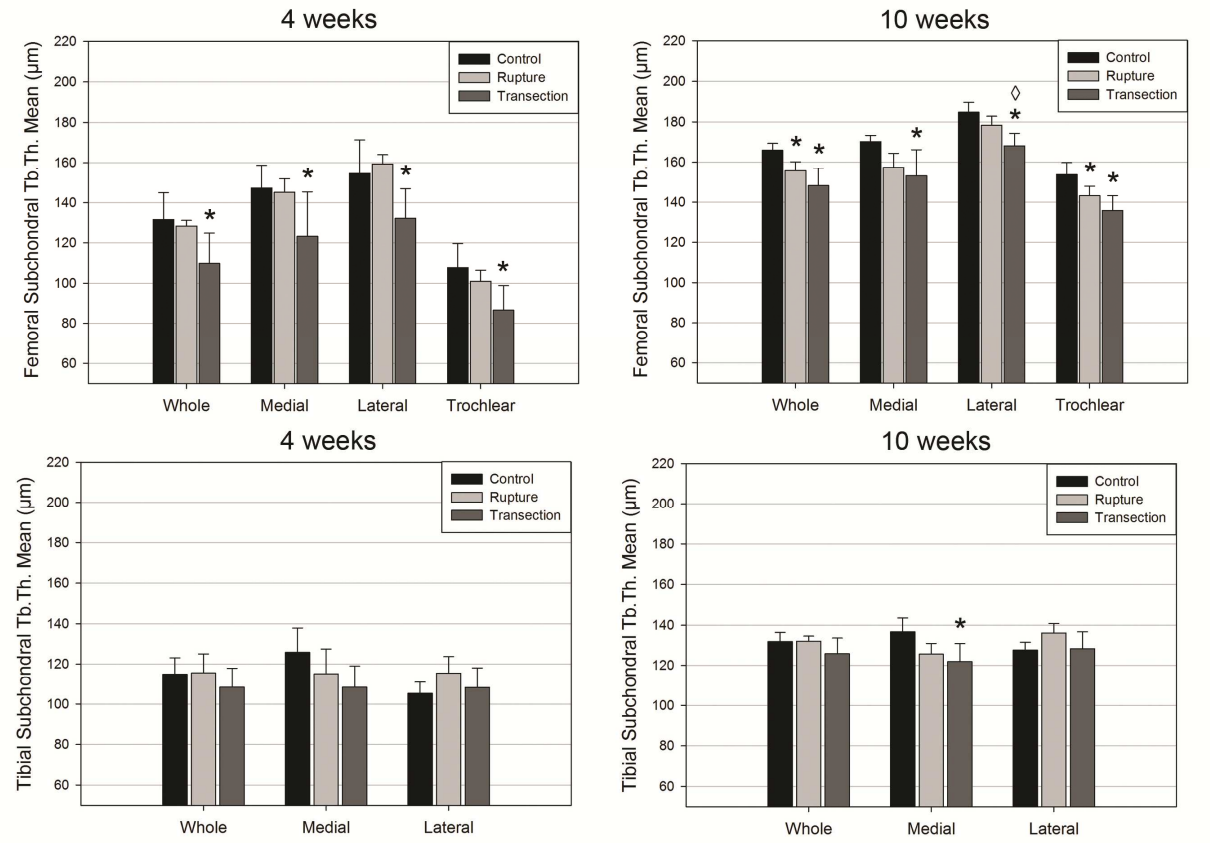

Figure 7.3.4 – *Femoral and Tibial Subchondral Trabecular Thickness (Tb.Th.) Mean at 4 weeks and 10 weeks. * denotes significant difference to Control. ◊ denotes significant difference between Rupture and Transection.*

Subchondral BV/TV correlated strongly with subchondral BMD in both the femur (r = 0.991, $P < 0.001$, Figure 7.3.5A) and tibia (r = 0.965, $P < 0.001$, Figure 7.3.5B), demonstrating the relationship between bone loss and subchondral bone mineral density. Furthermore, subchondral BV/TV correlated highly with subchondral TMD in both the femur (r = 0.804, $P < 0.001$) and the tibia (r = 0.816, $P < 0.001$) and with Tb .Th. Mean in both the femur (r = 0.969, $P < 0.001$) and the tibia (r = 0.813, $P < 0.001$), indicating a relationship between inherent bone tissue mineral density, trabecular morphology, and bone loss.

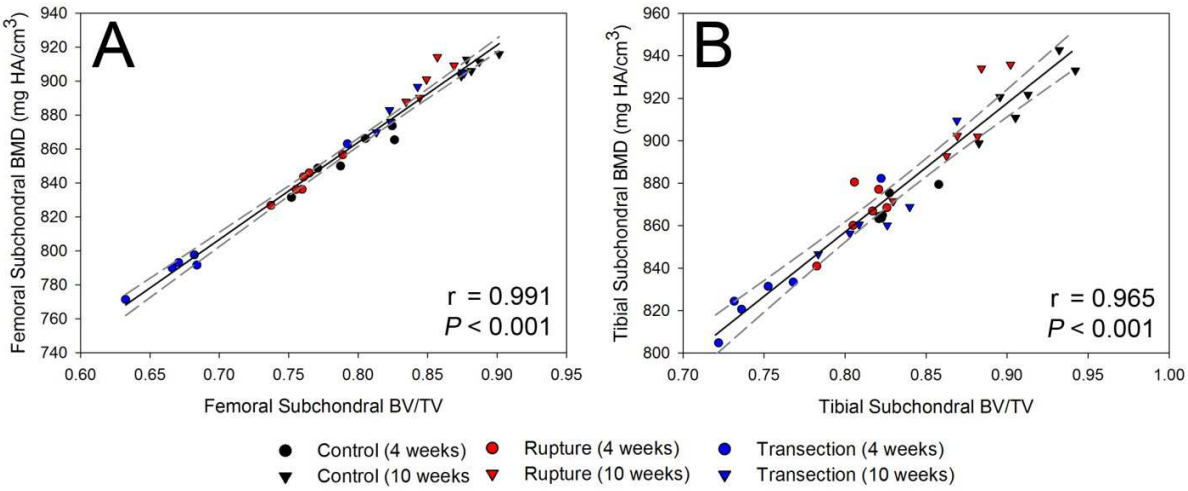

Figure 7.3.5 – *Correlation between subchondral BV/TV and subchondral BMD in the femur (A) and tibia (B). The solid line indicates the linear regression, and dashed lines indicate the 95% confidence interval of the regression.*

Epiphyseal Bone Remodeling

Bony remodeling of the femoral and tibial epiphysis was observed as a function of both age and injury. A comprehensive numerical summary of epiphyeal bone remodeling data can be found in Appendix 2, Femur: Tables A2.5, A2.6; Tibia: Tables A2.7, A2.8. Aging induced increases in epiphyseal BV/TV, BMD and TMD, and Tb.Th. mean increased in only the tibia. Compared to Control, femoral epiphyseal BV/TV was significantly lower in Rupture and Transection in the trochlear compartment and whole femur at 4 weeks and only in the trochlear compartment at 10 weeks. There were no direct differences in femoral epiphyseal BV/TV between Rupture and Transection. **(**Figure 7.3.6**)**

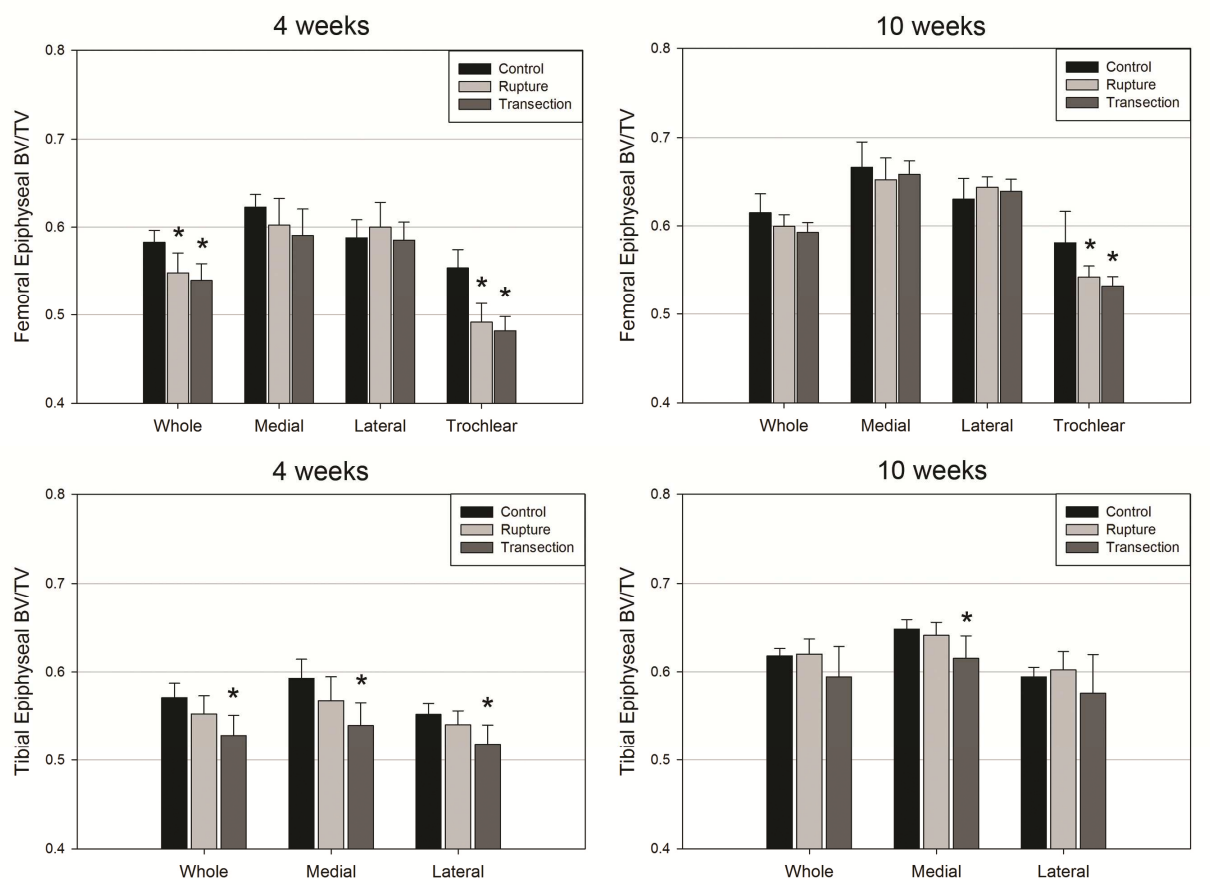

Figure 7.3.6 – *Femoral and Tibial Epiphyseal Bone Volume Fraction (BV/TV) Mean at 4 weeks and 10 weeks. * denotes significant difference to Control. ◊ denotes significant difference between Rupture and Transection.*

Femoral epiphyseal BMD was significantly lower in the trochlear compartment in both Rupture and Transection at 4 weeks. In general, compared to Control, Rupture exhibited increases in femoral epiphyseal bone mineral density whereas Transection exhibited slight decreases or no change. At 10 weeks, Rupture exhibited significant increases in femoral epiphyseal BMD in the lateral compartment and TMD in the medial compared to both Control and Transection. Rupture had significantly higher femoral epiphyseal TMD compared to Transection in all compartments at 10 weeks (Figure 7.3.7). Compared to Control, Rupture exhibited significantly higher femoral epiphyseal Tb.Th. Mean at both 4 and 10 weeks, whereas

Transection had increased Tb.Th. Mean at only 10 weeks (Figure 7.3.8). The same trend was observed for Tb.Th.Std.

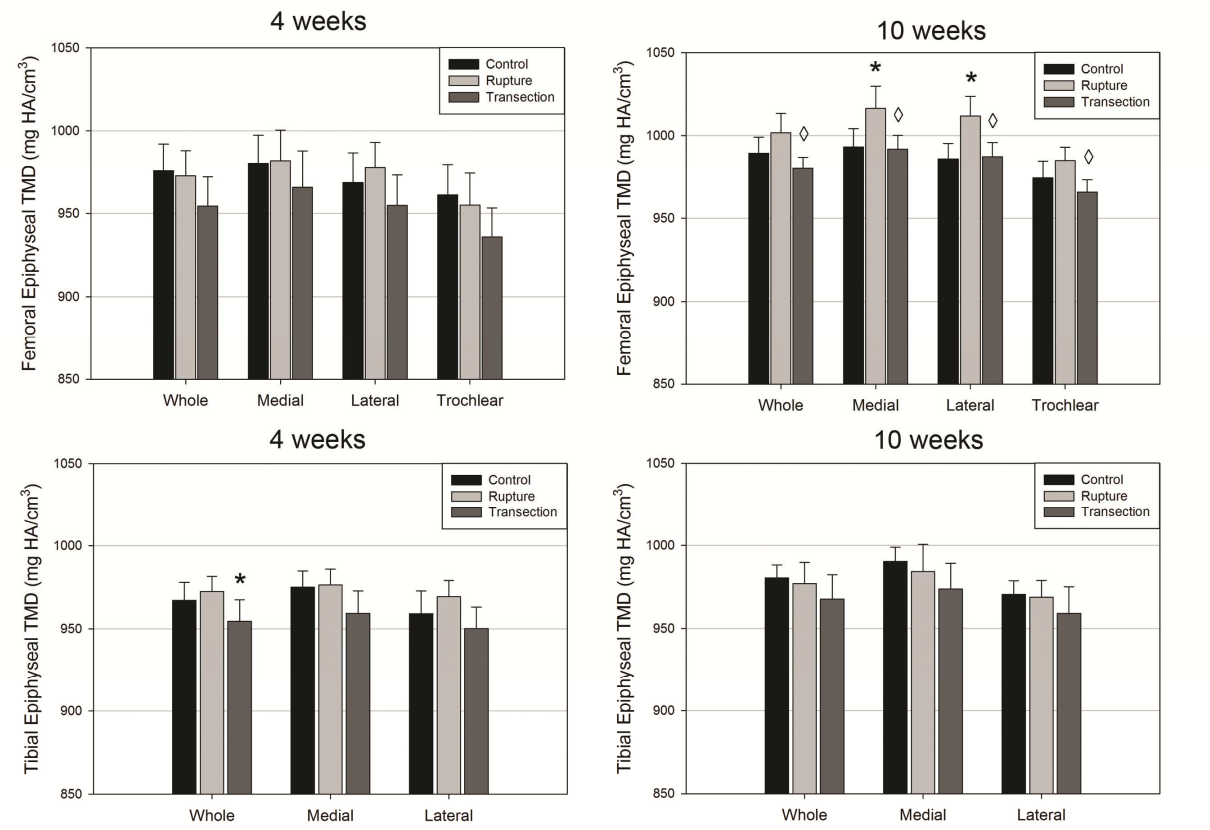

Figure 7.3.7 – *Femoral and Tibial Epiphyseal Bone Tissue Mineral Density (TMD) at 4 weeks and 10 weeks.* denotes significant difference to Control. ◊ denotes significant difference between Rupture and Transection.*

Injury-induced bony remodeling of epiphyseal bone of the tibia was less extensive than the femur (Appendix 2, Table A2.7, A2.8) . Transection induced a significant decrease in tibial epiphyseal BV/TV in all compartments at 4 weeks and only in the medial compartment at 10 weeks (Figure 7.3.6). BV/TV was not altered in the Rupture group at either time point, and there were no direct differences between Rupture and Transection. Rupture had significantly higher tibial epiphyseal BMD in the lateral compartment and whole tibia at 4 weeks compared to Transection, but no significant differences in bone mineral density were observed between the

two groups at 10 weeks. Transection exhibited significantly lower tibial epiphyseal TMD in the whole tibia compared to Control at 4 weeks, but no other changes in TMD were seen in either injury group at either time point (Figure 7.3.7) Tb.Th.Mean was significantly higher in the Rupture group compared to Control in the medial compartment at 10 weeks, but no other changes in Tb. Th. Mean were observed in either injury group (Figure 7.3.8).

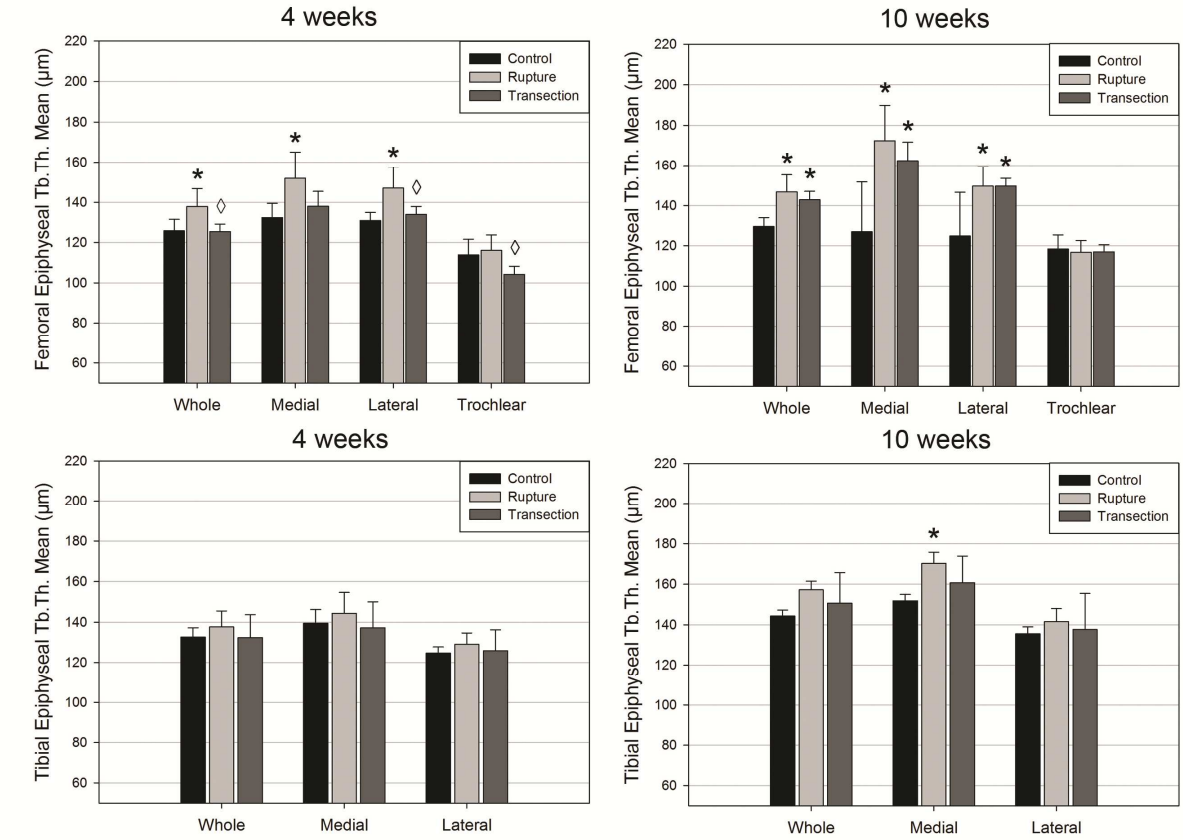

Figure 7.3.8 – *Femoral and Tibial Epiphyseal Trabecular Thickness (Tb.Th.) Mean at 4 weeks and 10 weeks. * denotes significant difference to Control. ◊ denotes significant difference between Rupture and Transection.*

Epiphyseal BV/TV correlated strongly with epiphyseal BMD in both the femur ($r = 0.850$, $P < 0.001$, Figure 7.3.9A) and the tibia **(**$r = 0.885$, $P < 0.001$, Figure 7.3.9**)**. Furthermore, there were significant correlations between epiphyseal BV/TV and epiphyseal TMD in both the

femur (r = 0.564, $P < 0.001$) and the tibia (r = 0.403, $P < 0.015$). Epiphyseal BV/TV correlated with epiphyseal Tb.Th. Mean only in the tibia (r = 0.770, $P < 0.001$).

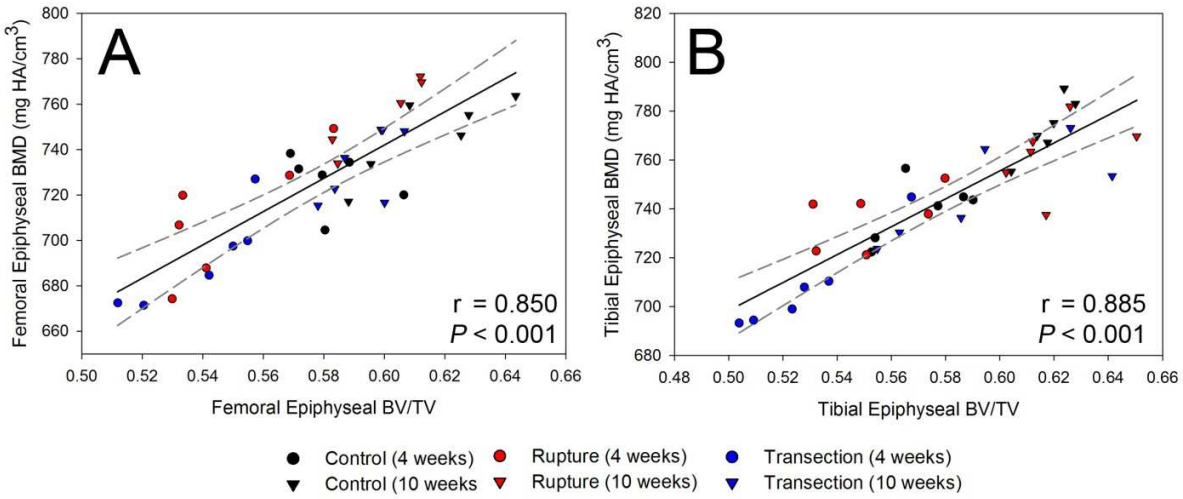

Figure 7.3.9 –*Correlation between epiphyseal BV/TV and epiphyseal BMD in the femur (A) and tibia (B). The solid line indicates the linear regression, and dashed lines indicate the 95% confidence interval of the regression.*

Articular Cartilage Morphology

Extensive changes in articular cartilage (AC) morphology were observed due to both Rupture and Transection. A comprehensive numerical summary of femoral and tibial articular cartilage thickness, peak-to-valley distance (P-V), and surface roughness between Control, Rupture, and Transection is shown in Appendix 3, Tables A3.1 – A3.4. Parameterized femoral cartilage thickness maps indicate profound compartmental and sub-compartmental changes in articular cartilage height due to injury, most notably on the medial condyle (Figure 7.3.11). Control animals exhibited smooth, congruent femoral articular cartilage with zones of slightly increased cartilage thickness at the weight-bearing regions of both condyles and the trochlear groove. A global decrease in AC thickness was observed in Control animals between 4 and 10 weeks due to aging, and this decrease was consistent throughout each compartment (Figure

7.3.10). At 4 weeks, both Rupture and Transection exhibited significant increases in whole femur AC thickness, with extensive sub-compartmental thickening in the medial zone of the medial condyle and thinning in the lateral zone of the medial condyle, evident numerically (Figure 7.3.10) and graphically on both parameterized height maps (Figure 7.3.11) and raw axial microCT slices (Figure 7.3.12). Thinning was observed to be with respect to the group's mean AC thickness rather than the Control's AC thickness, implying that although thinning was observed, these zones were still not significantly thinner than AC in Control animals. As such, cartilage thickness in the lateral zone of the medial condyle was significantly thinner than the medial zone of the medial condyle within both treatment groups. Both Rupture and Transection exhibited significant increases in AC thickness in the medial zone of the medial condyle, but only Rupture had a significant AC thickness increase in the whole medial condyle at 4 weeks**.** (Figure 7.3.10)

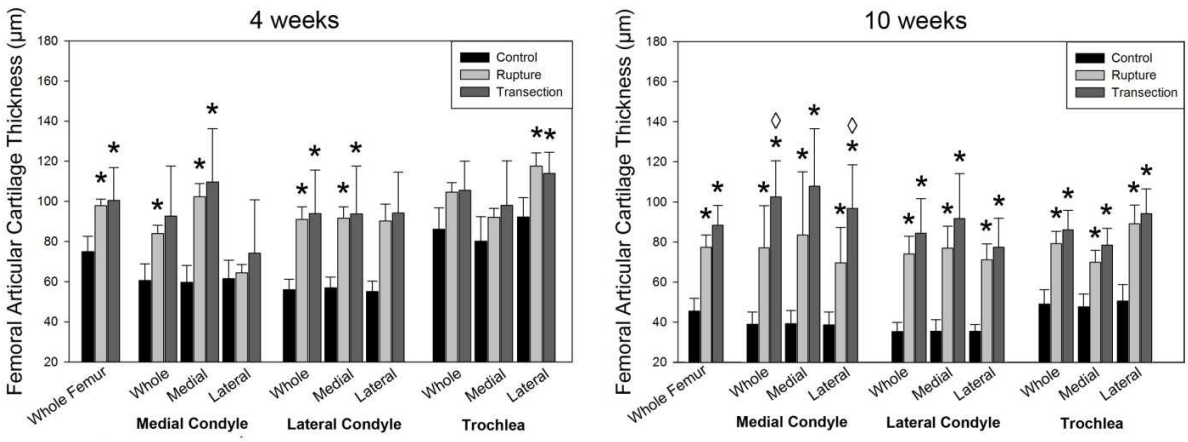

Figure 7.3.10 – *Femoral Articular Cartilage Thickness following Rupture and Transection at 4 weeks (left) and 10 weeks (right). * denotes significant difference to Control. ◊ denotes significant difference between Rupture and Transection.*

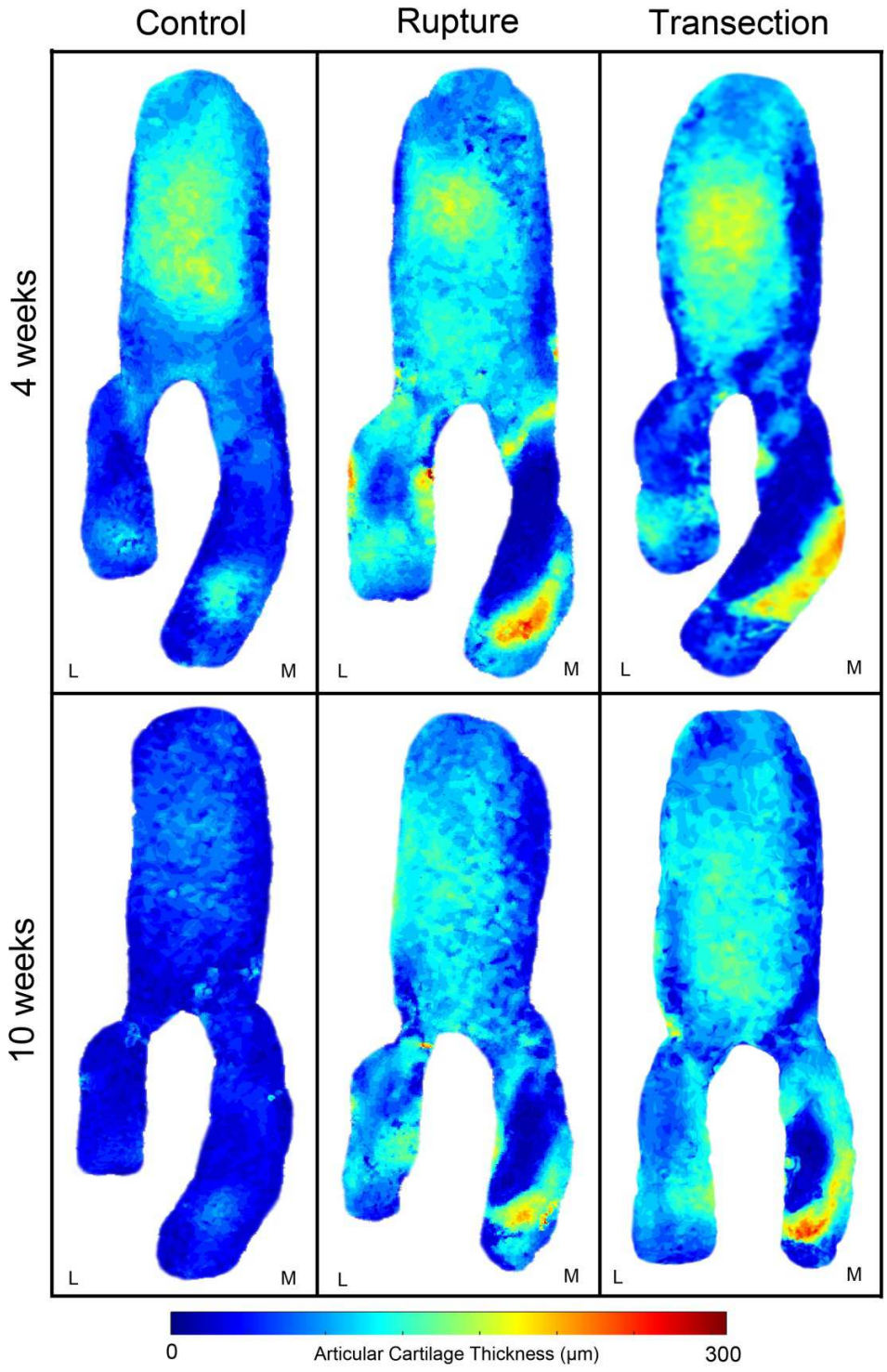

Figure 7.3.11 – *Representative Femoral Articular Cartilage Thickness Maps of Control (left column), Rupture (middle column) and Transection (right column) at 4 weeks (top row) and 10 weeks (bottom row). M = medial; L = lateral.*

At 10 weeks, AC remained globally thicker each in compartment of Rupture and Transection compared to Control. Whereas the lateral zone of the medial condyle was not significantly thicker in either group at 4 weeks, significantly thicker AC was observed at 10 weeks, and this same trend was observed in the trochlea. Differences between Transection and Rupture were observed in the medial condyle at 10 weeks: Transection exhibited significantly thicker AC compared to Rupture in the whole medial condyle and the lateral zone of the medial condyle (Figure 7.3.10). The Rupture group had a larger overall decrease in AC thickness between 4 and 10 weeks whereas the Transection group maintained AC thickening in most compartments and sub-compartments at 10 weeks (Appendix, Table A3.2). Specifically, whole-femur, lateral condylar, and trochlear AC thickness significantly decreased in the Rupture group between 4 and 10 weeks, whereas this was not observed in the Transection group.

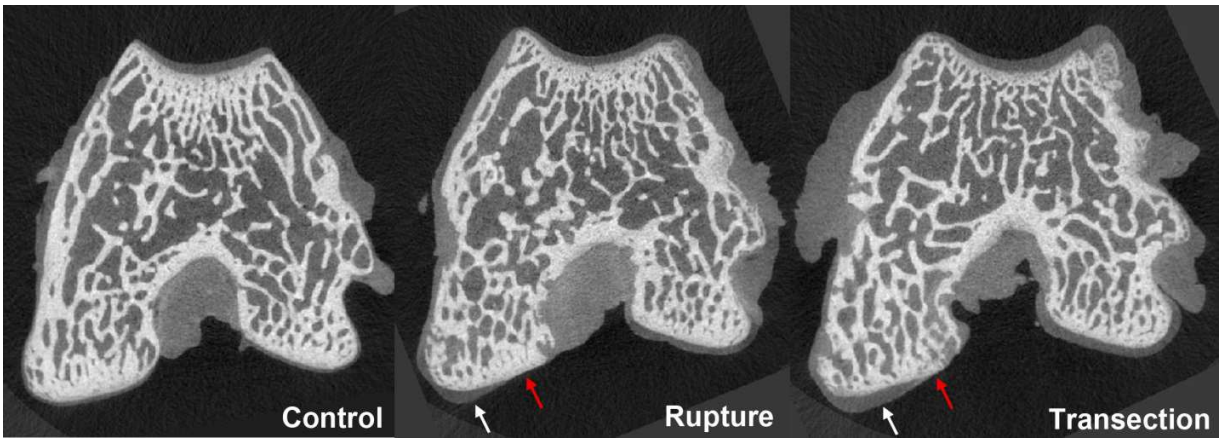

Figure 7.3.12 – *Representative axial contrast-enhanced μCT slices demonstrating sub-compartmental articular cartilage thickening (white arrows) and thinning (red arrows) on the medial femoral condyle in both Rupture (middle) and Transection (right).*

Surface roughness of AC was quantified using arithmetic surface roughness (S_a) and peak-to-valley distance (P-V). Both metrics of surface roughness were significantly increased in the whole femur, the medial condyle, and the lateral condyle at 4 and 10 weeks, but no drastic changes in surface roughness were observed in the trochlea (Appendix, Tables A3.1 and A3.2). S_a was highest in the medial condyle of both Rupture and Transection at 4 weeks, further elucidating the subcompartmental thickening and thinning observed on the medial femoral condyle. Compared to Control, S_a and P-V remained elevated at 10 weeks, with significant decreases between 4 and 10 weeks in only the lateral aspect of the lateral condyle in both the Rupture and Transection groups. Rupture exhibited significantly higher S_a in the whole trochlea compared to Control whereas Transection did not exhibit this finding. Furthermore, there was a significant increase in S_a of the medial trochlea between 4 and 10 weeks only in the Rupture group. However, no direct differences in S_a or P-V were observed between Rupture and Transection at either time point.

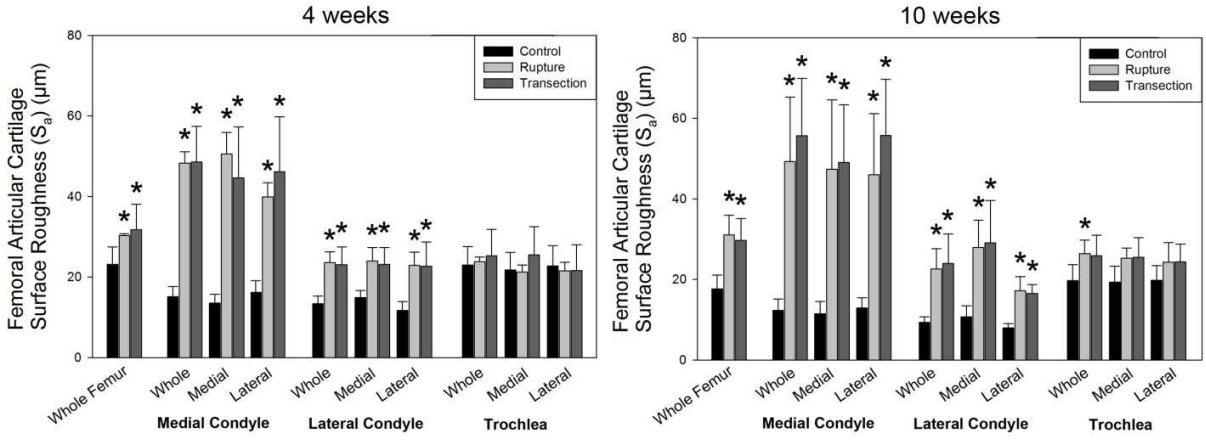

Figure 7.3.13 - *Femoral Articular Cartilage Surface Roughness (S_a) following Rupture and Transection at 4 weeks (left) and 10 weeks (right). * denotes significant difference to Control. ◊ denotes significant difference between Rupture and Transection.*

Changes in tibial articular cartilage were also observed in both injury groups at both time points. In contrast to the subcompartmental thickening and thinning observed in femoral articular cartilage of Rupture and Transection animals, tibial articular cartilage exhibited only global thickening, with the most extensive changes observed in the medial tibial compartment (Figure 7.3.14, Figure 7.3.15). At 4 weeks, both Rupture and Transection exhibited significantly higher AC thickness in the whole tibia, whole medial tibia, and whole lateral tibia (Figure 7.3.14). Compared to Control, all tibial subcompartments had increased thickness in the Transection group, whereas the Rupture group did not exhibit thicker AC in the medial zone of the medial compartment and the lateral zone of the lateral compartment. There were no direct differences in tibial AC thickness between Rupture and Transection in any compartment or subcompartment. At 10 weeks, tibial AC remained globally thicker in both groups compared to Control except for the medial zone of the medial compartment and lateral zone of the lateral compartment (Figure 7.3.14). As with femoral AC, only the Rupture group exhibited a significant decrease in whole-tibia AC thickness between 4 and 10 weeks, whereas the Transection group did not demonstrate this finding. There were no direct differences in tibial AC thickness between Rupture and Transection in any compartment or subcompartment at 10 weeks.

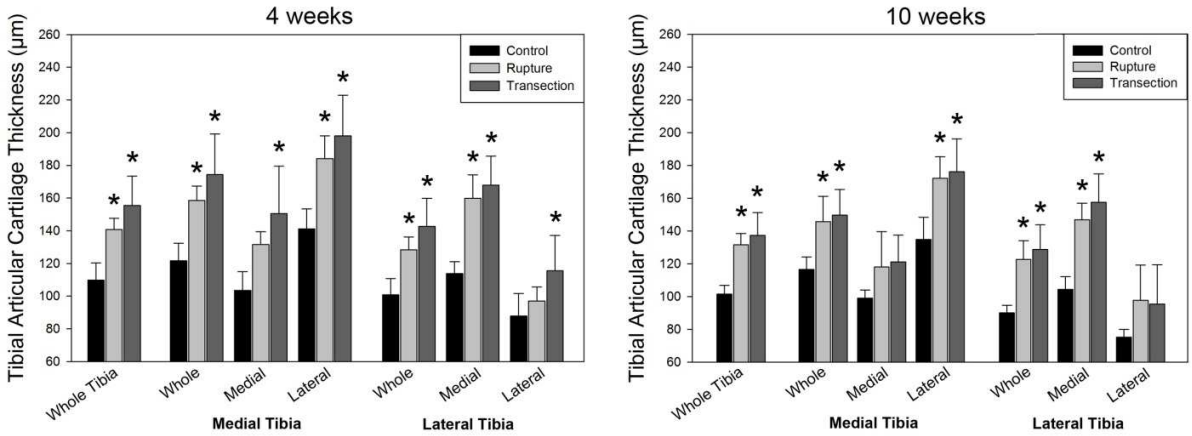

Figure 7.3.14 - *Tibial Articular Cartilage Thickness (S_a) following Rupture and Transection at 4 weeks (left) and 10 weeks (right). * denotes significant difference to Control. ◊ denotes significant difference between Rupture and Transection.*

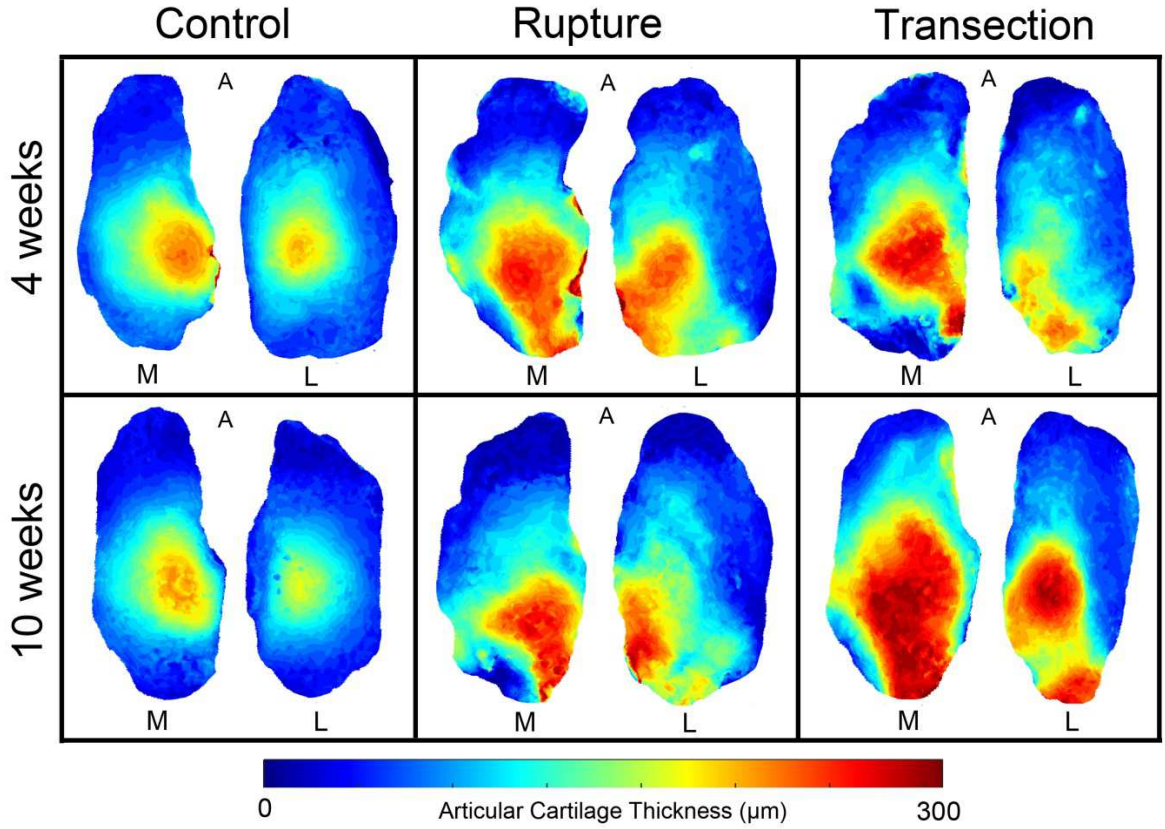

Figure 7.3.15 - *Representative Tibial Articular Cartilage Thickness Maps of Control (left column), Rupture (middle column) and Transection (right column) at 4 weeks (top row) and 10 weeks (bottom row). M = medial; L = lateral; A = anterior.*

Both P-V and S_a were significantly higher at 4 weeks compared to Control in all compartments and subcompartments of the tibia in the Transection group and in all compartments and subcompartments except for the lateral zone of the lateral tibia in the Rupture group. Transection exhibited significantly higher P-V in the lateral tibia compared to Rupture at 4 weeks, but no difference in P-V was observed between the groups at 10 weeks (Appendix, Table A3.3). Transection also exhibited significantly higher S_a in the medial and lateral zones of the medial tibia as well as the lateral zone of the lateral tibia and the whole lateral tibia (Figure 7.3.16). At 10 weeks, P-V remained significantly higher compared to Control in each subcompartment and compartment of the tibia in both Rupture and Transection, but only the whole lateral compartment in the Rupture group demonstrated a significant increase between 4 and 10 weeks. No significant increases in P-V were observed between 4 and 10 weeks in the Transection group (Appendix, Tables A3.3, A3.4). S_a remained significantly higher compared to Control in each compartment and subcompartment in the Transection group, and Rupture exhibited significantly higher S_a in all compartments and subcompartments except the lateral zones of the medial and lateral tibia. Transection had significantly higher S_a compared to Rupture in the whole tibia, the whole lateral tibia, and the medial zone of the lateral tibia. (Figure 7.3.16)

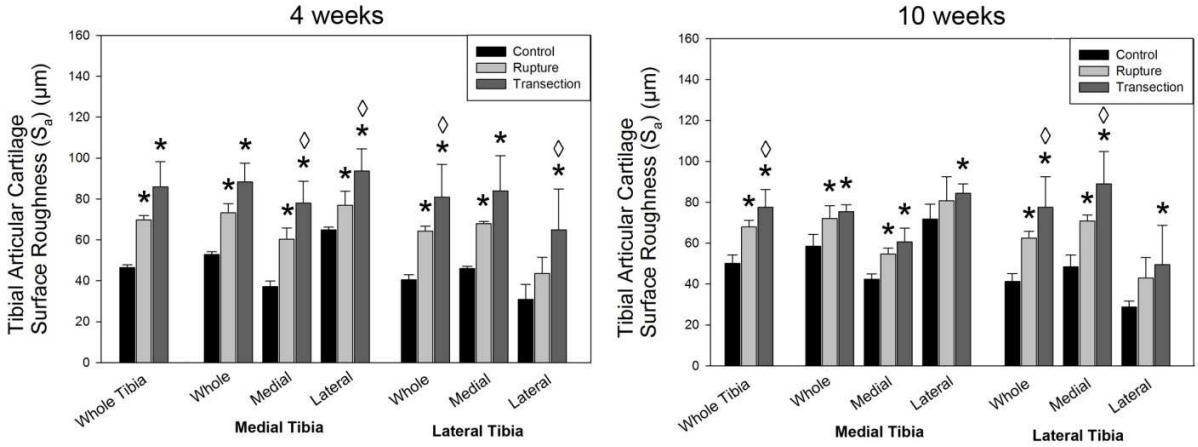

Figure 7.3.16 - *Tibial Articular Cartilage Surface Roughness (S_a) following Rupture and Transection at 4 weeks (left) and 10 weeks (right). * denotes significant difference to Control. ◊ denotes significant difference between Rupture and Transection.*

Metrics of articular cartilage morphology correlated with several epiphyseal and subchondral bone morphometric parameters. Femoral cartilage thickness correlated with epiphyseal BV/TV (r = -0.719, $P < 0.001$), epiphyseal TMD (r = -0.522, $P = 0.001$), epiphyseal BMD (r = -0.609, $P < 0.001$), subchondral BV/TV (r = -0.774, $P < 0.001$, Figure 7.3.17), subchondral TMD (r = -0.515, $P = 0.001$), subchondral BMD (r = -0.744, $P < 0.001$), and subchondral Tb.Th. Mean (r = -0.777, $P < 0.001$). Femoral cartilage P-V correlated only weakly with epiphyseal BV/TV (r = -0.334, $P = 0.046$) and epiphyseal Tb.Th. Mean (r = 0.429, $P = 0.009$). Femoral cartilage S_a correlated with epiphyseal BV/TV (r = -0.426, $P = 0.010$), epiphyseal TMD (r = -0.387, $P = 0.020$), epiphyseal BMD (r = -0.379, $P = 0.023$), epiphyseal Tb.Th. Mean (r = 0.377, $P = 0.024$) subchondral BV/TV (r = -0.522, $P = 0.001$), subchondral BMD (r = -0.466, $P = 0.004$), and subchondral Tb.Th. Mean (r = -0.485, $P = 0.003$).

Correlations between cartilage morphology and bone morphometry were also observed in the tibia. Tibial cartilage thickness correlated with epiphyseal BV/TV (r = -0.535, $P = 0.001$), epiphyseal TMD (r = -0.488, $P = 0.003$), epiphyseal BMD (r = -0.641, $P < 0.001$), subchondral BV/TV (r = -0.737, $P < 0.001$, Figure 7.3.17), subchondral TMD (r = -0.487, $P = 0.003$),

subchondral BMD (r = -0.651, $P < 0.001$), and subchondral Tb.Th. Mean (r = -0.513, $P = 0.001$). Tibial cartilage P-V correlated with epiphyseal BMD (r = -0.357, $P = 0.033$), subchondral BV/TV (r = -0.541, $P = 0.001$), subchondral TMD (r = -0.404, $P = 0.015$), and subchondral BMD (r = -0.500, $P = 0.002$). Tibial cartilage S_a correlated with epiphyseal BV/TV (r = -0.455, $P = 0.005$), epiphyseal TMD (r = -0.466, $P = 0.004$), epiphyseal BMD (r = -0.568, $P < 0.001$), subchondral BV/TV (r = -0.717, $P < 0.001$), subchondral TMD (r = -0.521, $P = 0.001$), subchondral BMD (r = -0.653, $P < 0.001$), and subchondral Tb.Th. Mean (r = -0.385, $P = 0.020$).

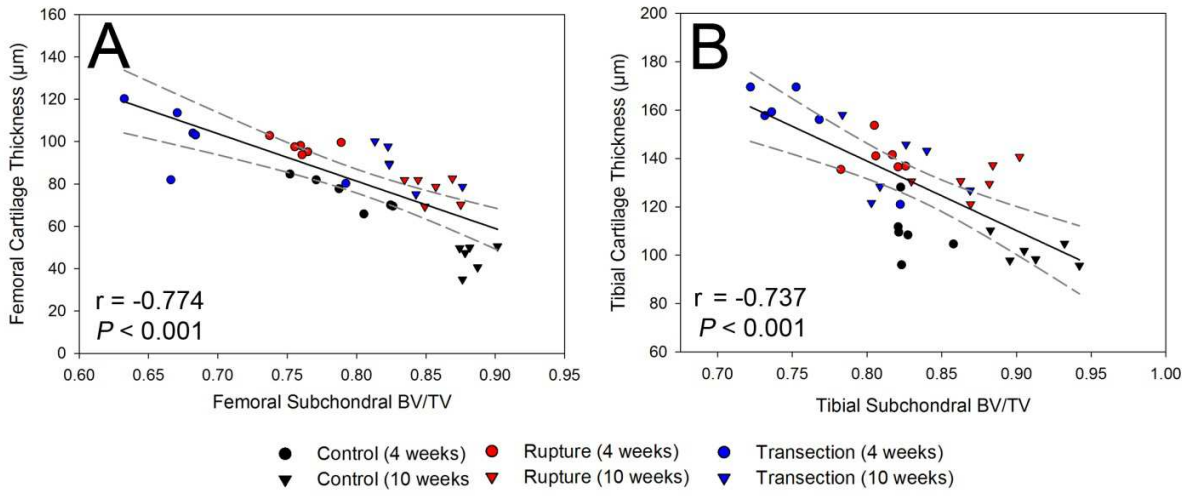

Figure 7.3.17 - *Correlation between subchondral BV/TV and articular cartilage thickness in the femur (A) and tibia (B). The solid line indicates the linear regression, and dashed lines indicate the 95% confidence interval of the regression.*

Histological Evaluation

Qualitative histologic assessment of H&E- and Saf-O-stained sections indicated extensive changes in AC structure, cellularity, and extracellular matrix (ECM) content as a function of treatment, and varying degrees of degenerative changes were observed in the compartments and subcompartments of both the femur and tibia. Healthy AC in the Control group exhibited a smooth, congruent surface with homogenous cellularity and Saf-O staining throughout the matrix. Aside from normal differences in thickness, trochlear and condylar cartilage appeared histologically identical. Chondrocytes in the Control group were observed as singlets or doublets within a chondron, and cellular size and orientation varied natively as a function of AC depth. A distinct, single, uninterrupted tidemark was observed between the deep zone and calcified zone in the Control group, and no capillaries penetrated into through the tidemark.

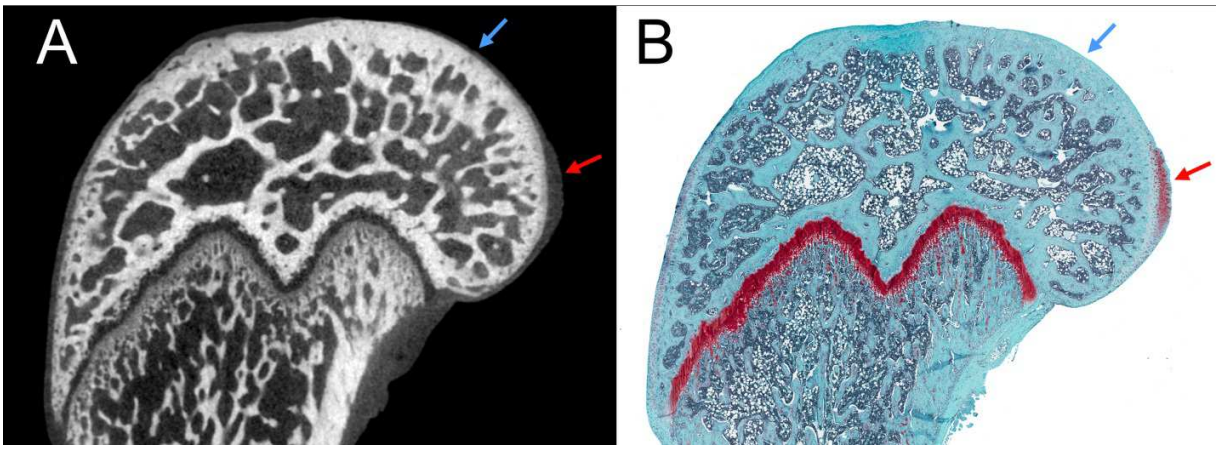

Figure 7.3.18 – *Articular cartilage morphology on µCT (A) and histology (B). Histologic evaluation confirmed µCT-based findings indicating zones of articular cartilage thickening (red arrow) immediately next to articular cartilage thinning (blue arrow) on the medial femoral condyle of both Rupture and Transection.*

Femoral AC exhibited histologic evidence of osteoarthritis-like changes in both Rupture and Transection, and these changes varied between compartments. Histologic assessment confirms µCT-based findings of AC morphology, namely subcompartmental thickening and thinning on the medial femoral condyle (MFC) (Figure 7.3.18). Magnified sections indicate that the zones of thickening are hypertrophic, hypercellular, and exhibit intense Saf-O staining (Figure 7.3.19B, D, black arrows). Chondrocytes exhibited abnormal clonality and clustering, and chondrons contained numerous chondrocytes in zones of hypercelluarity. Whereas the superficial layer of AC in healthy samples of the Control group exhibits flattened cells oriented parallel to the surface (Figure 7.3.19A, C), AC of the MFC in both Rupture and Transection exhibit nearly complete loss of the superficial layer with numerous fissures extending into the middle and deep zone (Figure 7.3.19B, D, red arrows). The zone of thinning was devoid of Saf-O staining and severely hypocellular with complete loss of the superficial, middle, and in some instances, deep zones of AC (Figure 7.3.19B, D, blue arrows). The tidemark was discontinuous and, at times, duplicated in zones of severe AC degeneration.

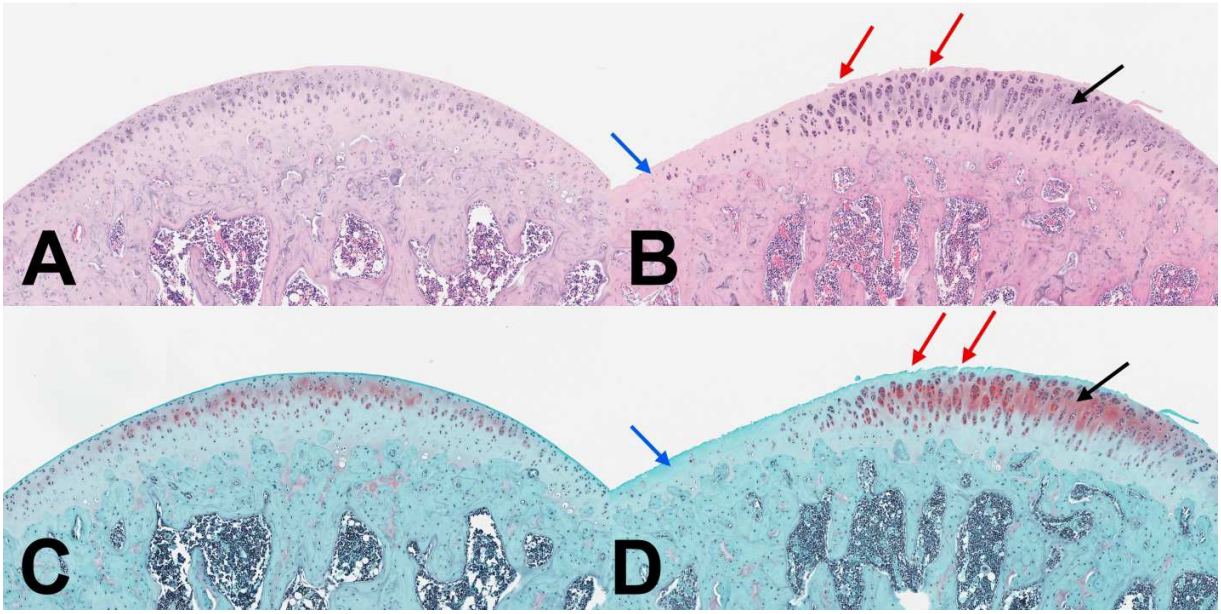

Figure 7.3.19 – *Histological Appearance of Subcompartmental Thickening and Thinning observed on the medial femoral condyle in both Rupture and Transection groups. Control cartilage (A,C) appears as a congruent tissue with even thickness, homogenous cell distribution and consistent Saf-O staining (C). Both treatment groups (B,D) exhibit a zone of severe cartilage thickening (black arrows) next to a zone of severe thinning (blue arrows). The cartilage tissue is hypocellular in the thin zone and hypercellular in the thick zone, with numerous fissures extending into the superficial zone (red arrows).*

The lateral femoral condyle and trochlea of both Rupture and Transection exhibited whole-compartment AC thickening with interspersed fissures and surface irregularities, but no zones of thinning were observed. These findings are also in accordance with µCT-based AC morphology results, demonstrating thickening in the medial and lateral subcompartments of the lateral and trochlear femoral compartment. Fissures generally extended into the superficial and middle zones, but whole-thickness lesions/fissures were rarely observed. Slight hypercellularity and cellular clustering were also observed in the lateral and trochlear compartments of both Rupture and Transection, and increased Saf-O staining was evident throughout the ECM. Numerous instances of bone marrow and vascular infiltration through the tidemark and into the deep zone of AC were noted in trochlear cartilage of both Rupture and Transection (Figure 7.3.20), consistent with decreases in BV/TV noted on µCT measurements.

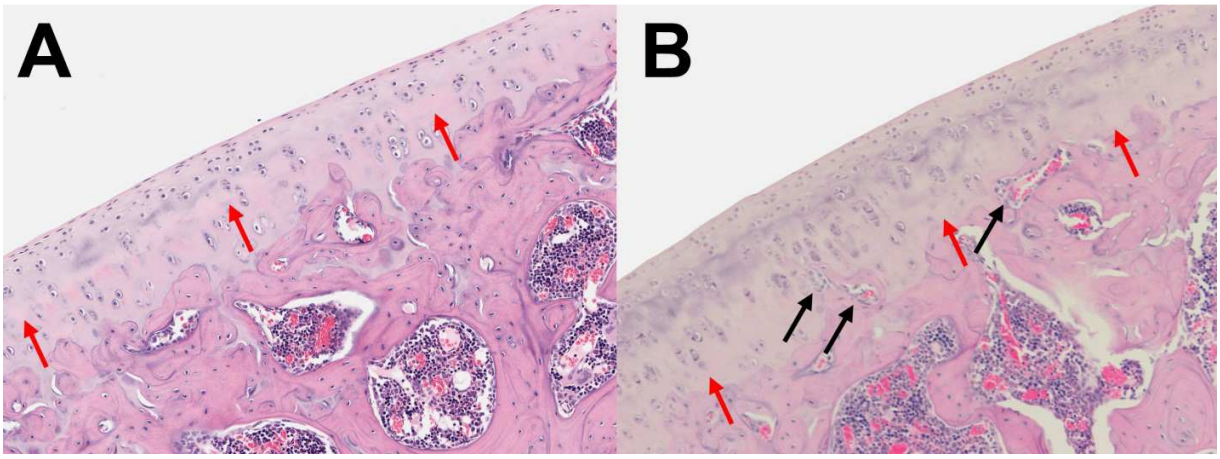

Figure 7.3.20 – *Infiltration of vasculature into the deep zone of trochlear articular cartilage. Healthy articular cartilage from Control animals exhibits a continuous tidemark (A, red arrows). Infiltration of subchondral vasculature (B, black arrows) into the deep zone of articular cartilage and a disrupted tidemark (B, red arrows) was observed in both Rupture and Transection animals.*

The OARSI Modified Mankin score was used to grade sagittal histologic sections. Inter-rater agreement between the three raters was calculated using the intraclass correlation coefficient (ICC). There was a high level of agreement in each subsection of the OARSI grade in the femur (Articular Cartilage Structure: ICC = 0.957; Proteoglycan Content: ICC = 0.881; Cellularity: ICC = 0.903; Tidemark Integrity: ICC = 0.739) as well as the averaged whole-femur grade (ICC = 0.966). A comprehensive numerical summary of histologic grading of the femur stratified by score subsection, treatment group, and time point can be found in Appendix 4, Tables A4.1 – A4.2. Both Rupture and Transection exhibited significantly higher whole femur, medial femur, and lateral femur histologic grade at both 4 and 10 weeks compared to Control (Figure 7.3.21). Each subsection of the score was significantly higher in both Rupture and Transection compared to Control, with the largest differences measured in the "Articular Cartilage Structure" subsection. The medial femur exhibited significantly higher histologic grade in both Rupture and Transection at both time points.

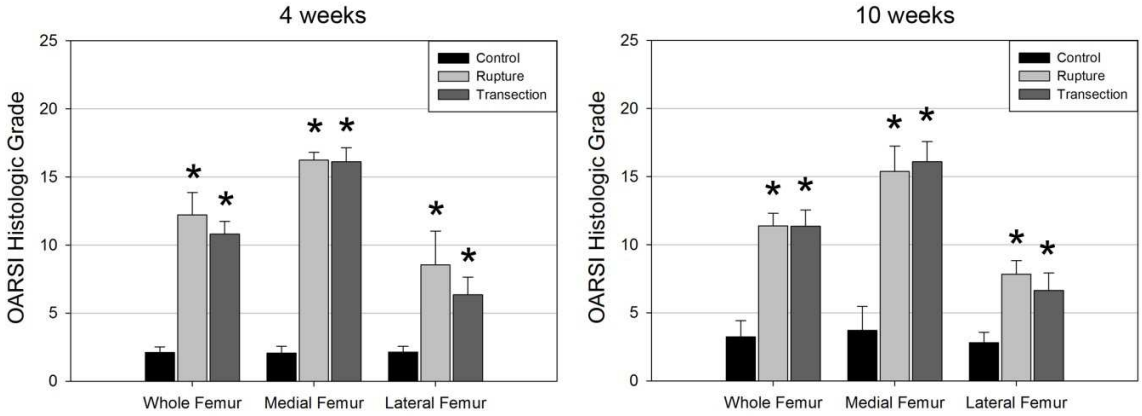

Figure 7.3.21 – *OARSI Modified Mankin Histologic Grading of the Femur in Control, Rupture, and Transection at 4 weeks (left) and 10 weeks (right).* denotes significant difference to Control.*

Rupture had a significantly higher Cellularity subsection grade compared to Transection in the whole femur and lateral femur at 4 weeks and in the lateral femur at 10 weeks (Figure 7.3.22). No other subsection grade differed significantly between Rupture and Control, and neither group exhibited significant changes in histologic grade or subsection grade between 4 and 10 weeks. Control animals exhibited a significant increase in Proteoglycan Content subsection grade in the medial femur between 4 and 10 weeks, but no other subsection grade varied between the two time points (Appendix 4, Tables A4.1 – A4.2).

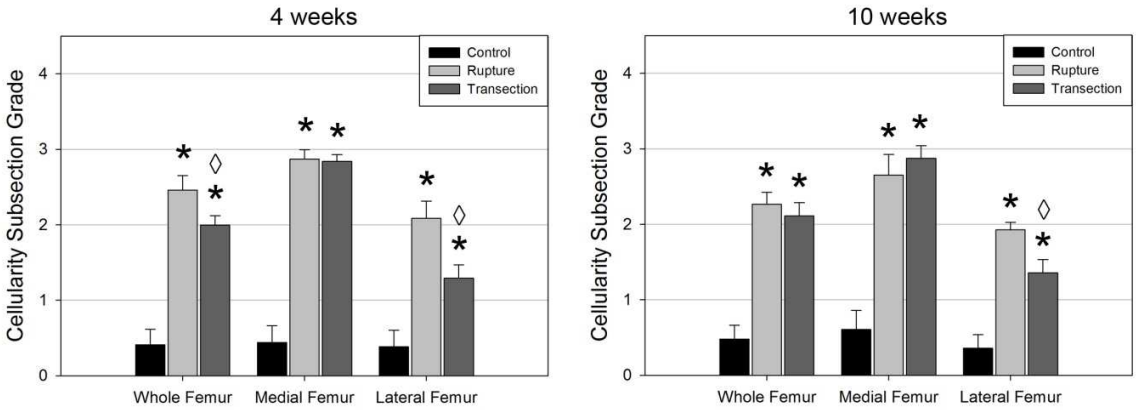

Figure 7.3.22 – *Histologic Cellularity Subsection Grade the Femur in Control, Rupture, and Transection at 4 weeks (left) and 10 weeks (right). Cellularity grade: 0 = normal cellularity; 1 = diffuse/slight hypercellularity; 2 = hypercellularity and clustering; 3 = Diffuse hypocellularity. * denotes significant difference to Control. ◊ denotes significant difference between Rupture and Transection.*

Degenerative changes were also noted on tibial cartilage of both Rupture and Transection. Though the overall extent of degeneration was milder on tibial cartilage compared to femoral cartilage, extensive evidence of structural, compositional, and cellular degeneration was evident in both the medial and lateral tibial compartments at 4 and 10 weeks. Structural damage was largely contained to the superficial zone, and no subcompartmental pattern of thickening and thinning was observed. Superficial structural degeneration coincided with hypocellularity and loss of Saf-O staining, and the middle and deep zones exhibited hypercellularity and cell clustering (Figure 7.3.23). The posterior aspect of tibial cartilage exhibited more extensive structural damage and erosion, likely due to anterior subluxation of the tibia with respect to the femur due to loss of anterior stability in both Rupture and Transection. Loss of Saf-O staining was largely localized to the superficial and middle zones, and the deep zone exhibit little to no loss of staining intensity.

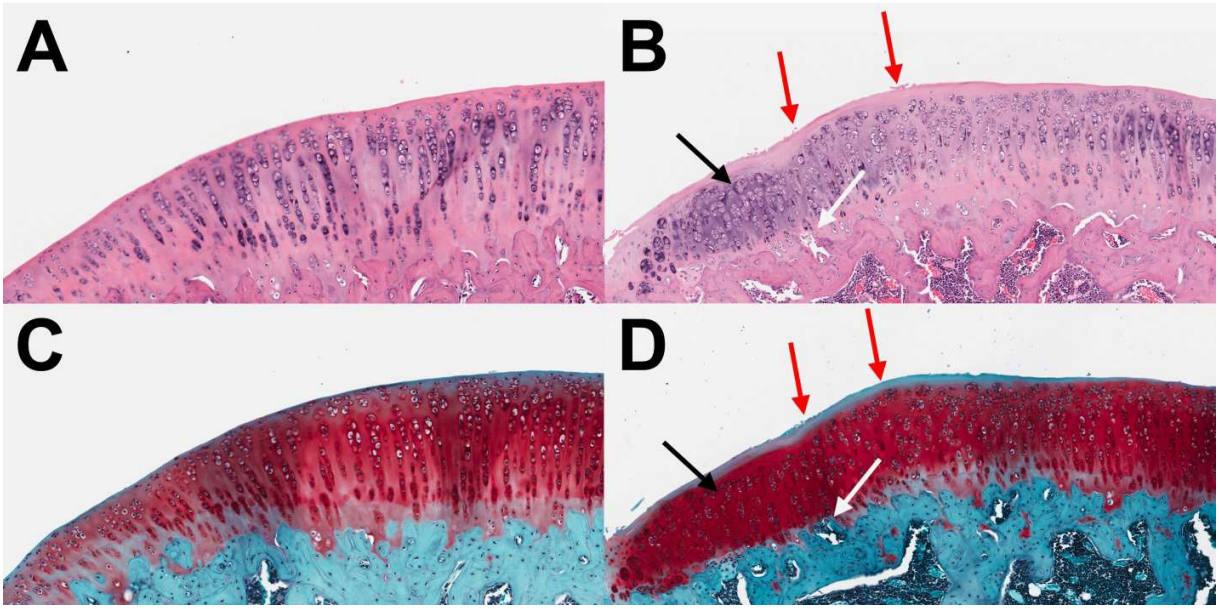

Figure 7.3.23 – *Histological appearance of superficial structural degeneration and hypocellularity on the posterior tibia in both Rupture and Transection. Control tibial cartilage (A, C) exhibits a smooth surface with homogenous cellularity and Saf-O staining intensity. Structural erosion of the superficial zone of cartilage was noted in both treatment groups (B, D). A thickened, hypocellular superficial zone with no Saf-O staining (red arrows), hypercellularity in the middle and deep zones (black arrow), and tidemark disruption with vascular infiltration (white arrow) were observed.*

Tibial histology was also graded using the OARSI Modified Mankin scale. There was a high level of agreement between the three raters in each subsection of the OARSI score (Articular Cartilage Structure: ICC = 0.847; Proteoglycan Content: ICC = 0.765; Cellularity: ICC = 0.935; Tidemark Integrity: ICC = 0.765) and in the averaged whole-tibia grade (ICC = 0.892). A comprehensive numerical summary of histologic grading of the tibia stratified by score subsection, treatment group, and time point can be found in Appendix 4, Tables A4.3 – A4.4. Both Rupture and Transection exhibited significantly higher whole tibia, medial tibia, and lateral tibia histologic grade at both 4 and 10 weeks compared to Control (Figure 7.3.24). Transection exhibited slightly lower whole tibia histologic grade compared to Rupture at 4 weeks, but this finding was not found to be statistically significant (P = 0.105). At 10 weeks, Transection

exhibited slightly higher histologic grade than Rupture, but this comparison was also not significant. There was no difference in histologic grade between the medial and lateral tibia in any of the groups. While the Control and Rupture group exhibited no differences in whole tibia, medial tibia, or lateral tibia histologic grade between the 4 and 10 week time points, there was a significant increase in whole tibia and lateral tibia histologic grade between the two time points in the Transection group. Furthermore, the Transection group had significant increases in the whole tibia Articular Cartilage and Proteoglycan Content subsection scores between the two time points (Appendix 4, Table A4.4).

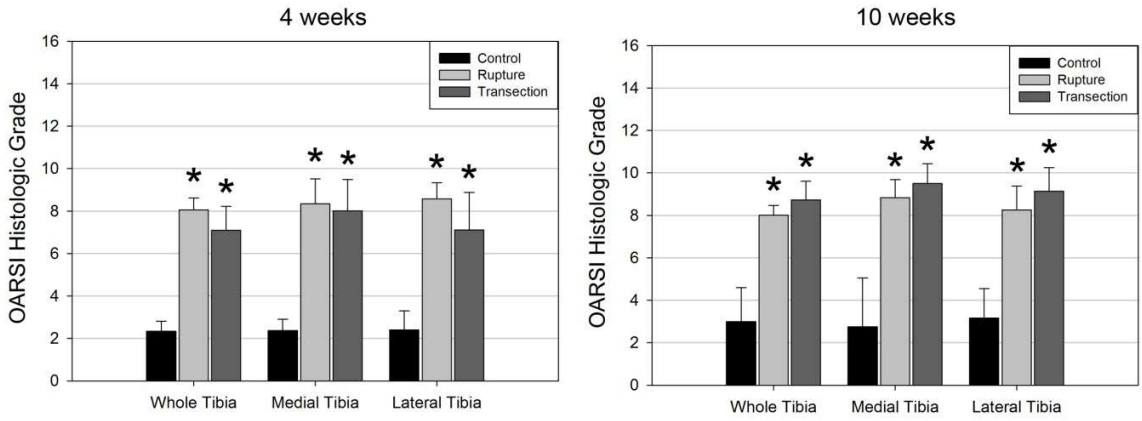

Figure 7.3.24 – *OARSI Modified Mankin Histologic Grading of the Tibia in Control, Rupture, and Transection at 4 weeks (left) and 10 weeks (right).* * denotes significant difference to Control.*

Serum-Level Biomarkers of Cartilage Metabolism and Breakdown

The concentrations of six articular cartilage biomarkers were measured in the serum of Control, Rupture, and Transection animals at both 4 and 10 weeks using commercially-available ELISA kits. Assay results of the six biomarkers are summarized in Figure 7.3.25. Compared to Rupture, Transection had significantly higher C2C concentration at both 4 and 10 weeks (Figure 7.3.25A), significantly higher COMP concentration at 4 weeks (Figure 7.3.25C), and significantly higher

CTxII concentration at 4 weeks (Figure 7.3.25F)**.** Furthermore, Transection had significantly higher COMP and CTxII concentration at 4 weeks compared to Control. There was no difference in the concentration of any analyte between Control and Rupture at either time point.

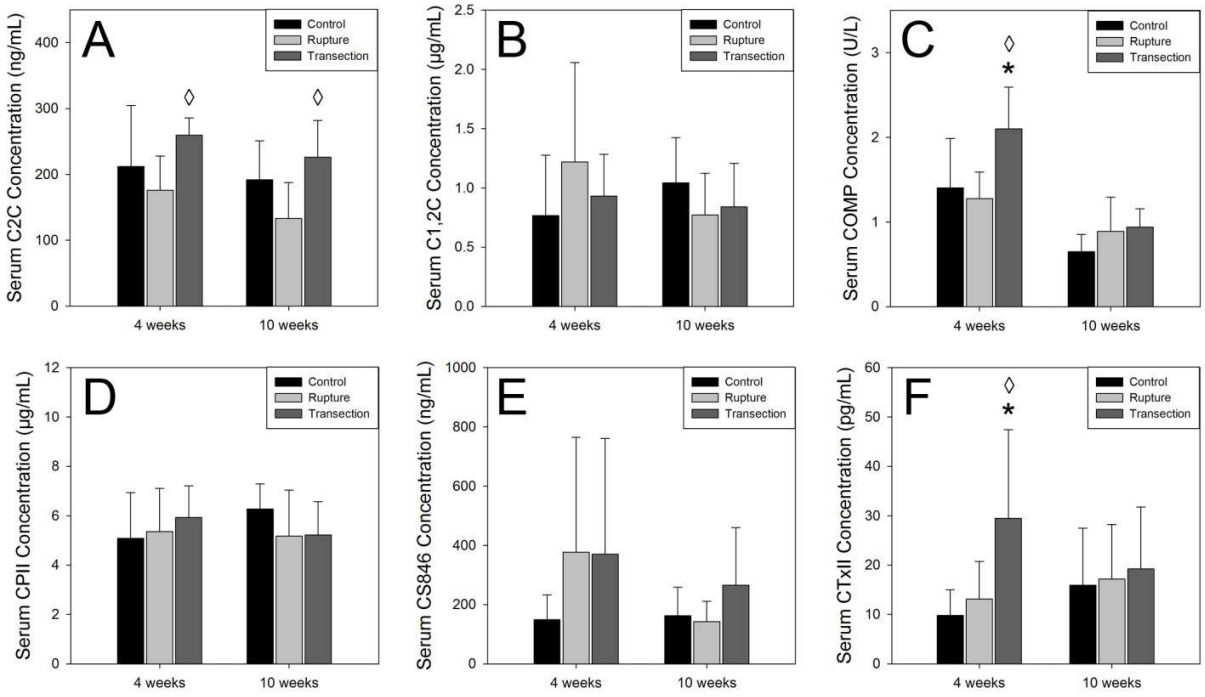

Figure 7.3.25 – *Quantification of C2C (A), C1,2C (B), COMP (C), CPII (D), CS846 (E), and CTxII (F) in serum of Control, Rupture, and Transection at 4 and 10 weeks. * denotes significant difference to Control. ◊ denotes significant difference between Rupture and Transection.*

Collagen cleavage-to-synthesis ratios were calculated using the four markers of Type I and/or Type II collagen cleavage C2C, C1,2C, CTxII, and COMP and the marker of collagen synthesis, CPII (Figure 7.3.26). Transection had a significantly higher C2C/CPII ratio compared to Rupture at 4 weeks and compared to both Control and Rupture at 10 weeks. There were no differences in C1,2C/CPII ratios between any of the groups at either time points. Transection had a significantly higher CTxII/CPII ratio compared to Control at 4 weeks, but there was no difference in CTxII/CPII ratio compared to Rupture at either time point. Lastly, Transection had

a significantly higher COMP/CPII ratio compared to Rupture at 4 weeks, and both treatment groups had a significantly higher COMP/CPII ratio compared to Control at 10 weeks.

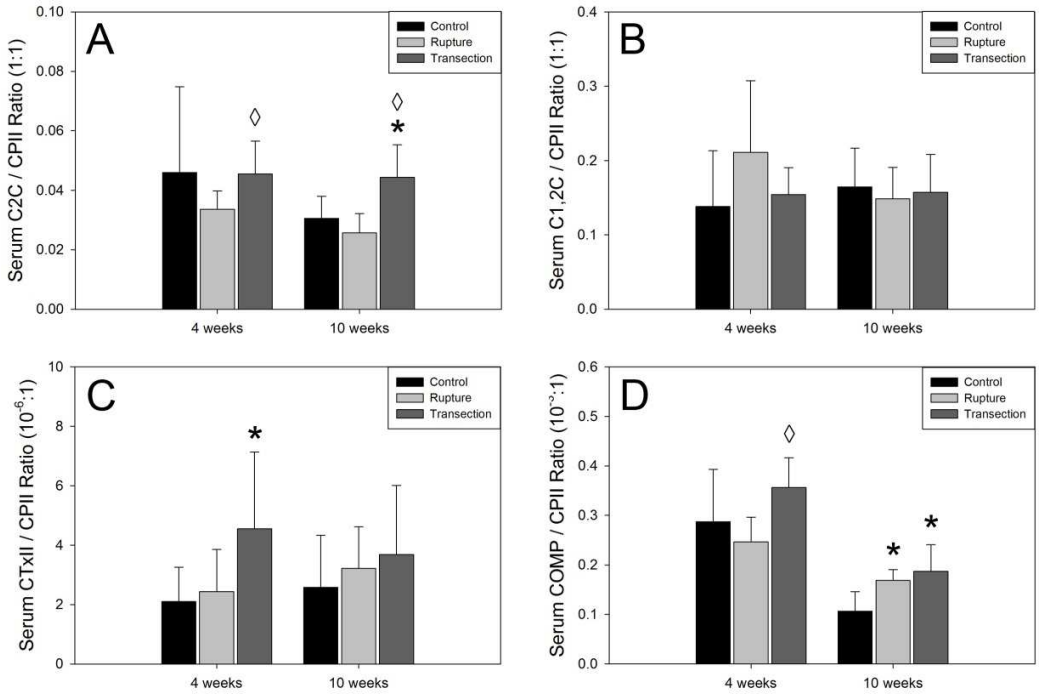

Figure 7.3.26 – *Collagen Cleavage-to-Synthesis Ratios of Serum-level biomarkers. Collagen cleavage-to-synthesis ratios were calculated using a marker of collagen synthesis, CPII, and four biomarkers of collagen cleavage C2C (A), C1,2C (B), CTxII (C), and COMP (D). * denotes significant difference to Control. ◊ denotes significant difference between Rupture and Transection.*

COMP Concentration in Synovial Lavage Fluid

Synovial lavage fluid was assayed for COMP concentration using a commercially-available ELISA kit. Although the assay was not expired and the manufacturer's protocol was followed precisely, the assay did not return usable results. No color development was noted in any assay well, and the standard curve samples all indicated optical density values below baseline. We conclude that one or more assay reagent(s) were impure, falsely packaged, or expired without indication, and given that all synovial fluid lavage samples were used up, no second quantification was able to be done.

7.4 – Discussion

Animal models are used to simulate a disease process in order to gain an understanding of its etiology and to screen potential therapeutic strategies. In the setting of PTOA, numerous animal models have been developed, and the most common ACL injury model is surgical ACL transection. While several studies have demonstrated that ACL transection induces degenerative changes, the extent to which this model mimics the biologic phenomena of human ACL rupture is unknown. The surgical nature of the ACL transection model may introduce several biological and biomechanical confounding factors, and models employing noninvasive injury could provide a more accurate representation of human injury. The purpose of this study was to characterize the onset and progression of PTOA in a new model of noninvasive ACL rupture in the rat, as characterized in Section 6 - Aim #1, and to compare the findings to the surgical ACL transection model. We hypothesized that the noninvasive rupture model would induce more extensive degenerative changes in articular cartilage and that a differential bony remodeling response would be observed. Our hypothesis regarding articular cartilage degeneration was proven false as both the Rupture and Transection groups exhibited extensive degeneration at both time points, and the Transection group exhibited more profound degeneration in femoral and tibial articular cartilage. Our hypothesis regarding differential bony remodeling was confirmed, and several differences in bone mineral density and morphometry were observed between the two groups.

A change in AC morphology is a hallmark sign of PTOA. While chronic OA is generally associated with global AC thinning (Lohmander et al., 2007), the acute and intermediate phases of PTOA have been shown to be associated with both AC thinning and thickening. In a clinical study of patients 2 years after ACL rupture and reconstruction, Su *et al* demonstrated AC thickening on the medial femoral condyle of patients with ACL injury and reconstruction

compared to healthy controls,(Su et al., 2013) a finding very similar to AC morphology results in the present study. However, Su *et al* also found AC thinning of the lateral tibia, an opposite finding to our results indicating AC thickening of the lateral tibia. In another clinical study, Buck *et al* used MRI to image 75 women with signs of mild to moderate OA and compared articular thickness of femoral and tibial compartments and subcompartments to 77 asymptomatic, healthy controls.(Buck et al., 2010) The study found that medial femoral thickening was as frequently detected as thinning in patient with moderate OA. The most extensive thickening was observed on the medial aspect of the medial femoral condyle, the same location where thickening was observed in our study. In a recent paper, Eckstein *et al* performed longitudinal quantification of AC thickness in the weight-bearing region of the tibiofemoral compartments following ACL rupture and reconstruction.(Eckstein et al., 2015) The study demonstrated thickening of the medial femoral condyle and medial tibial between baseline and 2-year follow-up and between 2-year and 5-year follow-up. The lateral tibia exhibited thinning between baseline and 2 years followed by thickening between 2 and 5 years. The overall cartilage thickness increase was 31 µm/year over the entire 5-year study duration, and more drastic overall, compartment-dependent changes were observed in the baseline-to-2 year interval.

Our results demonstrate that both noninvasive ACL rupture and surgical ACL transection cause subcompartmental cartilage thickening and thinning. We observed drastic thickening of the medial aspect of the medial femoral condyle in both treatment groups compared to Control animals, and a region of cartilage thinning on the lateral aspect of the medial femoral condyle was observed immediately next to the zone of thickening. The region of thinning was not significantly thinner than cartilage in Control animals, but since an overall, whole-joint increase in cartilage thickness was observed in treatment animals, the region of thinning was significantly

thinner than both groups' mean. Histologic analysis confirmed that this zone was in immediate proximity to the region of thickening and exhibited extensive loss of structure, cellularity, and proteoglycan content. AC surface roughness was globally elevated but highest in the medial femoral condyle in both groups, reiterating that cartilage degeneration is most profound in the medial compartment. This finding was subsequently supported by histologic analysis demonstrating higher histologic grades in the medial femoral compartment. Our data indicates several differences in AC morphology between the Rupture and Transection models. At 4 weeks, only the Rupture group exhibited a significant increase in whole femoral medial condyle AC thickness. Since both groups had significant increases in AC thickness in the medial zone of the medial condyle, this finding likely indicates that the Transection group had more profound thinning on the medial femoral condyle, thereby lowering the whole-condyle average. At 10 weeks, the Transection group had significantly thicker AC in the whole medial femoral condyle and the lateral zone of the medial femoral condyle compared to Rupture. While AC surface roughness was globally increased in the medial and lateral condyles of the femur, only the Rupture group exhibited significantly highly surface roughness in the trochlea at 10 weeks. Differences in AC morphology between the two groups were also observed on the tibia. Only the Transection group exhibited a significant increase in AC thickness of the medial zone of the medial tibia and the lateral zone of the lateral tibia at 4 weeks, and the Transection group exhibited significantly higher AC surface roughness on the medial and lateral tibia at 4 weeks in addition to the whole tibia and lateral tibia at 10 weeks. This data indicates that surgical ACL transection induces more profound degenerative response on the tibia compared to noninvasive ACL rupture.

Bony remodeling is a major part of the OA cascade.(Burr and Gallant, 2012; Karsdal et al., 2008) In the setting of PTOA, acute and chronic changes in joint kinematics alter the loading patterns of subchondral and epiphyseal bone, and the release of pro-inflammatory cytokines trigger cascades of bone resorption, causing remodeling to occur as a compensatory mechanism due to both mechanical loading and biologic signaling. The formation of osteophytes, sclerosis of subchondral bone, bone loss, change in bone mineral density, trabecular thinning and loss of trabecular elasticity are all known clinical symptoms of bony remodeling during OA(Karsdal et al., 2008), and these symptoms have been demonstrated thoroughly by several animal models of PTOA.(Boyd et al., 2000; Christiansen et al., 2012b; Florea et al., 2014; Hayami et al., 2006; Intema et al., 2010) In a model of noninvasive ACL injury using tibial compression in the mouse, Christiansen *et al* demonstrated that injured animals exhibit a drastic loss of femoral and tibial epiphyseal bone volume and apparent mineral density acutely.(Christiansen et al., 2012b) Both bone volume and density partially recovered but remained lower than uninjured controls at 8 weeks. A similar pattern was observed in femoral and tibial trabecular thickness, and the study demonstrates a drastic increase in heterotopic bone formation around the knee joint. Our study results also indicate bone loss following injury, and this was more pronounced in the Transection group than the Rupture group. Extensive differences in subchondral bone remodeling were observed between the Rupture and Transection group at 4 weeks, with the Transection group exhibiting significantly lower femoral and tibial subchondral BV/TV whereas the Rupture group showed no significant loss of either femoral or tibial subchondral BV/TV at 4 weeks. These differences largely disappeared in the femur at 10 weeks but remained in the tibia. Changes in epiphyseal BV/TV were less extensive, with both treatment groups exhibiting a whole-femur decrease at 4 weeks but not at 10 weeks. Only the Transection group had significant decreases in

tibial epiphyseal BV/TV whereas the Rupture group showed no change in tibial epiphyseal BV/TV at all. While the exact mechanism of bone loss following ACL injury is not yet known, the role of the injury-induced release of inflammatory factors in perpetuating bone resorption has been partially described. Pro-inflammatory cytokines such as interleukin (IL)-1β, tumor necrosis factor (TNF)-α, and IL-6 known to be released in the joint following ACL injury(Tang et al., 2009b; Tang et al., 2009c; Xue et al., 2009) perpetuate bone resorption directly or indirectly by promoting osteoclastogenesis.(Schett, 2011; Walsh et al., 2005; Wei et al., 2005) The surgical nature of the ACL transection model may cause a greater degree of pro-inflammatory cytokine expression in the knee joint compared to a noninvasive injury model due to the introduction of foreign bodies such as surgical tools and sutures, consequently causing increased bone loss, but future research is necessary to determine this.

Our data also indicates extensive differences in bone mineral density and trabecular morphology between the Rupture and Transection models. Whereas the Transection model exhibited a general decrease in both femoral BMD and femoral TMD, the Rupture model exhibited either no change or increases in BMD and TMD, and these differences were most pronounced at 10 weeks. Significant differences in BMD and TMD were noted between the Rupture and Transection groups in both epiphyseal and subchondral bone, and these findings indicate a differential bone remodeling response between the two models. We also found a difference in trabecular morphology between the two injury models in our study. Transection exhibited a decrease in femoral subchondral trabecular thickness at both 4 and 10 weeks whereas Rupture had no decrease at 4 weeks and slighter decreases at 10 weeks. In the femoral epiphysis, Rupture exhibited a drastic increase in trabecular thickness at both 4 and 10 weeks, whereas Transection did not exhibit an increase until 10 weeks. Significant differences were noted

between the two groups at 4 weeks, but these differences disappeared at 10 weeks. Interestingly, in their model of noninvasive ACL injury using the tibial compression model, Christiansen *et al* demonstrate an acute and chronic loss of femoral epiphyseal BMD and trabecular thickness in injured animals.(Christiansen et al., 2012b) This study represents the closest comparison to the noninvasive rupture model employed in the present study, and the causes leading to these differences in results between their study and the present study remain unknown.

Histologic evidence of OA was observed in both injury models. We found that extensive degenerative changes to femoral articular cartilage structure and proteoglycan content were equivalent between the two groups and that these changes are present at 4 weeks with minimal change between the 4 and 10 week time point. The Rupture group exhibited a higher Cellularity subsection histologic grade in the femur at both 4 and 10 weeks compared to Transection. As a higher cellularity grade indicates diffuse regions of hypocellularity within otherwise hypercellular AC, this data indicates that Rupture induces a greater loss of cellularity. End-stage OA can be characterized by extensive hypocellularity(Anderson et al., 2011), and this data may suggest that the Rupture model induces an earlier onset of the progressive loss of cellularity. Future studies involving immunohistochemical analysis of cell necrosis and/or apoptosis could clarify this differential cellular response. Tibial histology also indicated signs of OA-like degeneration with erosion of the superficial layer of AC, loss of superficial proteoglycan, whole-AC hypercellularity, and cellular clustering. Overall degeneration of tibial cartilage was, however, much milder than that observed on the femur, and our data does not indicate a differential degenerative state between the medial and lateral tibial compartment in either Rupture or Transection.

Biomarkers of cartilage degeneration have been used extensively to study the onset and progression of OA.(Catterall et al., 2010; Pruksakorn et al., 2009; Svoboda et al., 2013; Tourville et al., 2013) A biomarker can be any biochemical moiety indicating a disease state, and in the setting of OA, biomarkers of cartilage turnover and cleavage are most commonly employed due to the relative ease of detecting them in serum, synovial fluid, and urine. We quantified the concentrations of six cartilage biomarkers in the serum of injured and control rats, and our results indicate that Transection had higher absolute concentrations of C2C, COMP, and CTxII compared to Rupture. C2C and CTxII are byproducts of type II collagen cleavage, and COMP is a non-collagenous ECM protein expressed in increased amounts during OA-related cartilage turnover. We did not detect significant group-to-group differences in the absolute concentration of CPII, a marker of type II collagen synthesis, C1,2C, a byproduct of type I and type II collagen cleavage, or CS846, an epitope of chondroitin sulfate released during proteoglycan cleavage. The Rupture group did not have any elevated levels of biomarkers, and we partially attribute this finding to extensive animal-to-animal variability in our data. Due to the use of a cardiac puncture blood draw, we were unable to obtain baseline, pre-injury concentrations of the assayed biomarkers, thereby eliminating the possibility of an internal normalization. Furthermore, we did not normalize the absolute biomarker concentration to total serum protein, which represents a limitation of our study. However, we also compared the collagen cleavage-to-synthesis ratios C2C/CPII, C1,2C/CPII, CTxII/CPII, and COMP/CPII, as previously shown(Tourville et al., 2013), which inherently provided an internal normalization. This lowered overall animal-to-animal variability, and our data indicates that Transection had a significantly higher C2C/CPII ratio compared to Rupture at both 4 and 10 weeks, elevated CTxII/CPII ratio compared to Control at 4 weeks, higher COMP/CPII ratio compared to Rupture at 4 weeks, and higher

COMP/CPII ratio compared to Control at 10 weeks. Rupture animals had a higher COMP/CPII ratio compared to Control at 10 weeks, but no other ratios were elevated in the Rupture group. Given the drastic degenerative changes observed in our study, we expected highly elevated biomarker concentrations given their previous uses as indicators of OA in both human and animal studies, but our biomarker results do not fully corroborate our morphologic and histologic data. We attribute this to a lack of baseline normalization, the use of cardiac puncture, and inherent animal-to-animal variability. Future studies should employ a non-lethal venipuncture blood draw both pre- and postoperatively, which limits the total volume of serum able to be obtained but provides an important level of protein normalization.

This study is not without limitations. We did not perform imaging and histology on uninjured, contralateral limbs. The use of a healthy contralateral joint allows for internal normalization of results to limit the effect of animal-to-animal variability, but given the number of specimens used for analysis in this study, contralateral limbs were not analyzed. The imaging-based analysis of morphology of any tissue is limited by imaging resolution. To limit imaging time and time-dependent effects on tissue morphology during imaging, we employed a µCT protocol yielding an isotropic voxel size of 12 µm. While we believe this resolution to be more than sufficient for our analyses, the detection of small AC surface irregularities and the segmentation of the bone-cartilage interface was inherently limited. The contrast-enhanced imaging technique utilized in our studies necessitates the full dissection of the joint, incubation of the cartilage tissue in the contrast agent, and imaging in a humidified air chamber rather than in solution. As such, limiting acquisition time is of utmost importance to avoid tissue degradation and desiccation, which cause imaging and histologic artifacts. Histologic analyses are inherently limited by their 2D representation of a 3D tissue, and we made attempts to address this limitation

by obtaining 4 sagittal, 200 µm-spaced sections per compartment on both the tibia and femur. As mentioned above, our biomarker analysis was limited by the lack of a baseline, preoperative concentration with which to normalize post-operative concentrations, and future studies should obtain a baseline blood draw using non-lethal techniques. Lastly, our characterization of the noninvasive injury model in Section 6 – Aim #1 indicated that the injury protocol employed in the present study causes midsubstance ACL rupture, ACL avulsion of the femoral footprint, and a combination injury where one bundle avulses and one bundle ruptures. Since we did not confirm the exact injury type in each animal in the present study, we cannot rule out that animals in the Rupture group exhibited variable injury types, and this could have introduced variability in our dataset.

In conclusion, this study assessed differences in the onset and progression of PTOA in a model of noninvasive ACL injury compared to the frequently used model of surgical ACL transection. While both models cause the onset of PTOA with several similar results indicative of joint degeneration, numerous differences were found between the two models. Our study demonstrates that the two models exhibit a differential bony remodeling response, similar histologic findings with slight differences in cellularity, and that the surgical ACL transection model results in more extensive changes in articular cartilage morphology with correspondingly higher concentrations of serum-level cartilage biomarkers indicative of cartilage breakdown. We conclude that the surgical nature of the ACL transection model introduces several confounding biologic factors that perpetuate the OA cascade, and it may be overestimating the overall biological response of the joint following ligamentous injury. While some studies may benefit from a more rapid onset of OA-like joint degeneration, a more accurate representation of joint

biology following human ACL injury is, undoubtedly, obtained with a noninvasive injury model, and future studies assessing interventional treatment strategies can benefit its use.

CHAPTER 8: AIM #3 - ANALYZE AND COMPARE THE ACUTE BIOLOGICAL RESPONSE FOLLOWING BOTH NONINVASIVE ACL RUPTURE AND SURGICAL ACL TRANSECTION

8.1 - Introduction

Post-traumatic osteoarthritis (PTOA) is the consequence of a traumatic injury, acute inflammation, and chronic changes in joint kinematics and biology. Following ACL injury, surgical reconstruction has been shown to alleviate pain and restore joint stability by reducing anterior tibial translation, but the incidence of PTOA does not vary between surgically and nonsurgically-treated patients(Lohmander et al., 2007). While chronically unstable tibiofemoral articulation is known to increase the incidence of PTOA(Lohmander et al., 2007), current ACL reconstruction techniques do not appear to eliminate the risk for PTOA, and previous studies have indicated that the long-term risk for PTOA after ACL injury is as high as 100% . (Ait Si Selmi et al., 2006; Gillquist and Messner, 1999; Lohmander et al., 2004; Myklebust and Bahr, 2005; Nebelung and Wuschech, 2005; Roos et al., 1995; Von Porat et al., 2004)

Due to the lack of difference in PTOA incidence between surgically and nonsurgically treated patients, the PTOA cascade may be initiated at the time of injury and in the immediate, acute period following injury. However, the acute biological phenomena following ACL injury have yet to be fully elucidated (Section 2.3), and very little data exists regarding systemic cellular signaling, namely the mobilization and migration of mesenchymal stem cells. Morito *et al* have shown that synovial fluid-level MSC concentrations are increased after ACL rupture compared to healthy patients, (Morito et al., 2008) and these MSCs are more similar to synovium-derived MSCs than bone marrow-derived MSCs. No study has shown whether MSCs mobilize into circulation following ACL injury, and it is also unknown whether any mobilized

MSCs have the capacity to home to injured tissues in order to participate in immunomodulatory and/or regenerative processes.

The purpose of this aim was to assess the acute biological response following noninvasive ACL rupture and surgical transection. Specifically, we aimed to quantify MSC concentration in circulation, the concentration of cartilage metabolism biomarkers, and the concentration of stromal-derived factor-1 alpha (SDF-1α) in synovial fluid 72 hours after injury. We hypothesize that SDF-1 concentration will be elevated intraarticularly but neither noninvasive ACL rupture nor ACL transection induce systemic MSC mobilization. Furthermore, we hypothesize that serum-level increases in cartilage biomarker concentrations are only observed in the noninvasive ACL rupture group.

8.2 - Methods

Treatment Groups and Procedures

Eighteen adult, female Lewis rats 14 weeks of age were randomized to one of three groups: Control, Rupture, or Transection (n=6 per group). Noninvasive ACL rupture and surgical ACL transection were carried out exactly as described in Section 7. All animals were allowed *ad libitum* cage activity until sacrifice by CO_2 asphyxia at 72 hours. Five ml of whole blood were collected via cardiac puncture, and 4 ml were allowed to coagulate for 30 mins and processed for serum collection. One ml of blood was collected in EDTA-coated tubes at 4°C for flow cytometric analysis of MSCs. Synovial fluid aspirate was collected from the affected joint as outlined in Section 7 and frozen at -80°C until analysis.

Flow Cytometric Analysis of Circulating Mesenchymal Stem Cells

Whole blood was transferred to red blood cell lysis buffer (5 Prime Inc, Gaithersburg, Maryland, USA) and incubated for 10 mins at room temperature. Following centrifugation and washing, two samples of 10^6 cells from each animal were stained for cell-surface expression of CD29, CD34, CD45, and CD90. In brief, cells were incubated with 5 µg/ml sheep anti-rat CD34 primary antibody (R&D systems, Minneapolis, Minnesota, USA) for 30 mins at 4^0C. Following a wash, cells were incubated with 0.2 µg/ml donkey anti-sheep APC-conjugated secondary antibody (R&D systems). After another wash, cells were incubated with 2 µg/ml hamster anti-rat CD29-PE antibody (BD Biosciences, San Jose, California, USA), 2 µg/ml mouse anti-rat CD45-APC-Cy7 antibody (BD Biosciences), and 1 µg/ml mouse-anti rat CD90-PerCp antibody (BD Biosciences) for 30 mins at 4^0C. Another sample from each animal was also stained with isotype controls corresponding to each antibody. Cells were washed and transferred to flow cytometry tubes (BD Biosciences) and analyzed using a flow cytometer (FACSCanto II, BD Biosciences). Concentrations and flow cytometer voltages were optimized according to established protocols(Hulspas, 2010), and fluorescence compensation was performed using built-in compensation calculation following analysis of single-stained cells and an unstained control. Mesenchymal stem cells were identified by CD29+ CD90+ CD34- CD45- expression, and these cell surface markers have been previously used to identify MSCs in blood(Hong et al., 2009; Motawi et al., 2014; Nagaya et al., 2005; Yoshimura et al., 2007). The results of the two stained samples from each animal were averaged and analyzed as both absolute concentration and concentration normalized to control.

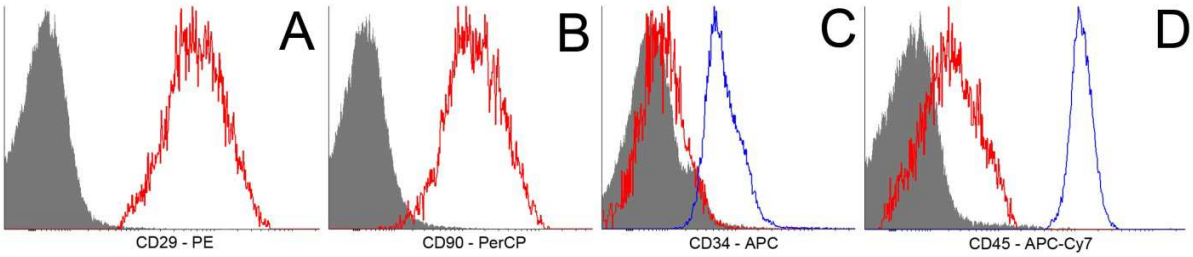

Figure 8.2.1 – *Panel of cell surface receptors analyzed using flow cytometry. The fraction of circulating MSCs was quantified using a CD29+ (A), CD90+ (B), CD34- (C), and CD45- (D) expression profile. Red = MSC expression profile. Blue = positive control. Grey = Isotype control.*

Serum Biomarker Quantification and Synovial Lavage Fluid SDF-1α Quantification

Collected serum was analyzed for cartilage biomarker concentrations of CS846, C2C, CTxII, CPII, C1,2C, and COMP as described in Section 7.2. Synovial lavage fluid was analyzed for SDF-1α concentration using ELISA (R&D Systems, Minneapolis, MN, USA).

Data Analysis and Statistical Comparison

All statistical analyses were performed in SPSS (v22, IBM, Armonk, NY). The normality and equal variance assumptions were assessed using the Shapiro-Wilk test and Levene's test, respectively. Differences in independent, normally distributed and non-normally distributed variables were compared between groups using one-way analysis of variance (ANOVA) and Kruskal-Wallis tests, respectively. Multiple comparisons were performed with a Sidak *P*-value correction at $\alpha = 95\%$. *P* values lower than 0.05 were considered significant.

8.3 - Results

Mesenchymal Stem Cell Mobilization Following ACL Rupture and Transection

The concentration of MSCs in blood of Control animals was 1.08% ± 0.75. MSC concentration was significantly higher in the Rupture group (6.81% ± 3.68, $P = 0.028$) and elevated in the Transection group, though not significantly (6.08% ± 4.49, $P = 0.059$) (Figure

8.3.1A). The fraction of CD34+ cells was decreased in both Rupture and Transection, though neither comparisons were statistically significant (P = 0.367 and P = 0.815, respectively) (Figure 8.3.1B). The same trend was observed for the cell fraction of CD45+ cells (P = 0.153 and P = 0.290, respectively) (Figure 8.3.1C).

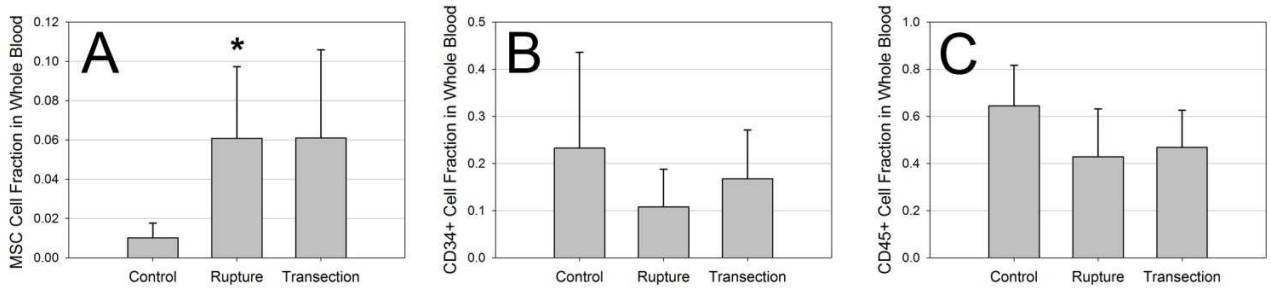

Figure 8.3.1 – *Flow Cytometric Analysis of cell fraction of MSCs (A), CD34+ cells (B), CD45+ cells (C) in whole blood 72 hours following injury. * denotes significant difference to Control.*

Serum-Level Biomarkers of Cartilage Metabolism and Breakdown

Biomarkers of cartilage breakdown and metabolism were quantified in the serum of Control, Rupture, and Transection animals. Results indicate that although small shifts in biomarker concentrations were observed between groups, neither Rupture nor Transection caused a significant increase in serum-level C2C, C1,2C, CPII, CS846, or CTxII concentration 72 hours after injury (Figure 8.3.2). Transection had a significantly higher COMP concentration compared to Rupture (P = 0.029), but no difference in COMP concentration was measured between Control and Transection or between Rupture and Transection (Figure 8.3.2C).

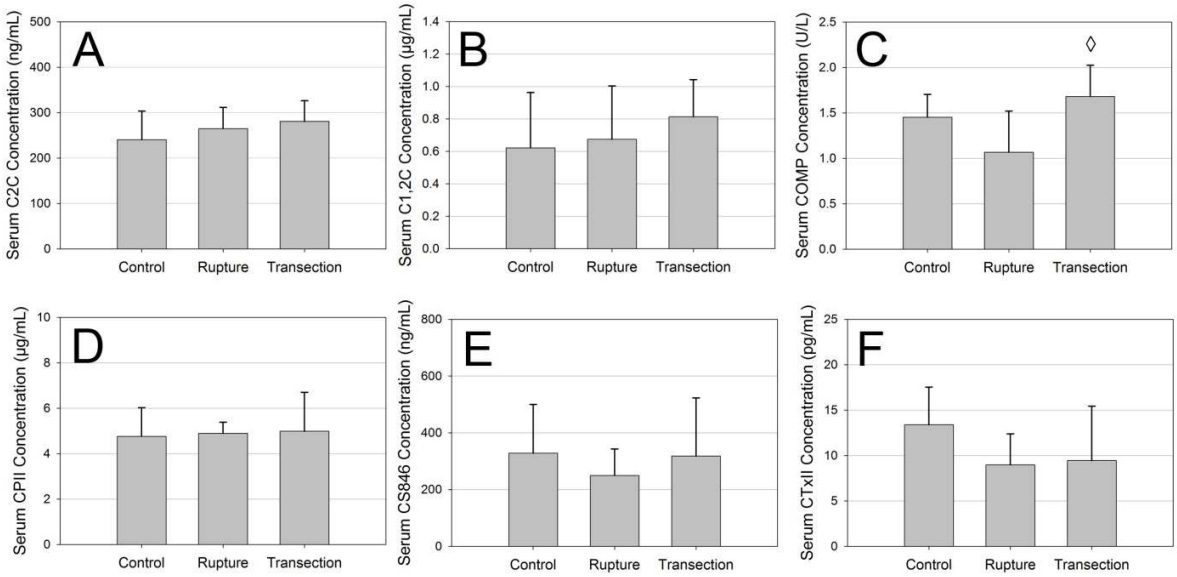

Figure 8.3.2 - *Serum C2C (A), C1,2C (B), COMP (C), CPII (D), CS846 (E), and CTxII (F) in Control, Rupture, and Transection at 72 hours. ◊ denotes significant difference between Rupture and Transection. ◊ denotes significant difference between Rupture and Transection.*

Collagen cleavage-to-synthesis ratios were calculated using the four markers of Type I and/or Type II collagen cleavage C2C, C1,2C, CTxII, and COMP and the marker of collagen synthesis, CPII (Figure 8.3.3). No group-to-group differences were found in C2C/CPII ratio, C1,2C/CPII ratio, or CTxII/CPII ratio. Transection had a significantly higher COMP/CPII ratio compared to Rupture, but neither group had a higher COMP/CPII ratio compared to Control.

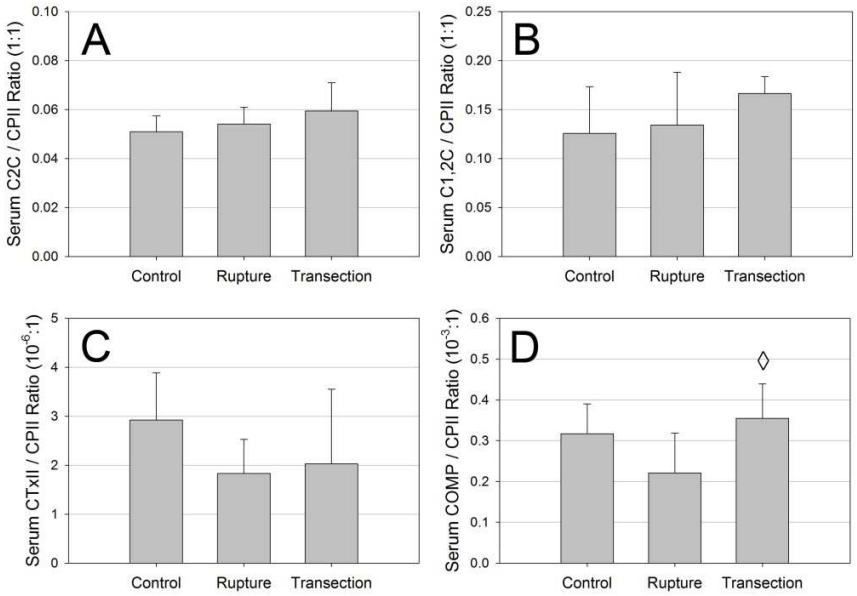

Figure 8.3.3 - *Collagen Cleavage-to-Synthesis Ratios of Serum-level Biomarkers 72 hrs after injury. Collagen cleavage-to-synthesis ratios were calculated using a marker of collagen synthesis, CPII, and four biomarkers of collagen cleavage C2C (A), C1,2C (B), CTxII (C), and COMP (D). ◊ denotes significant difference between Rupture and Transection.*

Synovial Fluid Lavage SDF-1α Concentration

Synovial lavage was assayed for SDF-1α, but several animals had undeterminable concentrations due to sub-threshold spectrophotometric optical densities. Two of six animals in the Control group, two of six animals in the Rupture group, and four of six animals in the Transection group had undeterminable SDF-1α concentrations, and final analysis and comparisons were performed with the remaining, usable data points. The concentration of SDF-1α in synovial fluid lavage was significantly higher in Rupture compared to Control ($P = 0.032$), but there was no difference between Transection and Control or between Rupture and Transection (Figure 8.3.4).

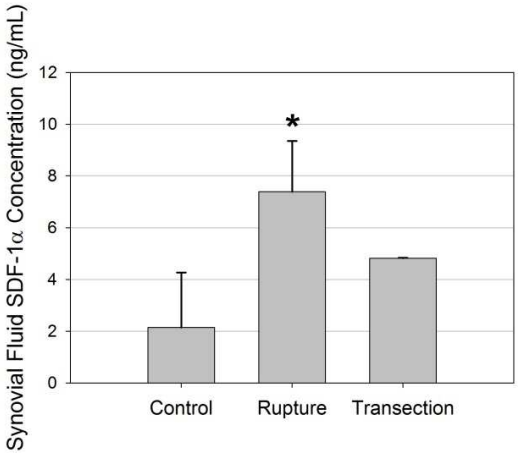

Figure 8.3.4 – *Synovial Fluid SDF-1α in Control, Rupture, and Transection at 72 hours. * denotes significant difference to Control.*

8.4 - Discussion

The biological phenomena leading to post-traumatic osteoarthritis (PTOA) following joint injury remain largely unknown. While chronic inflammation and altered joint kinematics are known perpetuators of the OA cascade, addressing these factors with surgical and pharmacological management has not been proven to lower the long-term incidence of PTOA. In the case of ACL rupture, clinical data does not indicate that the incidence of PTOA varies as a function of treatment(Lohmander et al., 2007), suggesting that while ACL reconstruction restores anterior knee stability, relieves pain, and allows patients to return to sporting activity, the risk for development of PTOA is equivalent between surgical and nonsurgical treatment. Due to the lack of evidence indicating that addressing chronic destabilization and inflammation lowers the overall risk for PTOA, it stands to reason that the acute biological events during and immediately after injury are major contributors to the onset and progression of PTOA. However, little data describing these acute events exists, and it is unclear whether existing animal models accurately reproduce the biological events present in humans. To this end, the purpose of this study was to employ the noninvasive ACL rupture model to study acute MSC mobilization, serum-level biomarkers of cartilage breakdown and metabolism, and synovial fluid SDF-1α concentrations and to compare these factors to the ACL transection model. Study results indicate that MSCs are mobilized into systemic circulation and that synovial fluid SDF-1α concentration is increased following ACL rupture. Biomarkers of cartilage breakdown were not significantly elevated in either injury group, but the Transection group exhibited a higher COMP concentration and COMP/CPII ratio compared to Rupture.

Stem cell mobilization has been shown to occur natively following myocardial infarction(Sprigg et al., 2006), stroke(Zohlnhöfer et al., 2006), fracture(Kitaori et al., 2009), lung

injury, (Yamada et al., 2004) and other trauma. Tissue trauma induces MSC and/or HSC mobilization, and mobilized stem or progenitor cells are able to migrate to injured tissue to participate in regenerative and immunomodulatory pathways.(Lapidot et al., 2005; Yagi et al., 2010) While the recruitment of synovium- and/or synovial fluid-derived MSCs has been shown following intraarticular ligament injury(Morito et al., 2008), no group has shown whether traumatic ligament injury induces systemic mobilization of MSCs into circulation. Our data indicates that both noninvasive ACL rupture and surgical ACL transection induce a ~6-fold increase in circulating CD29+ CD90+ CD34- CD45- MSCs. This data demonstrates that our hypothesis was incorrect and that ACL injury is indeed severe enough to mount a systemic response involving MSC mobilization. Since we did not measure any significant differences in circulating MSC concentration between the Rupture and Transection groups, we conclude that surgical trauma to the skin, joint capsule, and ACL is equivalent to noninvasive ACL rupture induced by biomechanical loading in its capacity to mount a systemic mobilization response. While flow cytometric analysis was performed using a panel of cell-surface receptors commonly used to identify bone marrow-derived MSCs, we cannot definitely conclude the source of the mobilized cells in our study. Although the bone marrow niche is the most likely source of mobilized cells, future studies are necessary in this regard.

The SDF-1 / CXCR-4 signaling axis is known to play an integral role in stem cell mobilization, migration, and homing. (Lau and Wang, 2011) SDF-1 is expressed by injured tissues and acts as a potent stem cell homing factor. In the setting of myocardial infarction, Abbott *et al* showed that SDF-1α is integral in the recruitment of bone marrow-derived stem cells following induced heart infarction.(Abbott et al., 2004) The study also showed that while exogenously-induced overexpression of SDF-1 is able to augment cellular recruitment, it is not

able to cause recruitment in the absence of tissue injury. Kitaori *et al* demonstrated that SDF-1 signaling dictates MSC migration to a healing long bone fracture site in a murine model.(Kitaori et al., 2009) The study demonstrated that intravenously-injected bone marrow-derived MSCs were present in the fracture site 7 days following injection, and an *in vitro* migration assay indicated that MSC migration is induced by SDF-1 in a dose-dependent manner. We measured SDF-1α concentration in synovial lavage fluid aspirated from knee joints 72 hours after injury and, although highly variable concentrations were measured in several rats, our data indicates SDF-1α concentration is elevated in the joint following noninvasive ACL rupture, confirming our hypothesis. Since SDF-1α expression following injury is known to contribute to stem cell mobilization, we conclude that the elevation in intraarticular SDF-1α is a driving factor in MSC mobilization observed after injury in the present study. However, it is unknown whether MSC migration into the joint occurred following systemic mobilization, and additional studies are underway to assess whether circulating MSCs are capable of migrating into the tissues of the knee joint.

We measured the concentration of six biomarkers of cartilage metabolism and turnover. Our results showed that animals treated with surgical ACL transection had a significantly higher COMP serum concentration and a significantly higher COMP/CPII ratio compared to the Rupture group. Our hypothesis that the Rupture group would exhibit higher cartilage biomarker levels was, therefore, disproven. Since neither treatment group exhibited significant increases in any biomarker concentration compared to Control, we conclude that the release of biomarkers indicative of cartilage turnover is minimal 72 hours following injury. Furthermore, we cannot conclude that the traumatic nature of the noninvasive rupture protocol causes acute structural damage to articular cartilage extensive enough to cause a release of the cartilage biomarkers

assayed in our study. Since rats in the Transection group were not subjected to any injury joint loading, our data indicates that surgical trauma and the inflammatory environment following surgery may be sufficient to initiate catabolic processes in cartilage to release COMP into serum, but this is not the case with other biomarkers. Furthermore, since cartilage degeneration and the onset of OA are known to be associated with increases in the serum concentration of all six biomarkers assayed in this study, we conclude that chronic inflammation and joint destabilization are necessary to cause measurable increases in serum biomarker concentration. Future research elucidating the temporal pattern of cartilage breakdown and biomarker release between surgical ACL transection and noninvasive ACL rupture using nonlethal blood draws are necessary.

The baseline concentration of MSCs in Control rats in our study was ~1%, which is higher than previously-reported values of the homeostatic concentration of circulating MSCs(Lapidot et al., 2005). We attribute this increased baseline MSC concentration to the use of cardiac puncture as a blood collection technique in addition to the anesthesia and CO_2 asphyxia-induced euthanasia procedures to which Control rats were subjected. We chose to subject Control rats to these procedures in order to avoid these as confounding factors, and our data should therefore be interpreted in the context of an increase over baseline concentration. Asphyxia/hypoxia have been shown to induce MSC mobilization (Rochefort et al., 2006), and cardiac puncture may have caused the release of myocardium-derived MSCs with a similar cell surface receptor expression profile as the one used in the present study. Future studies could benefit from blood collection via live venipuncture to avoid increased MSC mobilization due to cardiac puncture and CO_2 asphyxia.

This study is not without limitations. We employed cardiac puncture following CO_2 asphyxia to collect whole blood. This method was chosen to maximize the amount of blood available for analyses performed in our study, but we cannot rule out that this method of blood collection introduced confounding factors such as the release of myocardium-derived MSCs. Furthermore, as stated above, the use of CO_2 asphyxia may have caused a baseline increase in MSC concentration. We used ELISA to measure the concentration of six biomarkers, and our results indicate extensive variability between animals. While the technique is highly specific and yields an absolute concentration via the use of a known standard, it does not allow for normalization to total serum protein concentration, and animal-to-animal variability cannot be accounted for. Future studies should employ a non-lethal blood draw to obtain each animal's preoperative baseline biomarker concentration. However, by using CPII as a known biomarker of collagen II synthesis, we were able to compare cleavage-to-synthesis ratios, which were inherently normalized for each animal. Lastly, our method of synovial fluid lavage collection yielded highly variable amounts of product, and we attribute our high result variability to the collection method. Future work is required to optimize synovial fluid collection from the rat joint. Lastly, our characterization of the noninvasive injury model in Section 6 – Aim #1 indicated that the injury protocol employed in the present study causes midsubstance ACL rupture, ACL avulsion of the femoral footprint, and a combination injury where one bundle avulses and one bundle ruptures. Since we did not confirm the exact injury type in each animal in the present study, we cannot rule out that animals in the Rupture group exhibited variable injury types, and this could have introduced variability in our dataset.

In conclusion, this study demonstrated that both noninvasive ACL rupture and surgical ACL transection cause mobilization of MSCs into circulation to increase MSC concentration in

blood by ~6-fold over baseline. The two models of ACL injury causes varying levels of cartilage biomarker concentrations within serum, and the potent stem cell homing cytokine SDF-1α is released into the joint following injury. This data indicates that an acute, systemic response is triggered following ACL injury, and future studies can address acute biological events to develop interventional strategies to thwart the onset of PTOA.

CHAPTER 9: FUTURE WORK

The findings outlined in the present work open numerous avenues of future research. Three major categories of future research are, therefore, proposed: 1). Further characterization of the chronic changes following noninvasive ACL rupture; 2). further characterization of the acute biological phenomena following noninvasive ACL rupture; and 3). alterations to the noninvasive injury protocol to induce concomitant injuries or sub-rupture injuries.

To begin, as PTOA is a complex pathology with numerous interconnected pathways, further characterization of the chronic degenerative changes occurring in the knee joint following noninvasive ACL rupture is necessary. The μCT-based characterization of articular cartilage necessitated the full dissection of the knee joint, removing the meniscus, all ligaments, and the synovium. As these tissues are known to be intimately involved in degenerative mechanisms, characterization of biological changes in these tissues is an important topic for future work. Specifically, the assessment of synovial hyperplasia and meniscal degeneration could lend important information about the findings in the present study. Furthermore, the synovial fluid aspiration technique employed in the present study was proven to be imperfect. Future optimization of this technique is required as the consistent aspiration of uncontaminated synovial fluid is an important tool for future characterization of chronic joint biology. It can then be used to perform high throughput, proteome-wide analyses of synovial fluid to assess chronically-upregulated factors. These types of investigations can provide extremely useful information about the pathways responsible for chronic degeneration. As performed in the present study, all the proposed analyses can compare the noninvasive rupture model to the surgical ACL transection model in order to elucidate the source of their varying degenerative responses.

Secondly, in order to identify biological mechanisms triggering the onset of PTOA, extensive characterization of the acute phenomena following ACL injury are required. While current knowledge regarding the acute events after injury is limited, the noninvasive ACL rupture model can be employed to assess acute events leading to cartilage degeneration. As outlined above, following optimization of the synovial fluid aspiration technique, high throughput screening of the synovial fluid can identify specific moieties differentially expressed following injury. These can then be targeted using inhibitory strategies, which, in turn, may lead to the development of pharmacological therapies to lessen the degenerative effects of ACL rupture. Furthermore, one of the most significant findings of the present work is that ACL injury induces systemic MSC mobilization. Future experiments should isolate the mobilized cells by fluorescence-assisted cell sorting (FACS), magnetic-assisted cell sorting (MACS), or using conventional cell-culture based techniques such as density-gradient centrifugation followed by tissue culture plastic adherence. Isolated cells should be assessed for colony-forming unit capacity and tri-lineage differentiation capacity to confirm their MSC identity. Following this characterization, it will also be important to assess whether mobilized cells are able to migrate and home to the injured joint and to identify tissues into which MSCs have migrated. Subsequently, using tagged cells, one would be able to determine whether MSCs are differentiating into any of the joint tissues and/or whether they are participating in immunomodulatory mechanisms.

Lastly, the noninvasive ACL rupture model characterized in the present work can be modified in order to induce sub-rupture injury (i.e. ligament sprain) and/or concomitant injuries. Clinically, ACL sprains occur frequently during sporting activities, and while this injury is considered less severe than a complete rupture, joint injury undoubtedly occurs. Very little is

known about the relationship between an ACL sprain and the onset of PTOA, and the loading mechanism outlined in the present study can be utilized to induce a sub-rupture injury. Results outlined in Chapter 6: Aim #1 demonstrate that specimens that did not exhibit a complete injury still exhibited joint strain (assessed by tibiofemoral joint motion) and increased laxity. Small modifications in endpoint displacement could be made to the loading protocol in order to simulate rapid joint loading without complete ACL injury. This model can then be employed to assess how ACL sprains lead to PTOA. Furthermore, modification of the loading protocol to induce MCL injury via tibiofemoral rotation can provide a model for the commonly observed clinical injury of ACL-MCL rupture.

CHAPTER 10: FINISHING CONCLUSIONS

This work presented the biomechanical and biological development and characterization of a model of noninvasive ACL rupture in the rat. A complete, noninvasive ACL rupture can be repeatably induced with the application of a rapid 3 mm displacement of the tibia when the knee is flexed to 100°. This injury causes AP and varus laxity, indicating injury to the ACL as well as the LCL. Biological characterization of joint degeneration due to noninvasive ACL rupture and surgical ACL transection demonstrated that both injury models induce bony remodeling and changes in articular cartilage morphology indicative of PTOA-based degeneration. Histological evidence of articular cartilage degeneration was confirmed, and elevated serum-level concentrations were only observed in the surgical ACL transection group. Results from the present study lead us to conclude that the model of surgical ACL transection may be overestimating the degenerative response after injury, implying that confounding biological factors due to the surgical nature of the model introduce exacerbating degenerative effects. The investigation of acute phenomena following injury indicate that ACL injury triggers a systemic response, and to the authors' knowledge, this is the first study demonstrating that mobilization of MSCs occurs after ACL injury. We did not observe acute cartilage breakdown at 72 hrs after injury, measured by serum-level concentrations of established biomarkers, and we conclude that prolonged inflammation is necessary to release measurable levels of cartilage biomarkers within the serum. In conclusion, while the etiology of PTOA remains largely unknown, the noninvasive ACL injury model developed in this work can be employed in future investigations assessing pathologic mechanisms and therapeutic interventions.

APPENDIX

A1. Comprehensive Cartilage Parameterization Methods

Principle of the technique

Mesh parameterization refers to the bijective mapping of mesh vertices from a 3D (x,y,z) space onto a 2D (u,v) domain. Inherently, 3D surfaces are not able to be parameterized isometrically, and any parameterization algorithm needs to, therefore, be given criteria by which certain deformations are allowed to be introduced into the parameterization. As such, parameterizations can be either conformal (the angles between mesh vertices are preserved), equiareal (the areas of mesh triangles are preserved), or a combination of the two. The extent of deformation in either instance is directly correlated to the complexity of the 3D shape. In the application of analyzing cartilage morphology, accurate segmentation of compartments and subcompartments is crucial, and the delineation of compartmental borders is inherently challenging in 3D. Parameterization allows the mapping of the complex shape of an articular cartilage surface onto a relatively simple 2D surface, thereby allowing accurate segmentation and analysis.

Dodin *et al(Dodin et al., 2010)* proposed that by resampling the intensity information normal to the femoral bone-cartilage interface (BCI) at distance *h*, the parameterized BCI surface in the (*u*,*v*) domain can be extended into the 3D domain (*u*,*v*,*h*), producing a resampled image stack describing the local image intensity information normal to the BCI. The algorithm employed in the present study is based upon this principle.

Mesh generation

Cartilage volumes were segmented from µCT data sets as outlined in the Methods of Section 7 – Aim #2 (Figure A.1A). Each cartilage volume was triangulated into a mesh using MATLAB. Vertex normals were computed for each vertex (Figure A.1B), and the local image intensity was sampled normal to each vertex to determine adjacent tissues. Using intensity thresholding, vertices adjacent to bone (highly attenuating voxels) were defined part of the bone-cartilage interface (BCI) surface, while vertices adjacent to air or low attenuating soft tissue were excluded. The resultant BCI surface was cleaned, smoothed and resampled for even vertex spacing using open-source Meshlab software (http://meshlab.sourceforge.net) (Figure A.1C)(Cignoni et al., 2008).

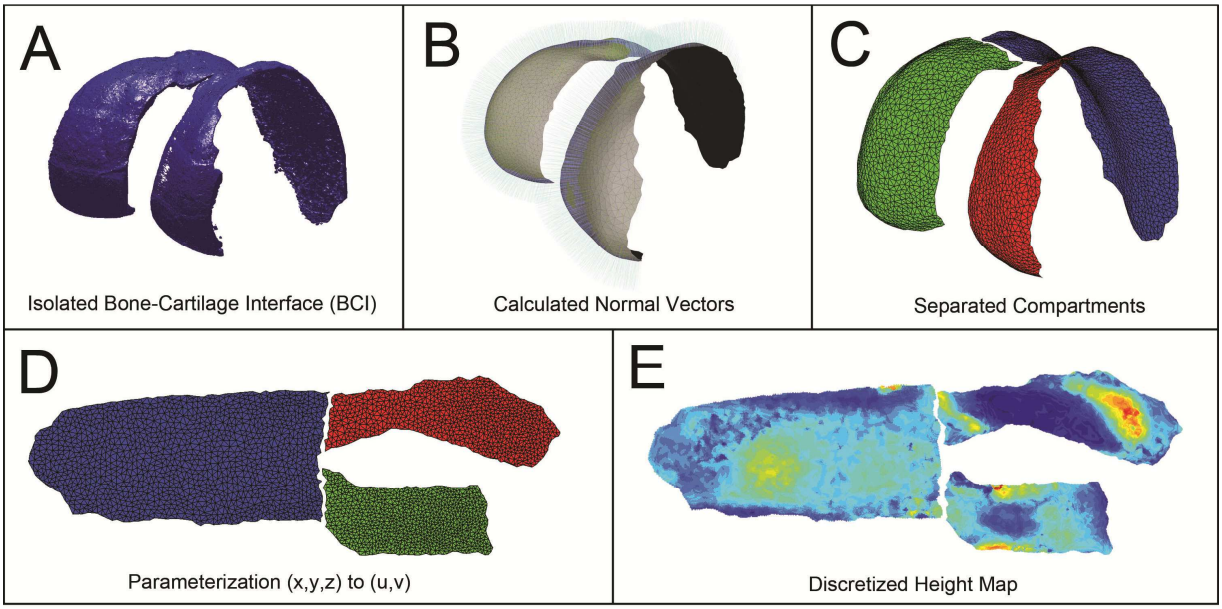

Figure A.1 – *Cartilage Parameterization Flow Chart. The bone-cartilage interface (BCI) is isolated using manual outling (A), and normal vectors are calculated following mesh generation (B). Individual compartments are isolated (C) and parameterized using conformal mesh parameterization (D). Meshes are discretized and height maps are generated (E).*

Parameterization

The cleaned mesh was reimported into MATLAB and mapped into the parameterized (*u*,*v*) space using an open-source Spectral Conformal Parameterization algorithm (Ryan Schmidt, http://dgp.toronto.edu/~rms/software/matlabmesh) based on the work of Mullen *et al(Mullen et al., 2008)* (Figure A.1D). The local attenuation around each vertex was then sampled along the normal line and discretized at a resolution of 12 μm/pixel to produce the (*u*,*v*,*h*) image stack. Parameterized image stacks were generated for the entire cartilage surface and for the individual sections (medial condyle, lateral condyle, trochlea) (Figure A.1E).

Thickness map generation

The cartilage layer of each parameterized image stack was segmented using fixed thresholds to eliminate air and bone, and a cartilage thickness map was generated from the resulting ROI (Figure A.1E). Because the *h* dimension describes the distance normal to the cartilage surface, the height of the cartilage at each position (*u*,*v*) corresponds to the normal cartilage thickness.

Surface roughness analysis

In addition to mean thickness, thickness maps were analyzed using metrics of areal surface roughness as defined by ISO 25178-6 (“Classification of methods for measuring surface texture,” International Organization for Standardization, 2014). The following areal surface roughness metrics were used: arithmetic surface roughness S_a and peak-to-valley distance (P-V). P-V is defined as the difference between the maximum and minimum thickness of the surface. The mathematical description of S_a is as follows:

$$S_a = \frac{1}{nm}\sum_{i=1}^{n}\sum_{j=1}^{m}\left|t^{ij} - \mu_t\right| \quad (1)$$

A2. Comprehensive Femoral and Tibial Bone Morphology and Densitometry Data

Table A2.1 – *Femoral Subchondral Bone Morphology and Densitometry (4 weeks)*

		Control	Rupture	Transection
BV/TV (Fraction ± Std. Dev.)	Medial	0.8411 ± 0.017	0.8203 ± 0.017 ◊	0.736 ± 0.075 *,◊
	Lateral	0.8391 ± 0.024	0.8696 ± 0.015 ◊	0.8101 ± 0.032 ◊
	Trochlear	0.7463 ± 0.039	0.6849 ± 0.027 ◊	0.6044 ± 0.055 *,◊
	Whole	0.7944 ± 0.02	0.7611 ± 0.016 ◊	0.6879 ± 0.054 *,◊
BMD (mg HA/cm^3 ± Std. Dev.)	Medial	883.2 ± 6.396	880.6 ± 11.37	837 ± 48.15 *
	Lateral	93.8 ± 18.47	927.6 ± 12.94	882 ± 25.31
	Trochlear	820.9 ± 16.92	783.3 ± 19.03 *,◊	743.5 ± 27.07 *,◊
	Whole	855.8 ± 15.44	840.8 ± 10.22	801 ± 31.66 *
TMD (mg HA/cm^3 ± Std. Dev.)	Medial	936.6 ± 8.957	945.5 ± 9.012	933.2 ± 20.14
	Lateral	944.6 ± 9.856	967.3 ± 7.315 *,◊	947.3 ± 15.66 ◊
	Trochlear	912.7 ± 5.955	905.3 ± 7.756	893.9 ± 13.74 *
	Whole	928.1 ± 7.859	932.5 ± 3.713	920 ± 14.73
Tb.Th. Mean (µm± Std. Dev.)	Medial	147.3 ± 11.47	145.2 ± 6.72	123.3 ± 22.09 *
	Lateral	154.6 ± 16.79	159.5 ± 4.621	132.2 ± 14.81 *
	Trochlear	107.8 ± 11.91	100.9 ± 5.505 ◊	86.59 ± 12.21 *
	Whole	131.6 ± 13.41	128.4 ± 2.769	109.8 ± 15.08 *
Tb.Th. Std (µm± Std. Dev.)	Medial	50.51 ± 4.014	49.16 ± 3.936	42.33 ± 8.248
	Lateral	51.06 ± 4.686	46.37 ± 2.397	40.97 ± 4.421*
	Trochlear	31.85 ± 3.711	30.1 ± 3.429	24.34 ± 5.392
	Whole	48.49 ± 4.037	48.43 ± 2.817	41.1 ± 5.891 *,◊
Tb.Th. Max (µm± Std. Dev.)	Medial	240.4 ± 10.23	245.7 ± 11.55	233.1 ± 21.93
	Lateral	250.1 ± 13.05	254.5 ± 5.284 ◊	230.6 ± 9.991 *,◊
	Trochlear	193.1 ± 17.36	191.7 ± 22.24	173.2 ± 31.34
	Whole	250.1 ± 13.05	256.9 ± 6.337	239.1 ± 13 ◊

* denotes significant difference to Control. ◊ denotes significant difference between Rupture and Transection.
‡ denotes significant difference between 4 and 10 weeks.

Table A2.2 - *Femoral Subchondral Bone Morphology and Densitometry (10 weeks)*

		Control	Rupture	Transection
BV/TV (Fraction ± Std. Dev.)	Medial	0.8867 ± 0.017 ‡	0.8640 ± 0.019 ‡	0.8334 ± 0.029 *, ‡
	Lateral	0.9063 ± 0.010 ‡	0.9135 ± 0.008 ◊, ‡	0.883 ± 0.022 ◊, ‡
	Trochlear	0.8703 ± 0.010 ‡	0.8241 ± 0.020 *, ‡	0.8131 ± 0.028 *, ‡
	Whole	0.8832 ± 0.011 ‡	0.8549 ± 0.015 *, ‡	0.8337 ± 0.023 *, ‡
BMD (mg HA/cm^3 ± Std. Dev.)	Medial	923.3 ± 10.42 ‡	924.3 ± 19.11 ‡	901.1 ± 25 ‡
	Lateral	939.1 ± 7.048 ‡	961.3 ± 11.72 *, ◊, ‡	920.4 ± 9.559 *, ◊, ‡
	Trochlear	886 ± 7.048 ‡	862.3 ± 11.88 *, ‡	859.7 ± 11.2 *, ‡
	Whole	908.9 ± 5.13 ‡	901.2 ± 10.44 ◊, ‡	884.2 ± 13.6 *, ◊, ‡
TMD (mg HA/cm^3 ± Std. Dev.)	Medial	956.3 ± 6.817 ‡	970.6 ± 17.23 ◊, ‡	948.5 ± 14.37 ◊
	Lateral	963.1 ± 6.036 ‡	982.7 ± 12.86 *, ◊, ‡	953.3 ± 10.32 ◊
	Trochlear	935.7 ± 5.657 ‡	938.7 ± 12.23 ‡	929.8 ± 2.593 ‡
	Whole	948.1 ± 4.91 ‡	957.9 ± 11.56 ◊, ‡	940.4 ± 6.484 ◊, ‡
Tb.Th. Mean (µm± Std. Dev.)	Medial	170.3 ± 3.137 ‡	157.5 ± 6.977 ‡	153.1 ± 13.13 *, ‡
	Lateral	184.7 ± 4.908 ‡	178.3 ± 4.539 ◊, ‡	168.2 ± 6.2 *, ◊, ‡
	Trochlear	153.7 ± 6.068 ‡	143.2 ± 4.761 *, ‡	135.8 ± 7.378 *, ‡
	Whole	165.9 ± 3.432 ‡	155.7 ± 4.552 *, ‡	148.1 ± 8.817 *, ‡
Tb.Th. Std (µm± Std. Dev.)	Medial	52.16 ± 1.897	46.84 ± 4.397	45.31 ± 4.377 *
	Lateral	54.36 ± 1.376	44.13 ± 1.729 *	46.34 ± 4.783 *
	Trochlear	44.15 ± 2.541 ‡	40.41 ± 2.147 ◊, ‡	43.79 ± 2.38 ◊, ‡
	Whole	50.78 ± 0.6049	45.45 ± 1.703 *	47.04 ± 1.459 *, ‡
Tb.Th. Max (µm± Std. Dev.)	Medial	255.8 ± 5.324 ‡	253.3 ± 12.68	246.6 ± 16.65
	Lateral	268.1 ± 1.587 ‡	260.7 ± 3.277	257.3 ± 11.71 ‡
	Trochlear	239.3 ± 8.211 ‡	239.4 ± 11.53 ‡	251.2 ± 20.46 ‡
	Whole	268.1 ± 1.587 ‡	262 ± 3.155	265.5 ± 8.065 ‡

* denotes significant difference to Control. ◊ denotes significant difference between Rupture and Transection.
‡ denotes significant difference between 4 and 10 weeks.

Table A2.3 - *Tibial Subchondral Bone Morphology and Densitometry (4 weeks)*

		Control	Rupture	Transection
BV/TV (Fraction ± Std. Dev.)	Medial	0.899 ± 0.025	0.842 ± 0.032 *, ◊	0.776 ± 0.044 *, ◊
	Lateral	0.774 ± 0.020	0.785 ± 0.018	0.742 ± 0.044
	Whole	0.828 ± 0.014	0.809 ± 0.015	0.755 ± 0.036 *
BMD (mg HA/cm^3 ± Std. Dev.)	Medial	909.9 ± 22.12	885.5 ± 19.16	846.4 ± 33.64 *
	Lateral	836.8 ± 7.955	851.5 ± 15.6 ◊	823.8 ± 23.84 ◊
	Whole	868.5 ± 7.04	865.6 ± 14.15	832.8 ± 26.27
TMD (mg HA/cm^3 ± Std. Dev.)	Medial	937.9 ± 14.51	931 ± 12.31	914.1 ± 18.67
	Lateral	904.5 ± 4.999	921.9 ± 9.655 *	906.5 ± 15.15
	Whole	920.3 ± 8.66	925.9 ± 9.412	909.7 ± 16.36
Tb.Th. Mean (µm± Std. Dev.)	Medial	125.8 ± 12.05	115.1 ± 12.35	108.3 ± 10.69
	Lateral	105.3 ± 5.628	115.6 ± 8.188	108.3 ± 9.802
	Whole	115 ± 8.126	115.6 ± 9.468	108.3 ± 9.654
Tb.Th. Std (µm± Std. Dev.)	Medial	35.42 ± 3.453	37.95 ± 1.142	35.53 ± 3.751
	Lateral	36.02 ± 3.334	44.56 ± 6.068 *	39.98 ± 2.852
	Whole	37.32 ± 3.873	42.11 ± 3.793	38.32 ± 2.874
Tb.Th. Max (µm± Std. Dev.)	Medial	206.5 ± 20.61	204.1 ± 11.01	191.7 ± 11.54
	Lateral	194.1 ± 17.63	225.4 ± 27.8	207.7 ± 13.24
	Whole	229.4 ± 10.87	250.2 ± 15.53	245.3 ± 16.45

* denotes significant difference to Control. ◊ denotes significant difference between Rupture and Transection.
‡ denotes significant difference between 4 and 10 weeks.

Table A2.4 – *Tibial Subchondral Bone Morphology and Densitometry (10 weeks)*

		Control	Rupture	Transection
BV/TV (Fraction ± Std. Dev.)	Medial	0.937 ± 0.017 ‡	0.873 ± 0.014 *, ◊	0.803 ± 0.031*, ◊
	Lateral	0.891 ± 0.031 ‡	0.871 ± 0.039 ‡	0.834 ± 0.037 *, ‡
	Whole	0.911 ± 0.022 ‡	0.871 ± 0.024 ◊ ‡	0.821 ± 0.030 *, ◊, ‡
BMD (mg HA/cm^3 ± Std. Dev.)	Medial	945.5 ± 18.18 ‡	911.7 ± 19.79 *, ◊, ‡	862.6 ± 26.1 *, ◊
	Lateral	901.5 ± 14.73 ‡	903.5 ± 29.47 ‡	870.1 ± 22.33 ‡
	Whole	921.3 ± 15.6 ‡	906.4 ± 24.79 ◊, ‡	867 ± 22.03 *, ◊, ‡
TMD (mg HA/cm^3 ± Std. Dev.)	Medial	962.8 ± 11.05 ‡	948.1 ± 17.26 ◊	920.5 ± 21.12 *, ◊
	Lateral	927.8 ± 9.429 ‡	944.4 ± 18.97 ◊, ‡	917.2 ± 12.05 ◊
	Whole	944 ± 9.915 ‡	946 ± 17.88 ‡	918.8 ± 15.41
Tb.Th. Mean (µm± Std. Dev.)	Medial	136.7 ± 6.793	125.6 ± 5.311	122 ± 8.888 *, ‡
	Lateral	127.6 ± 3.889 ‡	136.2 ± 4.632 ‡	128.4 ± 8.347 ‡
	Whole	131.8 ± 4.592 ‡	132 ± 2.515 ‡	125.9 ± 7.722 ‡
Tb.Th. Std (µm± Std. Dev.)	Medial	38.02 ± 2.927	41.86 ± 2.126 ‡	45.07 ± 4.426 *, ‡
	Lateral	43.66 ± 2.838 ‡	51.23 ± 4.671	48.91 ± 4.918 ‡
	Whole	41.5 ± 2.47	48.06 ± 2.395 *, ‡	47.69 ± 3.73 *, ‡
Tb.Th. Max (µm± Std. Dev.)	Medial	221.5 ± 15.1 1	218.6 ± 11.56	225.9 ± 17.04 ‡
	Lateral	223.1 ± 9.234 ‡	250.2 ± 15.53 *	243.7 ± 17.25 ‡
	Whole	229.4 ± 10.87 ‡	250.2 ± 15.53	245.3 ± 16.45 ‡

* denotes significant difference to Control. ◊ denotes significant difference between Rupture and Transection.
‡ denotes significant difference between 4 and 10 weeks.

Table A2.5 – *Femoral Epiphyseal Bone Morphology and Densitometry (4 weeks)*

		Control	Rupture	Transection
BV/TV (Fraction ± Std. Dev.)	Medial	0.622 ± 0.014	0.602 ± 0.03	0.59 ± 0.03
	Lateral	0.588 ± 0.02	0.6 ± 0.028	0.585 ± 0.02
	Trochlear	0.554 ± 0.021	0.492 ± 0.021*	0.482 ± 0.016*
	Whole	0.583 ± 0.014	0.548 ± 0.022*	0.539 ± 0.019*
BMD (mg HA/cm^3 ± Std. Dev.)	Medial	767.7 ± 8.01	767.6 ± 29.03	749.6 ± 30.76
	Lateral	741.8 ± 13.15	759.7 ± 28.74	729.3 ± 17.82
	Trochlear	701.5 ± 18.73	662.4 ± 31.56*	641.2 ± 17.1*
	Whole	726.2 ± 12.3	711.1 ± 27.4	692.1 ± 20.85
TMD (mg HA/ cm^3 ± Std. Dev.)	Medial	980.3 ± 17.03	981.9 ± 18.46	965.6 ± 22.14
	Lateral	968.4 ± 18.31	977.3 ± 15.59	954.8 ± 18.16
	Trochlear	961 ± 18.62	955 ± 19.12	935.8 ± 17.37
	Whole	975.5 ± 16.47	972.5 ± 15.47	954.2 ± 17.67
Tb.Th. Mean (µm± Std. Dev.)	Medial	132.4 ± 7.11	151.9 ± 13.14*	138.1 ± 7.36
	Lateral	130.8 ± 4.07	147 ± 10.54*, ◊	134 ± 3.91 ◊
	Trochlear	113.8 ± 7.79	116.1 ± 7.7 ◊	104.2 ± 3.97 ◊
	Whole	125.8 ± 5.67	137.8 ± 9.02*, ◊	125.5 ± 3.71 ◊
Tb.Th. Std (µm± Std. Dev.)	Medial	39.46 ± 3.91	68.76 ± 11.19*, ◊	51.55 ± 4.64 *, ◊
	Lateral	46.46 ± 1.85	61.42 ± 11.34*	55.21 ± 4.15
	Trochlear	36.29 ± 4.83	47.02 ± 7.64*, ◊	37.62 ± 3.95 ◊
	Whole	42.3 ± 3.14	62.94 ± 9.53*, ◊	50.34 ± 3.81 ◊
Tb.Th. Max (µm± Std. Dev.)	Medial	294.2 ± 22.64	385.1 ± 41.94*	334.4 ± 40.82
	Lateral	333.8 ± 26.95	373.1 ± 43.76	375.5 ± 25.28
	Trochlear	272.9 ± 39.21	316.9 ± 53.82	266.9 ± 30.51
	Whole	342 ± 18.05	401.9 ± 39.15*	371.9 ± 29.6

* denotes significant difference to Control. ◊ denotes significant difference between Rupture and Transection.
‡ denotes significant difference between 4 and 10 weeks.

Table A2.6 – *Femoral Epiphyseal Bone Morphology and Densitometry (10 weeks)*

		Control	Rupture	Transection
BV/TV (Fraction ± Std. Dev.)	Medial	0.666 ± 0.03 ‡	0.652 ± 0.024 ‡	0.658 ± 0.015 ‡
	Lateral	0.63 ± 0.023 ‡	0.643 ± 0.012 ‡	0.639 ± 0.014 ‡
	Trochlear	0.581 ± 0.035	0.542 ± 0.012*,‡	0.532 ± 0.011*, ‡
	Whole	0.615 ± 0.021 ‡	0.599 ± 0.013 ‡	0.592 ± 0.011 ‡
BMD (mg HA/cm^3 ± Std. Dev.)	Medial	796.8 ± 28.39 ‡	811.3 ± 22.18 ‡	799.8 ± 16.78 ‡
	Lateral	769.1 ± 17.28 ‡	806.4 ± 12*, ◊, ‡	780.6 ± 17.31 ◊, ‡
	Trochlear	723.2 ± 32.35	703.5 ± 13.39 ‡	686 ± 13.65*, ‡
	Whole	745.9 ± 17.71	754.9 ± 15.07 ‡	731.3 ± 15.2 ‡
TMD (mg HA/cm^3 ± Std. Dev.)	Medial	993.2 ± 11.02	1016 ± 13.43*, ◊, ‡	991.9 ± 8.45 ◊
	Lateral	985.9 ± 9.42	1012 ± 11.83*,◊, ‡	987.3 ± 8.52 ◊, ‡
	Trochlear	974 ± 10.67	984.9 ± 8.17 ◊, ‡	965.6 ± 7.46 ◊, ‡
	Whole	989.4 ± 9.71	1002 ± 11.55 ◊, ‡	979.9 ± 6.91 ◊
Tb.Th. Mean (µm± Std. Dev.)	Medial	126.9 ± 24.82	172.4 ± 17.4*, ‡	162.5 ± 9.11*, ‡
	Lateral	124.8 ± 21.75	149.6 ± 9.81*	149.7 ± 3.88*, ‡
	Trochlear	118.4 ± 7.06	116.7 ± 5.89	117 ± 3.54, ‡
	Whole	129.6 ± 4.48	146.7 ± 8.53*	142.8 ± 4.26*, ‡
Tb.Th. Std (µm± Std. Dev.)	Medial	38.24 ± 3.95	86.54 ± 15.8*, ‡	72.04 ± 7.93*, ‡
	Lateral	44.24 ± 3.99	60.81 ± 10.49*	65.29 ± 5.48*, ‡
	Trochlear	37.46 ± 4.09	45.76 ± 5.66*	49.52 ± 5.67*, ‡
	Whole	41.57 ± 2.57	72.6 ± 10.56*	67.87 ± 4.26*, ‡
Tb.Th. Max (µm± Std. Dev.)	Medial	278.9 ± 25.8	452.6 ± 49.28*, ‡	404.8 ± 32.18*, ‡
	Lateral	335 ± 43.89	371.3 ± 37.08	404.7 ± 41.51*, ‡
	Trochlear	284.1 ± 15.09	316 ± 35.05 ◊	375.4 ± 35.04*,◊, ‡
	Whole	350.6 ± 20.89	462.1 ± 64.31*	445.5 ± 25.16*, ‡

* denotes significant difference to Control. ◊ denotes significant difference between Rupture and Transection.
‡ denotes significant difference between 4 and 10 weeks.

Table A2.7 – *Tibial Epiphyseal Bone Morphology and Densitometry (4 weeks)*

		Control	Rupture	Transection
BV/TV (Fraction ± Std. Dev.)	Medial	0.592 ± 0.021	0.567 ± 0.026	0.539 ± 0.025 *
	Lateral	0.552 ± 0.012	0.540 ± 0.015	0.518 ± 0.022 *
	Whole	0.571 ± 0.016	0.552 ± 0.020	0.528 ± 0.022 *
BMD (mg HA/cm^3 ± Std. Dev.)	Medial	753.7 ± 13.17	747.5 ± 15.07	719.7 ± 22.58
	Lateral	726.8 ± 15.36	728.2 ± 12.3 ◊	700 ± 17.49 *,◊
	Whole	739.4 ± 12.37	736.4 ± 12.2 ◊	708.3 ± 19.2 *,◊
TMD (mg HA/cm^3 ± Std. Dev.)	Medial	975 ± 9.905	976.4 ± 9.566	959.3 ± 13.41
	Lateral	959.2 ± 13.7	969.4 ± 9.657	950.1 ± 12.88
	Whole	967 ± 10.86	972.4 ± 9.2	954.5 ± 12.97 *
Tb.Th. Mean (µm± Std. Dev.)	Medial	139.4 ± 6.8	144.4 ± 10.24	137.2 ± 12.8
	Lateral	124.7 ± 3.002	129 ± 5.638	125.9 ± 10.31
	Whole	132.6 ± 4.665	137.6 ± 7.871	132.4 ± 11.37
Tb.Th. Std (µm± Std. Dev.)	Medial	50.82 ± 3.282	60.88 ± 6.344 *	54.48 ± 6.206
	Lateral	43.58 ± 1.094	50.06 ± 5.308	50.28 ± 5.05 *
	Whole	48.4 ± 2.256	57.44 ± 5.741*	53.9 ± 4.859
Tb.Th. Max (µm± Std. Dev.)	Medial	317.4 ± 14.57	358.9 ± 36.11	328.6 ± 37.92
	Lateral	276.4 ± 5.141	333.8 ± 32.73 *	333.2 ± 36.47 *
	Whole	319.8 ± 14.87	362.4 ± 37.4	352.1 ± 29.77

* denotes significant difference to Control. ◊ denotes significant difference between Rupture and Transection.
‡ denotes significant difference between 4 and 10 weeks.

Table A2.8 – *Tibial Epiphyseal Bone Morphology and Densitometry (10 weeks)*

		Control	**Rupture**	**Transection**
BV/TV (Fraction ± Std. Dev.)	Medial	0.648 ± 0.010 ‡	0.641 ± 0.014 ‡	0.615 ± 0.025 *, ‡
	Lateral	0.594 ± 0.010 ‡	0.602 ± 0.020 ‡	0.575 ± 0.043 ‡
	Whole	0.617 ± 0.0082 ‡	0.619 ± 0.016 ‡	0.594 ± 0.034 ‡
BMD (mg HA/cm^3 ± Std. Dev.)	Medial	795.5 ± 12.79 ‡	777.8 ± 12.8 ‡	762.8 ± 13.78 *, ‡
	Lateral	756 ± 15.35 ‡	748.9 ± 18.94 ‡	731.8 ± 26.52 ‡
	Whole	773.3 ± 12.04 ‡	762.5 ± 15.06 ‡	746.9 ± 19.82 *, ‡
TMD (mg HA/cm^3 ± Std. Dev.)	Medial	990.2 ± 8.685 ‡	984.2 ± 16.33	973.7 ± 15.49
	Lateral	970.4 ± 8.357	968.7 ± 10.25	959 ± 16.04
	Whole	980.3 ± 7.931 ‡	977 ± 12.66	967.7 ± 14.58
Tb.Th. Mean (µm± Std. Dev.)	Medial	151.8 ± 3.075 ‡	170.2 ± 5.538 *, ‡	160.7 ± 13.18 ‡
	Lateral	135.5 ± 3.446 ‡	141.6 ± 6.409 ‡	137.6 ± 17.85
	Whole	144.2 ± 3.037 ‡	157.2 ± 4.255 ‡	150.6 ± 15.04 ‡
Tb.Th. Std (µm± Std. Dev.)	Medial	53.75 ± 3.75	82.01 ± 7.369 *, ‡	76.06 ± 13.5 *, ‡
	Lateral	49.34 ± 2.533 ‡	60.96 ± 5.284 *, ‡	59.66 ± 8.531 *, ‡
	Whole	53.34 ± 2.394 ‡	75.22 ± 5.152 *, ‡	71.12 ± 11.01 *, ‡
Tb.Th. Max (µm± Std. Dev.)	Medial	342.4 ± 25.14	428.6 ± 39.63 *, ‡	411.5 ± 53.09 *, ‡
	Lateral	319.9 ± 17.79 ‡	374.8 ± 19.67 *, ‡	377.5 ± 52.53 *
	Whole	353.1 ± 22.19 ‡	437 ± 33.44 *, ‡	418.6 ± 50.77 *, ‡

* denotes significant difference to Control. ◊ denotes significant difference between Rupture and Transection.
‡ denotes significant difference between 4 and 10 weeks.

A3. Comprehensive Femoral and Tibial Cartilage Morphology and Surface Roughness Data

Table A3.1 – *Femoral Cartilage Morphology and Surface Roughness by Compartment and Sub-Compartment (4 weeks)*

			Control	Rupture	Transection
Mean Height (µm± Std. Dev.)	Whole		74.95 ± 7.582	97.83 ± 3.221 *	100.5 ± 16.34 *
	Medial	Whole	60.52 ± 8.384	84.03 ± 4.148 *	92.67 ± 24.94
		Medial	59.6 ± 8.536	102.4 ± 6.548 *	109.7 ± 26.44 *
		Lateral	61.48 ± 9.261	64.37 ± 4.225	74.16 ± 26.6
	Lateral	Whole	55.94 ± 5.213	90.95 ± 6.276 *	93.9 ± 21.65 *
		Medial	56.88 ± 5.398	91.67 ± 5.659 *	93.72 ± 23.83 *
		Lateral	54.99 ± 5.328	90.23 ± 8.437 *	94.22 ± 20.35 *
	Trochlear	Whole	86.1 ± 10.67	104.6 ± 4.673 *	105.6 ± 14.47 *
		Medial	80.2 ± 12.21	92.08 ± 4.453	97.97 ± 22.31
		Lateral	92.24 ± 9.529	117.6 ± 6.565 *	113.9 ± 10.6 *
Peak-to-Valley (µm± Std. Dev.)	Whole		186 ± 33.73	266 ± 36.73 *	264 ± 39.44 *
	Medial	Whole	144 ± 21.47	254 ± 45.8 *	256 ± 47.8 *
		Medial	124 ± 9.798	254 ± 45.8 *	236 ± 36.13 *
		Lateral	144 ± 21.47	206 ± 15.95 *	238 ± 55.99 *
	Lateral	Whole	132 ± 16.97	210 ± 41.4 *	192 ± 46.16 *
		Medial	120 ± 7.589	206 ± 47.04 *	184 ± 50.15 *
		Lateral	126 ± 21.13	150 ± 39.98	160 ± 31.9
	Trochlear	Whole	172 ± 29.07	224 ± 25.92	204 ± 26.29
		Medial	156 ± 30.36	204 ± 16.97 *	196 ± 23.6 *
		Lateral	170 ± 29.8	198 ± 42.09	198 ± 21.13
S_a (µm± Std. Dev.)	Whole		23.14 ± 4.329	30.32 ± 0.4788 *	31.78 ± 6.318 *
	Medial	Whole	15.11 ± 2.555	48.27 ± 2.874 *	48.59 ± 8.809 *
		Medial	13.52 ± 2.224	50.56 ± 5.38 *	44.66 ± 12.65 *
		Lateral	16.24 ± 2.871	39.94 ± 3.461 *	46.19 ± 13.6 *
	Lateral	Whole	13.43 ± 1.855	23.62 ± 2.65 *	23.09 ± 4.375 *
		Medial	14.88 ± 1.811	24.02 ± 3.295 *	23.12 ± 4.223 *
		Lateral	11.71 ± 2.242	22.89 ± 3.276 *	22.65 ± 6.073 *
	Trochlear	Whole	23.03 ± 4.496	23.8 ± 1.17	25.32 ± 6.521
		Medial	21.76 ± 4.368	21.23 ± 1.788	25.55 ± 6.972
		Lateral	22.79 ± 5.054	21.57 ± 2.067	21.62 ± 6.364

* denotes significant difference to Control. ◊ denotes significant difference between Rupture and Transection.
‡ denotes significant difference between 4 and 10 weeks.

Table A3.2– *Femoral Cartilage Morphology and Surface Roughness by Compartment and Sub-Compartment (10 weeks)*

			Control	Rupture	Transection
Mean Height (µm± Std. Dev.)	Whole		45.51 ± 6.361 ‡	77.41 ± 6.117 *, ‡	88.39 ± 9.964 *
	Medial	Whole	38.97 ± 6.153 ‡	77.07 ± 21.05 *,◊	102.6 ± 17.88 *,◊
		Medial	39.31 ± 6.512 ‡	83.42 ± 31.55 *	107.8 ± 28.62 *
		Lateral	38.64 ± 6.475 ‡	69.67 ± 17.59 *,◊	96.75 ± 21.85 *,◊
	Lateral	Whole	35.4 ± 4.437‡	73.95 ± 8.926 *, ‡	84.41 ± 17.27 *
		Medial	35.41 ± 5.853 ‡	77 ± 10.85 *, ‡	91.74 ± 22.3 *
		Lateral	35.41 ± 3.428 ‡	71.07 ± 8.078 *, ‡	77.36 ± 14.55 *
	Trochlear	Whole	49.05 ± 7.118 ‡	79.23 ± 6.116 *, ‡	86.05 ± 9.749 *, ‡
		Medial	47.65 ± 6.337 ‡	69.84 ± 5.969 *, ‡	78.45 ± 8.399 *
		Lateral	50.51 ± 8.244 ‡	89.05 ± 9.4 *, ‡	94.18 ± 12.39 *, ‡
Peak-to-Valley (µm± Std. Dev.)	Whole		152 ± 23.6	282 ± 44.74 *	304 ± 39.19 *
	Medial	Whole	112 ± 21.01 ‡	262 ± 67.63 *	302 ± 42.54 *
		Medial	100 ± 28.06	248 ± 63.8 *	268 ± 60.56 *
		Lateral	100 ± 19.6 ‡	232 ± 59.6 *	288 ± 44.25 *
	Lateral	Whole	108 ± 36.4	180 ± 37.95 *	206 ± 39.01 *
		Medial	70 ± 20.67 ‡	166 ± 29.8 *	178 ± 49.43 *
		Lateral	104 ± 39.19	174 ± 41.4 *	178 ± 48.84 *
	Trochlear	Whole	142 ± 26.74	196 ± 39.92	198 ± 56.67
		Medial	122 ± 27.8	166 ± 32.57, ‡	162 ± 39.25
		Lateral	130 ± 25.64 ‡	190 ± 38.26	196 ± 52.4 *
S_a (µm± Std. Dev.)	Whole		17.68 ± 3.389 ‡	31.07 ± 4.869 *	29.73 ± 5.332 *
	Medial	Whole	12.35 ± 2.789	49.3 ± 15.99 *	55.71 ± 14.19 *
		Medial	11.51 ± 3.04	47.38 ± 17.25 *	49.06 ± 14.29 *
		Lateral	12.91 ± 2.536	46.03 ± 15.11 *	55.74 ± 13.95 *
	Lateral	Whole	9.353 ± 1.405 ‡	22.63 ± 4.995 *	23.98 ± 7.335 *
		Medial	10.7 ± 2.782 ‡	27.93 ± 6.789 *	29.07 ± 10.54 *
		Lateral	7.967 ± 1.09 ‡	17.22 ± 3.519 *, ‡	16.51 ± 2.211 *, ‡
	Trochlear	Whole	19.73 ± 3.94	26.47 ± 3.282 *	25.92 ± 5.063
		Medial	19.3 ± 3.985	25.3 ± 2.478 ‡	25.47 ± 4.934
		Lateral	19.79 ± 3.645	24.3 ± 4.913	24.33 ± 4.476

* denotes significant difference to Control. ◊ denotes significant difference between Rupture and Transection.
‡ denotes significant difference between 4 and 10 weeks.

Table A3.3– *Tibial Cartilage Morphology and Surface Roughness by Compartment and Sub-Compartment (4 weeks)*

			Control	Rupture	Transection
Mean Height (µm± Std. Dev.)	Whole		109.7 ± 10.55	140.8 ± 6.765*	155.5 ± 17.9*
	Medial	Whole	121.7 ± 10.67	158.5 ± 8.871*	174.3 ± 24.91*
		Medial	103.6 ± 11.32	131.7 ± 7.706	150.4 ± 29.07*
		Lateral	141.2 ± 12.13	184.2 ± 13.86*	198 ± 24.93*
	Lateral	Whole	100.7 ± 10.09	128.4 ± 7.785*	142.6 ± 17.14*
		Medial	113.8 ± 7.18	159.9 ± 14.33*	167.9 ± 17.7*
		Lateral	87.8 ± 13.84	97.03 ± 8.484	115.5 ± 21.64*
Peak-to-Valley (µm± Std. Dev.)	Whole		284 ± 22.34	350 ± 23.29*	382 ± 33.44*
	Medial	Whole	282 ± 19.72	340 ± 27.01*	370 ± 40.46*
		Medial	222 ± 36.99	296 ± 28.06*	348 ± 40.87*
		Lateral	278 ± 14.03	338 ± 23.29*	364 ± 39.92*
	Lateral	Whole	252 ± 30.36	314 ± 19.22*, ◊	360 ± 33.08*, ◊
		Medial	252 ± 30.36	312 ± 22.77*, ◊	360 ± 33.08*, ◊
		Lateral	222 ± 31.06	246 ± 28.14 ◊	330 ± 39.25*, ◊
S_a (µm± Std. Dev.)	Whole		46.43 ± 1.397	69.77 ± 2.182*	85.91 ± 12.33*
	Medial	Whole	52.79 ± 1.493	73.29 ± 4.378*	88.34 ± 9.085*
		Medial	37.16 ± 2.707	60.28 ± 5.531*, ◊	77.91 ± 10.69*, ◊
		Lateral	64.84 ± 1.385	76.97 ± 6.845*, ◊	93.64 ± 10.82*, ◊
	Lateral	Whole	40.46 ± 2.489	64.3 ± 2.388 *, ◊	80.91 ± 15.92*, ◊
		Medial	45.97 ± 1.158	67.87 ± 1.196*	83.92 ± 17.25*
		Lateral	30.93 ± 7.233	43.59 ± 7.959 ◊	64.91 ± 19.84*, ◊

* denotes significant difference to Control. ◊ denotes significant difference between Rupture and Transection.
‡ denotes significant difference between 4 and 10 weeks.

Table A3.4– *Tibial Cartilage Morphology and Surface Roughness by Compartment and Sub-Compartment (10 weeks)*

			Control	Rupture	Transection
Mean Height (µm± Std. Dev.)	Whole		101.5 ± 5.383	131.6 ± 6.767*, ‡	137.3 ± 13.95*
	Medial	Whole	116.5 ± 7.663	145.8 ± 15.36*	149.6 ± 15.69*
		Medial	99.04 ± 4.959	118 ± 21.58	121.1 ± 16.49
		Lateral	134.9 ± 13.5	172.2 ± 13.16*	176.1 ± 19.99*
	Lateral	Whole	90 ± 4.727‡	122.7 ± 11.48*	128.7 ± 15.03*
		Medial	104.4 ± 7.644	146.9 ± 9.939*	157.5 ± 17.31*
		Lateral	75.16 ± 4.771	97.71 ± 21.44	95.46 ± 23.93
Peak-to-Valley (µm± Std. Dev.)	Whole		284 ± 23.6	364 ± 23.6*	408 ± 25.17*
	Medial	Whole	284 ± 23.6	354 ± 39.25*	390 ± 14.7*
		Medial	226 ± 9.033	288 ± 42.93*	322 ± 25.64*
		Lateral	282 ± 21.13	352 ± 40.63*	386 ± 11.8*
	Lateral	Whole	230 ± 14.03	344 ± 9.798*, ‡	380 ± 54.02*
		Medial	230 ± 14.03	338 ± 14.03*	378 ± 53.53*
		Lateral	196 ± 12.39	280 ± 50.72*	300 ± 67.46*
S_a (µm± Std. Dev.)	Whole		50.12 ± 4.083	67.85 ± 3.363*, ◊	77.52 ± 8.642*, ◊
	Medial	Whole	58.55 ± 5.712‡	72.12 ± 6.226*	75.38 ± 3.356*
		Medial	42.37 ± 2.579‡	54.74 ± 2.796*	60.54 ± 6.834*, ‡
		Lateral	71.79 ± 7.253‡	80.73 ± 11.7	84.39 ± 4.636*
	Lateral	Whole	41.21 ± 3.79	62.53 ± 3.269*, ◊	77.51 ± 14.95*, ◊
		Medial	48.44 ± 5.701	70.81 ± 2.837*, ◊	89.02 ± 15.85*, ◊
		Lateral	28.8 ± 2.818	42.93 ± 10.1	49.42 ± 19.27*

* denotes significant difference to Control. ◊ denotes significant difference between Rupture and Transection.
‡ denotes significant difference between 4 and 10 weeks.

A4. Comprehensive Femoral and Tibial OARSI Modified Mankin Grades

Table A4.1– *Femoral OARSI Histologic Grade by Subsection and Compartment (4 weeks)*

		Control	Rupture	Transection
Articular Cartilage Structure (Mean ± Std. Dev.)	Medial	0.6713 ± 0.359	7.245 ± 0.417*	7.25 ± 0.457*
	Lateral	0.7824 ± 0.375	3.278 ± 1.33*	2.699 ± 0.648*
	Whole	0.7259 ± 0.349	5.194 ± 0.844*	4.78 ± 0.451*
Proteoglycan Content (Mean ± Std. Dev.)	Medial	0.6898 ± 0.233	5.13 ± 0.282*	5.014 ± 0.529*
	Lateral	0.6389 ± 0.253	2.38 ± 0.874*	1.745 ± 0.557*
	Whole	0.6669 ± 0.231	3.668 ± 0.566*	3.222 ± 0.454*
Cellularity (Mean ± Std. Dev.)	Medial	0.4398 ± 0.223	2.87 ± 0.125*	2.838 ± 0.0903*
	Lateral	0.3843 ± 0.218	2.083 ± 0.23*, ◊	1.292 ± 0.175*, ◊
	Whole	0.4102 ± 0.207	2.459 ± 0.195*, ◊	1.997 ± 0.123*, ◊
Tidemark Integrity (Mean ± Std. Dev.)	Medial	0.2685 ± 0.0738	0.9722 ± 0.068*	1.000 ± 0.000*
	Lateral	0.3287 ± 0.117	0.7824 ± 0.125*	0.588 ± 0.234
	Whole	0.3016 ± 0.0853	0.873 ± 0.0981*	0.7789 ± 0.122*
Total Score (Mean ± Std. Dev.)	Medial	2.069 ± 0.477	16.22 ± 0.577*	16.1 ± 1.04*
	Lateral	2.134 ± 0.427	8.523 ± 2.50*	6.343 ± 1.3*
	Whole	2.105 ± 0.412	12.19 ± 1.66*	10.79 ± 0.935*

* denotes significant difference to Control. ◊ denotes significant difference between Rupture and Transection.
‡ denotes significant difference between 4 and 10 weeks.

Table A4.2– *Femoral OARSI Histologic Grade by Subsection and Compartment (10 weeks)*

		Control	Rupture	Transection
Articular Cartilage Structure (Mean ± Std. Dev.)	Medial	1.31 ± 0.981	6.866 ± 0.823*	7.222 ± 0.76*
	Lateral	1.208 ± 0.332	2.866 ± 0.602*	2.657 ± 0.806*
	Whole	1.258 ± 0.623	4.741 ± 0.545*	4.934 ± 0.67*
Proteoglycan Content (Mean ± Std. Dev.)	Medial	1.468 ± 0.708 ‡	4.889 ± 0.906*	4.991 ± 0.566*
	Lateral	0.9769 ± 0.535	2.181 ± 0.581*	1.931 ± 0.436*
	Whole	1.199 ± 0.538	3.45 ± 0.271*	3.449 ± 0.42*
Cellularity (Mean ± Std. Dev.)	Medial	0.6065 ± 0.255	2.653 ± 0.271*	2.875 ± 0.165*
	Lateral	0.3565 ± 0.179	1.926 ± 0.0989*, ◊	1.356 ± 0.174*, ◊
	Whole	0.4795 ± 0.185	2.265 ± 0.16*	2.109 ± 0.176*
Tidemark Integrity (Mean ± Std. Dev.)	Medial	0.2963 ± 0.139	0.9537 ± 0.0517*	1.000 ± 0.00*
	Lateral	0.2407 ± 0.156	0.838 ± 0.143*	0.6852 ± 0.135*
	Whole	0.2692 ± 0.134	0.8942 ± 0.0855*	0.8455 ± 0.0612*
Total Score (Mean ± Std. Dev.)	Medial	3.694 ± 1.76	15.36 ± 1.88*	16.09 ± 1.46*
	Lateral	2.796 ± 0.772	7.833 ± 0.978*	6.63 ± 1.30*
	Whole	3.22 ± 1.20	11.38 ± 0.925*	11.34 ± 1.20*

* denotes significant difference to Control. ◊ denotes significant difference between Rupture and Transection.
‡ denotes significant difference between 4 and 10 weeks.

Table A4.3– *Tibial OARSI Histologic Grade by Subsection and Compartment (4 weeks)*

		Control	Rupture	Transection
Articular Cartilage Structure (Mean ± Std. Dev.)	Medial	0.7407 ± 0.218	3.269 ± 0.619*	3.051 ± 0.621*
	Lateral	0.8519 ± 0.303	3.236 ± 0.31*	2.593 ± 0.725*
	Whole	0.7836 ± 0.232	3.27 ± 0.347*	2.817 ± 0.503*
Proteoglycan Content (Mean ± Std. Dev.)	Medial	0.8611 ± 0.66	2.755 ± 0.462*	2.431 ± 0.803*
	Lateral	0.8565 ± 0.141	2.838 ± 0.246*	2.315 ± 0.716*
	Whole	0.8753 ± 0.447	2.784 ± 0.156*	2.38 ± 0.629*
Cellularity (Mean ± Std. Dev.)	Medial	0.6435 ± 0.188	1.843 ± 0.311*	1.662 ± 0.133*
	Lateral	0.4815 ± 0.427	1.759 ± 0.27*	1.519 ± 0.285*
	Whole	0.5728 ± 0.232	1.789 ± 0.198*	1.599 ± 0.129*
Tidemark Integrity (Mean ± Std. Dev.)	Medial	0.2083 ± 0.131	0.9722 ± 0.043*	0.9861 ± 0.034*
	Lateral	0.3981 ± 0.193	0.9861 ± 0.034*	0.8889 ± 0.272
	Whole	0.3032 ± 0.138	0.9782 ± 0.035*	0.9375 ± 0.153*
Total Score (Mean ± Std. Dev.)	Medial	2.366 ± 0.537	8.343 ± 1.18*	8.009 ± 1.48*
	Lateral	2.407 ± 0.893	8.579 ± 0.761*	7.116 ± 1.76*
	Whole	2.338 ± 0.482	8.049 ± 0.574*	7.094 ± 1.13*

* denotes significant difference to Control. ◊ denotes significant difference between Rupture and Transection.
‡ denotes significant difference between 4 and 10 weeks.

Table A4.4– *Tibial OARSI Histologic Grade by Subsection and Compartment (10 weeks)*

		Control	Rupture	Transection
Articular Cartilage Structure (Mean ± Std. Dev.)	Medial	0.9667 ± 0.496	3.236 ± 0.42*	3.62 ± 0.191*
	Lateral	1.204 ± 0.495	3.468 ± 0.927*	3.694 ± 0.481*, ‡
	Whole	1.043 ± 0.441	3.258 ± 0.365*	3.666 ± 0.248*, ‡
Proteoglycan Content (Mean ± Std. Dev.)	Medial	1.628 ± 1.37	3.083 ± 0.224*	3.634 ± 0.371*, ‡
	Lateral	1.296 ± 0.85	3.157 ± 0.51*	3.5 ± 0.51*, ‡
	Whole	1.422 ± 1.09	3.065 ± 0.186*, ‡	3.541 ± 0.395*, ‡
Cellularity (Mean ± Std. Dev.)	Medial	0.6389 ± 0.34	1.819 ± 0.226*	1.787 ± 0.234*
	Lateral	0.6528 ± 0.374	1.833 ± 0.284*	1.782 ± 0.239*
	Whole	0.6676 ± 0.312	1.802 ± 0.173*	1.791 ± 0.179*
Tidemark Integrity (Mean ± Std. Dev.)	Medial	0.3222 ± 0.398	0.9583 ± 0.0697	0.9815 ± 0.045
	Lateral	0.4167 ± 0.329	0.9074 ± 0.103	1.000 ± 0.00*
	Whole	0.3685 ± 0.347	0.9286 ± 0.0584	0.9907 ± 0.022*
Total Score (Mean ± Std. Dev.)	Medial	2.75 ± 2.29	8.833 ± 0.856*	9.500 ± 0.940*
	Lateral	3.157 ± 1.39	8.259 ± 1.13*	9.139 ± 1.12*, ‡
	Whole	2.987 ± 1.61	8.006 ± 0.465*	8.73 ± 0.872*, ‡

* denotes significant difference to Control. ◊ denotes significant difference between Rupture and Transection.
‡ denotes significant difference between 4 and 10 weeks.

A5. Abbreviations

AC - articular cartilage

ACL - Anterior Cruciate Ligament

AMB - Anteromedial bundle

ANOVA - Analysis of Variance

BM- MSC - Bone marrow-derived mesenchymal stem cell

C1,2C - type I and II degradation Col2 3/4 short assay

C2C - collagen type II cleavage

CD - cluster of differentiation

CDC - Center for Disease Control

CO_2 - Carbon Dioxide

Col - Collagen, gene

CPII - procollagen II carboxy propeptide

CRP - C-Reactive Protein

CS846 - aggrecan chondroitin sulfate 846 epitope

CT - computed tomography

ECM - extracellular matrix

ELISA - enzyme-linked immunosorbent assay

EPIC - Equilibrium Partitioning of an anionic Contrast Agent

GAG - glycosaminoglycan

GFP - green fluorescent protein

HA - hyaluronic acid

HSC - Hematopoeitic Stem Cell

IL - interleukin

KOOS - Knee Injury and Osteroarthritis score

LCL - Lateral Collateral Ligament

MCL - Medial Collateral Ligament

MFC – Medial Femoral Condyle

LFC – Lateral Femoral Condyle

MMP - matrix metalloproteinase

MRI - magnetic resonance imaging

MSC - Mesenchymal Stem Cell

OA - Osteoarthritis

PBS - phosphate-buffered saline

PG - proteoglycan

PLB - posterolateral bundle

PTOA - Post-traumatic Osteoarthritis

RBC - red blood cell

ROI - region of interest

Saf-O - safranin-O

sCPII - procollagen II C-propeptide

SD - Standard Deviation

SDF-1 - Stromal Derived Factor -1

sGAG - sulfated glycosaminoglycan

snoRNA - serum-level small non-coding RNA

TIMP - Tissue Inhibitor of Matrix Metalloproteinase

TNF-α - tumor necrosis factor alpha

uCTX-I - type I collagen C-telopeptide

uCTX-II - type II collagen C-telopeptide

WF6 - chondroitin sulfate epitope

WHO - World Health Organization

REFERENCES

Abbott, J.D., Huang, Y., Liu, D., Hickey, R., Krause, D.S., Giordano, F.J., 2004. Stromal cell–derived factor-1α plays a critical role in stem cell recruitment to the heart after myocardial infarction but is not sufficient to induce homing in the absence of injury. Circulation 110, 3300-3305.

Agung, M., Ochi, M., Yanada, S., Adachi, N., Izuta, Y., Yamasaki, T., Toda, K., 2006. Mobilization of bone marrow-derived mesenchymal stem cells into the injured tissues after intraarticular injection and their contribution to tissue regeneration. Knee Surgery, Sports Traumatology, Arthroscopy 14, 1307-1314.

Ait Si Selmi, T., Fithian, D., Neyret, P., 2006. The evolution of osteoarthritis in 103 patients with ACL reconstruction at 17 years follow-up. The Knee 13, 353-358.

Altman, R., Tenenbaum, J., Latta, L., Riskin, W., Blanco, L.N., Howell, D.S., 1984a. Biomechanical and biochemical properties of dog cartilage in experimentally induced osteoarthritis. Annals of the rheumatic diseases 43, 83-90.

Altman, R.D., Tenenbaum, J., Latta, L., Riskin, W., Blanco, L.N., Howell, D.S., 1984b. Biomechanical and biochemical properties of dog cartilage in experimentally induced osteoarthritis. Annals of the rheumatic diseases 43, 83-90.

Amis, A., Dawkins, G., 1991. Functional anatomy of the anterior cruciate ligament. Fibre bundle actions related to ligament replacements and injuries. Journal of Bone & Joint Surgery, British Volume 73, 260-267.

Anderson, D.D., Chubinskaya, S., Guilak, F., Martin, J.A., Oegema, T.R., Olson, S.A., Buckwalter, J.A., 2011. Post-traumatic osteoarthritis: Improved understanding and opportunities for early intervention. Journal of Orthopaedic Research 29, 802-809.

Appleton, C.T.G., McErlain, D.D., Pitelka, V., Schwartz, N., Bernier, S.M., Henry, J.L., Holdsworth, D.W., Beier, F., 2007. Forced mobilization accelerates pathogenesis: characterization of a preclinical surgical model of osteoarthritis. Arthritis research & therapy 9, R13.

Argentieri, E., Sturnick, D., DeSarno, M., Gardner-Morse, M., Slauterbeck, J., Johnson, R., Beynnon, B., 2014. Changes to the articular cartilage thickness profile of the tibia following anterior cruciate ligament injury. Osteoarthritis and Cartilage 22, 1453-1460.

Ashraf, S., Mapp, P.I., Walsh, D.A., 2011. Contributions of angiogenesis to inflammation, joint damage, and pain in a rat model of osteoarthritis. Arthritis & Rheumatism 63, 2700-2710.

Bayliss, M.T., Venn, M., Maroudas, A., Ali, S.Y., 1983. Structure of proteoglycans from different layers of human articular cartilage. Biochemical Journal 209, 387.

Benninghoff, A., 1925. Form und Bau der Gelenkknorpel in ihren Beziehungen zur Funktion. Cell and Tissue Research 2, 783-862.

Bin, S.-I., Nam, T.-S., 2007. Surgical outcome of 2-stage management of multiple knee ligament injuries after knee dislocation. Arthroscopy: The Journal of Arthroscopic & Related Surgery 23, 1066-1072.

Boden, B.P., Dean, G.S., Feagin, J., Garrett, W., 2000a. Mechanisms of anterior cruciate ligament injury. Orthopedics 23, 573-578.

Boden, B.P., Dean, G.S., Feagin Jr, J.A., Garrett Jr, W.E., 2000b. Mechanisms of anterior cruciate ligament injury. Orthopedics 23, 573-578.

Boden, B.P., Sheehan, F.T., Torg, J.S., Hewett, T.E., 2010. Noncontact anterior cruciate ligament injuries: mechanisms and risk factors. Journal of the American Academy of Orthopaedic Surgeons 18, 520-527.

Borrelli, J., Jr., Silva, M.J., Zaegel, M.A., Franz, C., Sandell, L.J., 2009. Single high-energy impact load causes posttraumatic OA in young rabbits via a decrease in cellular metabolism. J Orthop Res 27, 347-352.

Boyd, S.K., Matyas, J.R., Wohl, G.R., Kantzas, A., Zernicke, R.F., 2000. Early regional adaptation of periarticular bone mineral density after anterior cruciate ligament injury. Journal of applied physiology 89, 2359-2364.

Brophy, R.H., Kovacevic, D., Imhauser, C.W., Stasiak, M., Bedi, A., Fox, A.J., Deng, X.-H., Rodeo, S.A., 2011. Effect of short-duration low-magnitude cyclic loading versus immobilization on tendon-bone healing after ACL reconstruction in a rat model. The Journal of Bone & Joint Surgery 93, 381-393.

Brown, T.D., Johnston, R.C., Saltzman, C.L., Marsh, J.L., Buckwalter, J.A., 2006. Posttraumatic osteoarthritis: a first estimate of incidence, prevalence, and burden of disease. Journal of orthopaedic trauma 20, 739-744.

Buck, R., Wyman, B., Le Graverand, M.-P.H., Hudelmaier, M., Wirth, W., Eckstein, F., 2010. Osteoarthritis may not be a one-way-road of cartilage loss–comparison of spatial patterns of cartilage change between osteoarthritic and healthy knees. Osteoarthritis and Cartilage 18, 329-335.

Buckwalter, J., 2002. Articular cartilage injuries. Clinical Orthopaedics and Related Research 402, 21-37.

Buckwalter, J.A., Brown, T.D., 2004. Joint injury, repair, and remodeling: roles in post-traumatic osteoarthritis. Clinical Orthopaedics and Related Research 423, 7-16.

Burr, D.B., Gallant, M.A., 2012. Bone remodelling in osteoarthritis. Nature Reviews Rheumatology 8, 665-673.

Catterall, J., Stabler, T., Flannery, C., Kraus, V., 2010. Changes in serum and synovial fluid biomarkers after acute injury (NCT00332254). Arthritis Research and Therapy 12, R229.

Chen, F.H., Tuan, R.S., 2008. Mesenchymal stem cells in arthritic diseases. Arthritis Res Ther 10, 223.

Chockalingam, P.S., Glasson, S.S., Lohmander, L.S., 2012. Tenascin-C levels in synovial fluid are elevated after injury to the human and canine joint and correlate with markers of inflammation and matrix degradation. Osteoarthritis and Cartilage.

Christiansen, B., Anderson, M., Lee, C., Williams, J., Yik, J., Haudenschild, D., 2012a. Musculoskeletal changes following non-invasive knee injury using a novel mouse model of post-traumatic osteoarthritis. Osteoarthritis and Cartilage 20, 773-782.

Christiansen, B.A., Anderson, M.J., Lee, C.A., Williams, J.C., Yik, J.H., Haudenschild, D.R., 2012b. Musculoskeletal changes following non-invasive knee injury using a novel mouse model of post-traumatic osteoarthritis. Osteoarthritis Cartilage 20, 773-782.

Cignoni, P., Callieri, M., Corsini, M., Dellepiane, M., Ganovelli, F., Ranzuglia, G., Year Meshlab: an open-source mesh processing tool. In Eurographics Italian Chapter Conference.

Coates, E.E., Fisher, J.P., 2010. Phenotypic variations in chondrocyte subpopulations and their response to in vitro culture and external stimuli. Annals of biomedical engineering 38, 3371-3388.

Cohen, M., Amaro, J.T., Ejnisman, B., Carvalho, R.T., Nakano, K.K., Peccin, M.S., Teixeira, R., Laurino, C.F., Abdalla, R.J., 2007. Anterior cruciate ligament reconstruction after 10 to 15 years: association between meniscectomy and osteoarthrosis. Arthroscopy: The Journal of Arthroscopic & Related Surgery 23, 629-634.

Craig, J.G., Go, L., Blechinger, J., Hearshen, D., Bouffard, J.A., Diamond, M., van Holsbeeck, M.T., 2005. Three-tesla imaging of the knee: initial experience. Skeletal radiology 34, 453-461.

Crisan, M., Yap, S., Casteilla, L., Chen, C.-W., Corselli, M., Park, T.S., Andriolo, G., Sun, B., Zheng, B., Zhang, L., 2008. A perivascular origin for mesenchymal stem cells in multiple human organs. Cell stem cell 3, 301-313.

da Silva Meirelles, L., Chagastelles, P.C., Nardi, N.B., 2006. Mesenchymal stem cells reside in virtually all post-natal organs and tissues. Journal of cell science 119, 2204-2213.

Dell'Accio, F., Bari, C.D., Luyten, F.P., 2003. Microenvironment and phenotypic stability specify tissue formation by human articular cartilage-derived cells in vivo. Experimental cell research 287, 16-27.

DeMorat, G., Weinhold, P., Blackburn, T., Chudik, S., Garrett, W., 2004. Aggressive quadriceps loading can induce noncontact anterior cruciate ligament injury. The American journal of sports medicine 32, 477-483.

Dirschl, D.R., Marsh, J.L., Buckwalter, J.A., Gelberman, R., Olson, S.A., Brown, T.D., Llinias, A., 2004. Articular fractures. Journal of the American Academy of Orthopaedic Surgeons 12, 416-423.

Dodin, P., Pelletier, J.-P., Martel-Pelletier, J., Abram, F., 2010. Automatic human knee cartilage segmentation from 3-D magnetic resonance images. Biomedical Engineering, IEEE Transactions on 57, 2699-2711.

Doube, M., Kłosowski, M.M., Arganda-Carreras, I., Cordelières, F.P., Dougherty, R.P., Jackson, J.S., Schmid, B., Hutchinson, J.R., Shefelbine, S.J., 2010. BoneJ: Free and extensible bone image analysis in ImageJ. Bone 47, 1076-1079.

Duthon, V., Barea, C., Abrassart, S., Fasel, J., Fritschy, D., Menetrey, J., 2006. Anatomy of the anterior cruciate ligament. Knee Surgery, Sports Traumatology, Arthroscopy 14, 204-213.

Eckstein, F., Wirth, W., Lohmander, L., Hudelmaier, M., Frobell, R., 2015. Five-Year Followup of Knee Joint Cartilage Thickness Changes After Acute Rupture of the Anterior Cruciate Ligament. Arthritis & Rheumatology 67, 152-161.

Englund, M., Hunter, D., Gale, D., Clancy, M., Guermazi, A., Aliabadi, P., Felson, D., 2006. Prevalence of anterior cruciate ligament tear and its association with knee osteoarthritis and giving way among older adults in the community. Osteoarthritis and Cartilage 14, S121.

Eyre, D., Wu, J., 1987. Type XI or 1a2a3a collagen, in: Mayne, R., Burgeson, R. (Eds.), Structure and Function of Collagen Types. Academic Prress, New York, NY, pp. 261-281.

Feller, J., 2004. Anterior cruciate ligament rupture: is osteoarthritis inevitable? British Journal of Sports Medicine 38, 383-384.

Ferry, T., Bergström, U., Hedström, E.M., Lorentzon, R., Zeisig, E., 2013. Epidemiology of acute knee injuries seen at the Emergency Department at Umeå University Hospital, Sweden, during 15 years. Knee Surgery, Sports Traumatology, Arthroscopy, 1-7.

Florea, C., Malo, M., Rautiainen, J., Mäkelä, J., Fick, J., Nieminen, M., Jurvelin, J., Davidescu, A., Korhonen, R., 2014. Alterations in subchondral bone plate, trabecular bone and articular cartilage properties of rabbit femoral condyles at 4 weeks after anterior cruciate ligament transection. Osteoarthritis and Cartilage.

Fox, A.J.S., Bedi, A., Rodeo, S.A., 2009. The basic science of articular cartilage: structure, composition, and function. Sports Health: A Multidisciplinary Approach 1, 461-468.

Frobell, R., Lohmander, L., Roos, H., 2007. Acute rotational trauma to the knee: poor agreement between clinical assessment and magnetic resonance imaging findings. Scandinavian journal of medicine & science in sports 17, 109-114.

Furman, B.D., Strand, J., Hembree, W.C., Ward, B.D., Guilak, F., Olson, S.A., 2007. Joint degeneration following closed intraarticular fracture in the mouse knee: a model of posttraumatic arthritis. J Orthop Res 25, 578-592.

Gao, B., Zheng, N.N., 2010. Alterations in three-dimensional joint kinematics of anterior cruciate ligament-deficient and-reconstructed knees during walking. Clinical Biomechanics 25, 222-229.

Gardiner, J.C., Weiss, J.A., 2003. Subject-specific finite element analysis of the human medial collateral ligament during valgus knee loading. Journal of Orthopaedic Research 21, 1098-1106.

Gianotti, S.M., Marshall, S.W., Hume, P.A., Bunt, L., 2009. Incidence of anterior cruciate ligament injury and other knee ligament injuries: a national population-based study. Journal of Science and Medicine in Sport 12, 622-627.

Gillquist, J., Messner, K., 1999. Anterior cruciate ligament reconstruction and the long term incidence of gonarthrosis. Sports Medicine 27, 143-156.

Goodwin, W., McCabe, D., Sauter, E., Reese, E., Walter, M., Buckwalter, J.A., Martin, J.A., 2010. Rotenone prevents impact-induced chondrocyte death. Journal of Orthopaedic Research 28, 1057-1063.

Green, D., Noble, P., BocellJr, J., Ahuero, J., Poteet, B., Birdsall, H., 2006. Effect of early full weight-bearing after joint injury on inflammation and cartilage degradation. The Journal of Bone & Joint Surgery 88, 2201-2209.

Guilak, F., Ratcliffe, A., Lane, N., Rosenwasser, M.P., Mow, V.C., 1994a. Mechanical and biochemical changes in the superficial zone of articular cartilage in canine experimental osteoarthritis. Journal of Orthopaedic Research 12, 474-484.

Guilak, F., Ratcliffe, A., Lane, N., Rosenwasser, M.P., Mow, V.C., 1994b. Mechanical and biochemical changes in the superficial zone of articular cartilage in canine experimental osteoarthritis. J Orthop Res 12, 474-484.

Hagg, R., Bruckner, P., Hedbom, E., 1998. Cartilage fibrils of mammals are biochemically heterogeneous: differential distribution of decorin and collagen IX. The Journal of cell biology 142, 285-294.

Hashimoto, S., Creighton-Achermann, L., Takahashi, K., Amiel, D., Coutts, R., Lotz, M., 2002a. Development and regulation of osteophyte formation during experimental osteoarthritis. Osteoarthritis and Cartilage 10, 180-187.

Hashimoto, S., Creighton-Achermann, L., Takahashi, K., Amiel, D., Coutts, R.D., Lotz, M., 2002b. Development and regulation of osteophyte formation during experimental osteoarthritis. Osteoarthritis Cartilage 10, 180-187.

Haugen, I.K., Englund, M., Aliabadi, P., Niu, J., Clancy, M., Kvien, T.K., Felson, D.T., 2011. Prevalence, incidence and progression of hand osteoarthritis in the general population: the Framingham Osteoarthritis Study. Annals of the rheumatic diseases 70, 1581-1586.

Hayami, T., Pickarski, M., Zhuo, Y., Wesolowski, G.A., Rodan, G.A., Duong le, T., 2006. Characterization of articular cartilage and subchondral bone changes in the rat anterior cruciate ligament transection and meniscectomized models of osteoarthritis. Bone 38, 234-243.

Helmick, C.G., Felson, D.T., Lawrence, R.C., Gabriel, S., Hirsch, R., Kwoh, C.K., Liang, M.H., Kremers, H.M., Mayes, M.D., Merkel, P.A., 2008. Estimates of the prevalence of arthritis and other rheumatic conditions in the United States: Part I. Arthritis & Rheumatism 58, 15-25.

Higuchi, H., Shirakura, K., Kimura, M., Terauchi, M., Shinozaki, T., Watanabe, H., Takagishi, K., 2006. Changes in biochemical parameters after anterior cruciate ligament injury. International orthopaedics 30, 43-47.

Hollis, J., Takai, S., Adams, D., Horibe, S., Woo, S., 1991. The effects of knee motion and external loading on the length of the anterior cruciate ligament (ACL): a kinematic study. Journal of biomechanical engineering 113, 208.

Hong, H.S., Lee, J., Lee, E., Kwon, Y.S., Lee, E., Ahn, W., Jiang, M.H., Kim, J.C., Son, Y., 2009. A new role of substance P as an injury-inducible messenger for mobilization of CD29+ stromal-like cells. Nature medicine 15, 425-435.

Horie, M., Sekiya, I., Muneta, T., Ichinose, S., Matsumoto, K., Saito, H., Murakami, T., Kobayashi, E., 2009. Intra-articular Injected Synovial Stem Cells Differentiate into Meniscal Cells Directly and Promote Meniscal Regeneration Without Mobilization to Distant Organs in Rat Massive Meniscal Defect. Stem Cells 27, 878-887.

Hulspas, R., 2010. Titration of Fluorochrome-Conjugated Antibodies for Labeling Cell Surface Markers on Live Cells. Current Protocols in Cytometry, 6.29. 21-26.29. 29.

Hunter, W., 1995. Of the structure and disease of articulating cartilages. 1743. Clin Orthop Relat Res 317, 3-6.

Intema, F., Hazewinkel, H., Gouwens, D., Bijlsma, J., Weinans, H., Lafeber, F., Mastbergen, S., 2010. In early OA, thinning of the subchondral plate is directly related to cartilage damage: results from a canine ACLT-meniscectomy model. Osteoarthritis and Cartilage 18, 691-698.

Jansen, H., Frey, S.P., Paletta, J., Meffert, R.H., 2011. Effects of low-energy NMR on posttraumatic osteoarthritis: observations in a rabbit model. Archives of orthopaedic and trauma surgery 131, 863-868.

Jansen, H., Meffert, R., Birkenfeld, F., Petersen, W., Pufe, T., 2012. Detection of vascular endothelial growth factor (VEGF) in moderate osteoarthritis in a rabbit model. Annals of Anatomy-Anatomischer Anzeiger 194, 452-456.

Järvelä, T., Paakkala, T., Kannus, P., Järvinen, M., 2001. The incidence of patellofemoral osteoarthritis and associated findings 7 years after anterior cruciate ligament reconstruction with a bone-patellar tendon-bone autograft. The American journal of sports medicine 29, 18-24.

Jones, E.A., Crawford, A., English, A., Henshaw, K., Mundy, J., Corscadden, D., Chapman, T., Emery, P., Hatton, P., McGonagle, D., 2008. Synovial fluid mesenchymal stem cells in health and early osteoarthritis: Detection and functional evaluation at the single-cell level. Arthritis & Rheumatism 58, 1731-1740.

Jones, H., Rocha, P.C., 2012. Prevention in ACL Injuries, Sports Injuries. Springer, pp. 33-42.

Jones, M.D., Tran, C.W., Li, G., Maksymowych, W.P., Zernicke, R.F., Doschak, M.R., 2010. In vivo microfocal computed tomography and micro-magnetic resonance imaging evaluation of antiresorptive and antiinflammatory drugs as preventive treatments of osteoarthritis in the rat. Arthritis Rheum 62, 2726-2735.

Kadonishi, Y., Deie, M., Takata, T., Ochi, M., 2012. Acceleration of tendon–bone healing in anterior cruciate ligament reconstruction using an enamel matrix derivative in a rat model. Journal of Bone & Joint Surgery, British Volume 94, 205-209.

Karsdal, M., Leeming, D., Dam, E., Henriksen, K., Alexandersen, P., Pastoureau, P., Altman, R., Christiansen, C., 2008. Should subchondral bone turnover be targeted when treating osteoarthritis? Osteoarthritis and cartilage 16, 638-646.

Kitaori, T., Ito, H., Schwarz, E.M., Tsutsumi, R., Yoshitomi, H., Oishi, S., Nakano, M., Fujii, N., Nagasawa, T., Nakamura, T., 2009. Stromal cell–derived factor 1/CXCR4 signaling is critical for the recruitment of mesenchymal stem cells to the fracture site during skeletal repair in a mouse model. Arthritis & Rheumatism 60, 813-823.

Koga, H., Nakamae, A., Shima, Y., Iwasa, J., Myklebust, G., Engebretsen, L., Bahr, R., Krosshaug, T., 2010. Mechanisms for noncontact anterior cruciate ligament injuries knee joint kinematics in 10 injury situations from female team handball and basketball. Am J Sports Med 38, 2218-2225.

Kotwal, N., Li, J., Sandy, J., Plaas, A., Sumner, D.R., 2012. Initial application of EPIC-μCT to assess mouse articular cartilage morphology and composition: effects of aging and treadmill running. Osteoarthritis and Cartilage 20, 887-895.

Kraus, V.B., Huebner, J.L., DeGroot, J., Bendele, A., 2010. The OARSI histopathology initiative–recommendations for histological assessments of osteoarthritis in the guinea pig. Osteoarthritis and Cartilage 18, S35-S52.

Krosshaug, T., Nakamae, A., Boden, B.P., Engebretsen, L., Smith, G., Slauterbeck, J.R., Hewett, T.E., Bahr, R., 2007. Mechanisms of anterior cruciate ligament injury in basketball video analysis of 39 cases. The American journal of sports medicine 35, 359-367.

Lapidot, T., Dar, A., Kollet, O., 2005. How do stem cells find their way home? Blood 106, 1901-1910.

Lau, T.T., Wang, D.-A., 2011. Stromal cell-derived factor-1 (SDF-1): homing factor for engineered regenerative medicine. Expert opinion on biological therapy 11, 189-197.

Lawrence, R.C., Felson, D.T., Helmick, C.G., Arnold, L.M., Choi, H., Deyo, R.A., Gabriel, S., Hirsch, R., Hochberg, M.C., Hunder, G.G., 2008. Estimates of the prevalence of arthritis and other rheumatic conditions in the United States: Part II. Arthritis & Rheumatism 58, 26-35.

Lee, J.K., Yao, L., Phelps, C.T., Wirth, C., Czajka, J., Lozman, J., 1988. Anterior cruciate ligament tears: MR imaging compared with arthroscopy and clinical tests. Radiology 166, 861-864.

Levine, J.W., Kiapour, A.M., Quatman, C.E., Wordeman, S.C., Goel, V.K., Hewett, T.E., Demetropoulos, C.K., 2013. Clinically relevant injury patterns after an anterior cruciate ligament injury provide insight into injury mechanisms. Am J Sports Med 41, 385-395.

Levy, B.A., Dajani, K.A., Whelan, D.B., Stannard, J.P., Fanelli, G.C., Stuart, M.J., Boyd, J.L., MacDonald, P.A., Marx, R.G., 2009. Decision making in the multiligament-injured knee: an evidence-based systematic review. Arthroscopy: The Journal of Arthroscopic & Related Surgery 25, 430-438.

Lindhorst, E., Vail, T., Guilak, F., Wang, H., Setton, L., Vilim, V., Kraus, V., 2000. Longitudinal characterization of synovial fluid biomarkers in the canine meniscectomy model of osteoarthritis. Journal of Orthopaedic Research 18, 269-280.

Lockwood, K.A., Chu, B.T., Anderson, M.J., Haudenschild, D.R., Christiansen, B.A., 2013. Comparison of loading rate-dependent injury modes in a murine model of post-traumatic osteoarthritis. J Orthop Res.

Lockwood, K.A., Chu, B.T., Anderson, M.J., Haudenschild, D.R., Christiansen, B.A., 2014. Comparison of loading rate-dependent injury modes in a murine model of post-traumatic osteoarthritis. J Orthop Res 32, 79-88.

Lohmander, L., Östenberg, A., Englund, M., Roos, H., 2004. High prevalence of knee osteoarthritis, pain, and functional limitations in female soccer players twelve years after anterior cruciate ligament injury. Arthritis & Rheumatism 50, 3145-3152.

Lohmander, L.S., Atley, L.M., Pietka, T.A., Eyre, D.R., 2003. The release of crosslinked peptides from type II collagen into human synovial fluid is increased soon after joint injury and in osteoarthritis. Arthritis & Rheumatism 48, 3130-3139.

Lohmander, L.S., Englund, P.M., Dahl, L.L., Roos, E.M., 2007. The long-term consequence of anterior cruciate ligament and meniscus injuries osteoarthritis. The American journal of sports medicine 35, 1756-1769.

Lohmander, S., Roos, H., Dahlberg, L., Hoerrner, L.A., Lark, M.W., 1994. Temporal patterns of stromelysin-1, tissue inhibitor, and proteoglycan fragments in human knee joint fluid after injury to the cruciate ligament or meniscus. Journal of Orthopaedic Research 12, 21-28.

Louboutin, H., Debarge, R., Richou, J., Selmi, T.A.S., Donell, S.T., Neyret, P., Dubrana, F., 2009. Osteoarthritis in patients with anterior cruciate ligament rupture: a review of risk factors. The Knee 16, 239-244.

Maerz, T., Kurdziel, M., Davidson, A., Baker, K., Anderson, K., Matthew, H., 2015. Biomechanical Characterization of a Model of Noninvasive, Traumatic Anterior Cruciate Ligament Injury in the Rat. Annals of biomedical engineering Accepted and processing.

Mankin, H.J., Grodzinsky, A., Buckwalter, J.A., 2007. Articular Cartilage and Osteoarthritis, in: Einhorn, T. (Ed.), Orthopaedic Basic Science: Foundations of Clinical Practice, 3 ed. American Academy of Orthopaedic Surgeons, Chicago, IL.

Martin, J., Buckwalter, J., 2006a. Post-traumatic osteoarthritis: the role of stress induced chondrocyte damage. Biorheology 43, 517-521.

Martin, J.A., Buckwalter, J.A., 2006b. Post-traumatic osteoarthritis: the role of stress induced chondrocyte damage. Biorheology 43, 517-521.

Martin, J.A., McCabe, D., Walter, M., Buckwalter, J.A., McKinley, T.O., 2009. N-acetylcysteine inhibits post-impact chondrocyte death in osteochondral explants. The Journal of Bone & Joint Surgery 91, 1890-1897.

Mazzocca, A.D., Nissen, C.W., Geary, M., Adams, D.J., 2003. Valgus medial collateral ligament rupture causes concomitant loading and damage of the anterior cruciate ligament. The journal of knee surgery 16, 148-151.

Meyer, E.G., Haut, R.C., 2005. Excessive compression of the human tibio-femoral joint causes ACL rupture. Journal of biomechanics 38, 2311-2316.

Meyer, E.G., Haut, R.C., 2008. Anterior cruciate ligament injury induced by internal tibial torsion or tibiofemoral compression. Journal of biomechanics 41, 3377-3383.

Mifune, Y., Matsumoto, T., Takayama, K., Terada, S., Sekiya, N., Kuroda, R., Kurosaka, M., Fu, F.H., Huard, J., 2013. Tendon graft revitalization using adult anterior cruciate ligament (ACL)-derived CD34+ cell sheets for ACL reconstruction. Biomaterials 34, 5476-5487.

Mollenhauer, J., Bee, J.A., Lizarbe, M.A., Von Der Mark, K., 1984. Role of anchorin CII, a 31,000-mol-wt membrane protein, in the interaction of chondrocytes with type II collagen. The Journal of cell biology 98, 1572-1579.

Morito, T., Muneta, T., Hara, K., Ju, Y.-J., Mochizuki, T., Makino, H., Umezawa, A., Sekiya, I., 2008. Synovial fluid-derived mesenchymal stem cells increase after intra-articular ligament injury in humans. Rheumatology 47, 1137-1143.

Motawi, T.M., Atta, H.M., Sadik, N.A., Azzam, M., 2014. The therapeutic effects of bone marrow-derived mesenchymal stem cells and simvastatin in a rat model of liver fibrosis. Cell biochemistry and biophysics 68, 111-125.

Mullen, P., Tong, Y., Alliez, P., Desbrun, M., Year Spectral conformal parameterization. In Computer Graphics Forum.

Myklebust, G., Bahr, R., 2005. Return to play guidelines after anterior cruciate ligament surgery. British Journal of Sports Medicine 39, 127-131.

Nagaya, N., Kangawa, K., Itoh, T., Iwase, T., Murakami, S., Miyahara, Y., Fujii, T., Uematsu, M., Ohgushi, H., Yamagishi, M., 2005. Transplantation of mesenchymal stem cells

improves cardiac function in a rat model of dilated cardiomyopathy. Circulation 112, 1128-1135.

Nakamae, A., Engebretsen, L., Bahr, R., Krosshaug, T., Ochi, M., 2006. Natural history of bone bruises after acute knee injury: clinical outcome and histopathological findings. Knee Surgery, Sports Traumatology, Arthroscopy 14, 1252-1258.

Nebelung, W., Wuschech, H., 2005. Thirty-five Years of Follow-up of Anterior Cruciate Ligament—Deficient Knees in High-Level Athletes. Arthroscopy: The Journal of Arthroscopic & Related Surgery 21, 696-702.

Neuman, P., Kostogiannis, I., Friden, T., Roos, H., Dahlberg, L., Englund, M., 2009. Patellofemoral osteoarthritis 15 years after anterior cruciate ligament injury–a prospective cohort study. Osteoarthritis and Cartilage 17, 284-290.

Newman, A.P., 1998. Articular cartilage repair. The American journal of sports medicine 26, 309-324.

Nohmi, S., Yamamoto, Y., Mizukami, H., Ishibashi, Y., Tsuda, E., Maniwa, K., Yagihashi, S., Motomura, S., Toh, S., Furukawa, K.-I., 2012. Post injury changes in the properties of mesenchymal stem cells derived from human anterior cruciate ligaments. International orthopaedics 36, 1515-1522.

Onur, T.S., Wu, R., Chu, S., Chang, W., Kim, H.T., Dang, A.B., 2013. Joint instability and cartilage compression in a mouse model of posttraumatic osteoarthritis. J Orthop Res.

Onur, T.S., Wu, R., Chu, S., Chang, W., Kim, H.T., Dang, A.B., 2014. Joint instability and cartilage compression in a mouse model of posttraumatic osteoarthritis. J Orthop Res 32, 318-323.

Palmer, A.W., Guldberg, R.E., Levenston, M.E., 2006. Analysis of cartilage matrix fixed charge density and three-dimensional morphology via contrast-enhanced microcomputed tomography. Proceedings of the National Academy of Sciences 103, 19255-19260.

Peterfy, C., Guermazi, A., Zaim, S., Tirman, P., Miaux, Y., White, D., Kothari, M., Lu, Y., Fye, K., Zhao, S., 2004. Whole-organ magnetic resonance imaging score (WORMS) of the knee in osteoarthritis. Osteoarthritis and Cartilage 12, 177-190.

Pruksakorn, D., Rojanasthien, S., Pothacharoen, P., Luevitoonvechkij, S., Wongtreratanachai, P., Ong-chai, S., Kongtawelert, P., 2009. Chondroitin sulfate epitope (WF6) and hyaluronic acid as serum markers of cartilage degeneration in patients following anterior cruciate ligament injury. Journal of Science and Medicine in Sport 12, 445-448.

Quatman, C.E., Hewett, T.E., 2009. The anterior cruciate ligament injury controversy: is “valgus collapse” a sex-specific mechanism? British journal of sports medicine 43, 328-335.

Quatman, C.E., Kiapour, A.M., Demetropoulos, C.K., Kiapour, A., Wordeman, S.C., Levine, J.W., Goel, V.K., Hewett, T.E., 2013. Preferential Loading of the ACL Compared With the MCL During Landing A Novel In Sim Approach Yields the Multiplanar Mechanism of Dynamic Valgus During ACL Injuries. Am J Sports Med, 0363546513506558.

Rochefort, G.Y., Delorme, B., Lopez, A., Herault, O., Bonnet, P., Charbord, P., Eder, V., Domenech, J., 2006. Multipotential mesenchymal stem cells are mobilized into peripheral blood by hypoxia. Stem Cells 24, 2202-2208.

Roemer, F.W., Frobell, R., Lohmander, L.S., Niu, J., Guermazi, A., 2014. Anterior Cruciate Ligament OsteoArthritis Score (ACLOAS): Longitudinal MRI-based whole joint assessment of anterior cruciate ligament injury. Osteoarthritis and Cartilage 22, 668-682.

Roos, H., Adalberth, T., Dahlberg, L., Lohmander, L.S., 1995. Osteoarthritis of the knee after injury to the anterior cruciate ligament or meniscus: the influence of time and age. Osteoarthritis and Cartilage 3, 261-267.

Roughley, P.J., White, R., 1980. Age-related changes in the structure of the proteoglycan subunits from human articular cartilage. J Biol Chem 255, 217-224.

Ruan, M.Z., Dawson, B., Jiang, M.M., Gannon, F., Heggeness, M., Lee, B.H., 2013a. Quantitative imaging of murine osteoarthritic cartilage by phase-contrast micro–computed tomography. Arthritis & Rheumatism 65, 388-396.

Ruan, M.Z., Erez, A., Guse, K., Dawson, B., Bertin, T., Chen, Y., Jiang, M.M., Yustein, J., Gannon, F., Lee, B.H., 2013b. Proteoglycan 4 expression protects against the development of osteoarthritis. Sci Transl Med 5, 176ra134.

Sage, D., Prodanov, D., Tinevez, J., Schindelin, J., Year MIJ: Making Interoperability Between ImageJ and Matlab Possible. In ImageJ User & Developer Conference. Luxembourg.

Sakaguchi, Y., Sekiya, I., Yagishita, K., Muneta, T., 2005. Comparison of human stem cells derived from various mesenchymal tissues: superiority of synovium as a cell source. Arthritis & Rheumatism 52, 2521-2529.

Sankar, W.N., Wells, L., Sennett, B.J., Wiesel, B.B., Ganley, T.J., 2006. Combined anterior cruciate ligament and medial collateral ligament injuries in adolescents. Journal of Pediatric Orthopaedics 26, 733-736.

Schaible, H.G., von Banchet, G.S., Boettger, M., Bräuer, R., Gajda, M., Richter, F., Hensellek, S., Brenn, D., Natura, G., 2010. The role of proinflammatory cytokines in the generation and maintenance of joint pain. Annals of the New York Academy of Sciences 1193, 60-69.

Schett, G., 2011. Effects of inflammatory and anti-inflammatory cytokines on the bone. European journal of clinical investigation 41, 1361-1366.

Schindelin, J., Arganda-Carreras, I., Frise, E., Kaynig, V., Longair, M., Pietzsch, T., Preibisch, S., Rueden, C., Saalfeld, S., Schmid, B., 2012. Fiji: an open-source platform for biological-image analysis. Nature methods 9, 676-682.

Sekiya, I., Ojima, M., Suzuki, S., Yamaga, M., Horie, M., Koga, H., Tsuji, K., Miyaguchi, K., Ogishima, S., Tanaka, H., 2012. Human mesenchymal stem cells in synovial fluid increase in the knee with degenerated cartilage and osteoarthritis. Journal of Orthopaedic Research 30, 943-949.

Shelbourne, K.D., Davis, T.J., Klootwyk, T.E., 1998. The relationship between intercondylar notch width of the femur and the incidence of anterior cruciate ligament tears A prospective study. The American journal of sports medicine 26, 402-408.

Shin, C.S., Chaudhari, A.M., Andriacchi, T.P., 2009. The effect of isolated valgus moments on ACL strain during single-leg landing: a simulation study. Journal of biomechanics 42, 280-285.

Singer, N.G., Caplan, A.I., 2011. Mesenchymal stem cells: mechanisms of inflammation. Annual Review of Pathology: Mechanisms of Disease 6, 457-478.

Sprigg, N., Bath, P.M., Zhao, L., Willmot, M.R., Gray, L.J., Walker, M.F., Dennis, M.S., Russell, N., 2006. Granulocyte-Colony–Stimulating Factor Mobilizes Bone Marrow Stem Cells in Patients With Subacute Ischemic Stroke The Stem Cell Trial of Recovery EnhanceMent After Stroke (STEMS) Pilot Randomized, Controlled Trial (ISRCTN 16784092). Stroke 37, 2979-2983.

Steinert, A.F., Kunz, M., Prager, P., Barthel, T., Jakob, F., Nöth, U., Murray, M.M., Evans, C.H., Porter, R.M., 2011. Mesenchymal stem cell characteristics of human anterior cruciate ligament outgrowth cells. Tissue Engineering Part A 17, 1375-1388.

Strobel, M.J., Schulz, M.S., Petersen, W.J., Eichhorn, H.J., 2006. Combined anterior cruciate ligament, posterior cruciate ligament, and posterolateral corner reconstruction with autogenous hamstring grafts in chronic instabilities. Arthroscopy: The Journal of Arthroscopic & Related Surgery 22, 182-192.

Su, F., Hilton, J., Nardo, L., Wu, S., Liang, F., Link, T., Ma, C., Li, X., 2013. Cartilage morphology and T< sub> 1ρ</sub> and T< sub> 2</sub> quantification in ACL-reconstructed knees: a 2-year follow-up. Osteoarthritis and Cartilage 21, 1058-1067.

Svoboda, S.J., Harvey, T.M., Owens, B.D., Brechue, W.F., Tarwater, P.M., Cameron, K.L., 2013. Changes in Serum Biomarkers of Cartilage Turnover After Anterior Cruciate Ligament Injury. The American journal of sports medicine 41, 2108-2116.

Tang, Z., Yang, L., Wang, Y., Xue, R., Zhang, J., Huang, W., Chen, P.C., Sung, K.L., 2009a. Contributions of different intraarticular tissues to the acute phase elevation of synovial fluid MMP-2 following rat ACL rupture. J. Orthop. Res. 27, 243-248.

Tang, Z., Yang, L., Wang, Y., Xue, R., Zhang, J., Huang, W., Chen, P.C., Sung, K.L., 2009b. Contributions of different intraarticular tissues to the acute phase elevation of synovial fluid MMP-2 following rat ACL rupture. Journal of orthopaedic research 27, 243-248.

Tang, Z., Yang, L., Zhang, J., Xue, R., Wang, Y., Chen, P.C., Sung, K.-L.P., 2009c. Coordinated expression of MMPs and TIMPs in rat knee intra-articular tissues after ACL injury. Connective tissue research 50, 315-322.

Tchetverikov, I., Lohmander, L., Verzijl, N., Huizinga, T., TeKoppele, J., Hanemaaijer, R., DeGroot, J., 2005. MMP protein and activity levels in synovial fluid from patients with joint injury, inflammatory arthritis, and osteoarthritis. Annals of the rheumatic diseases 64, 694-698.

Tourville, T.W., Johnson, R.J., Slauterbeck, J.R., Naud, S., Beynnon, B.D., 2013. Relationship Between Markers of Type II Collagen Metabolism and Tibiofemoral Joint Space Width Changes After ACL Injury and Reconstruction. The American journal of sports medicine 41, 779-787.

Uhorchak, J.M., Scoville, C.R., Williams, G.N., Arciero, R.A., Pierre, P.S., Taylor, D.C., 2003. Risk Factors Associated with Noncontact Injury of the Anterior Cruciate Ligament A Prospective Four-Year Evaluation of 859 West Point Cadets. The American journal of sports medicine 31, 831-842.

Viskontas, D.G., Giuffre, B.M., Duggal, N., Graham, D., Parker, D., Coolican, M., 2008. Bone Bruises Associated With ACL Rupture Correlation With Injury Mechanism. The American journal of sports medicine 36, 927-933.

Von Porat, A., Roos, E., Roos, H., 2004. High prevalence of osteoarthritis 14 years after an anterior cruciate ligament tear in male soccer players: a study of radiographic and patient relevant outcomes. Annals of the rheumatic diseases 63, 269-273.

Walsh, N.C., Crotti, T.N., Goldring, S.R., Gravallese, E.M., 2005. Rheumatic diseases: the effects of inflammation on bone. Immunological reviews 208, 228-251.

Wei, S., Kitaura, H., Zhou, P., Ross, F.P., Teitelbaum, S.L., 2005. IL-1 mediates TNF-induced osteoclastogenesis. Journal of Clinical Investigation 115, 282.

Widuchowski, W., Widuchowski, J., Trzaska, T., 2007. Articular cartilage defects: study of 25,124 knee arthroscopies. The Knee 14, 177-182.

Williams, A., Qian, Y., Golla, S., Chu, C., 2012. UTE-T2∗ mapping detects sub-clinical meniscus injury after anterior cruciate ligament tear. Osteoarthritis and Cartilage 20, 486-494.

Woolf, A.D., Pfleger, B., 2003. Burden of major musculoskeletal conditions. Bulletin of the World Health Organization 81, 646-656.

Wu, Y., Yang, R., Chen, P., Sung, K.P., 2009. The profile of MMP and TIMP in injured rat ACL. Mol Cell Biomech 7, 115-1124.

Xie, L., Lin, A.S., Guldberg, R.E., Levenston, M.E., 2010. Nondestructive assessment of sGAG content and distribution in normal and degraded rat articular cartilage< i> via</i> EPIC-μCT. Osteoarthritis and Cartilage 18, 65-72.

Xue, R., Yang, L., Tang, Z., Zhang, J., Wang, Y., Tang, X., Jiang, J., Wu, Y., Yang, R., Chen, P., Sung, K.P., 2009. The profile of MMP and TIMP in injured rat ACL. Molecular Cellular 7, 115-124.

Yagi, H., Soto-Gutierrez, A., Parekkadan, B., Kitagawa, Y., Tompkins, R.G., Kobayashi, N., Yarmush, M.L., 2010. Mesenchymal stem cells: mechanisms of immunomodulation and homing. Cell transplantation 19, 667.

Yamada, M., Kubo, H., Kobayashi, S., Ishizawa, K., Numasaki, M., Ueda, S., Suzuki, T., Sasaki, H., 2004. Bone marrow-derived progenitor cells are important for lung repair after lipopolysaccharide-induced lung injury. The Journal of Immunology 172, 1266-1272.

Yoon, K.H., Yoo, J.H., Kim, K.-I., 2011. Bone contusion and associated meniscal and medial collateral ligament injury in patients with anterior cruciate ligament rupture. The Journal of Bone & Joint Surgery 93, 1510-1518.

Yoshimura, H., Muneta, T., Nimura, A., Yokoyama, A., Koga, H., Sekiya, I., 2007. Comparison of rat mesenchymal stem cells derived from bone marrow, synovium, periosteum, adipose tissue, and muscle. Cell and tissue research 327, 449-462.

Yu, B., Garrett, W.E., 2007. Mechanisms of non-contact ACL injuries. British Journal of Sports Medicine 41, i47-i51.

Zhang, L., Yang, M., Marks, P., White, L., Hurtig, M., Divine, G., Gibson, G., 2012. Serum non-coding RNAs as biomarkers for osteoarthritis progression after ACL injury. Osteoarthritis and Cartilage.

Zohlnhöfer, D., Ott, I., Mehilli, J., Schömig, K., Michalk, F., Ibrahim, T., Meisetschläger, G., von Wedel, J., Bollwein, H., Seyfarth, M., 2006. Stem cell mobilization by granulocyte colony-stimulating factor in patients with acute myocardial infarction. JAMA: the journal of the American Medical Association 295, 1003-1010.

ABSTRACT

BIOMECHANICAL AND BIOLOGICAL EVALUATION OF A MODEL OF POST-TRAUMATIC OSTEOARTHRITIS FOLLOWING NONINVASIVE, TRAUMATIC RUPTURE OF THE ANTERIOR CRUCIATE LIGAMENT

by

TRISTAN MAERZ

August 2015

Advisor: Dr. Howard Matthew

Major: Biomedical Engineering

Degree: Doctor of Philosophy

Post-traumatic osteoarthritis (PTOA) is a prevalent condition following rupture of the anterior cruciate ligament (ACL). While numerous animal models of PTOA exist, most are based on surgical disruption of a stabilizing structure. In the rat, surgical ACL transection is the most commonly employed model, but it may introduce confounding biological factors due to surgery. The purpose of this dissertation was to utilize the tibial compression model of ACL injury to induce a noninvasive ACL rupture in the rat. First, a biomechanical characterization of four different loading protocols was undertaken, and a high-speed, high-displacement protocol was deemed optimal for inducing a repeatable, complete ACL injury. Tibiofemoral joint motion was found to be representative of motion during human injury. Next, a chronic, biological comparison of the noninvasive injury model to the surgical ACL transection model was performed. Results indicate that the two models both cause extensive degenerative joint changes, and articular cartilage degeneration was most profound in the medial compartment of the femur. The two models yield in a differential bony remodeling response, and surgical ACL transection causes more drastic degenerative changes of articular cartilage. Furthermore, the ACL

transection group had elevated biomarkers of cartilage breakdown compared to the noninvasive rupture group. Lastly, the acute response following noninvasive and surgical injury was investigated. Both injuries cause the systemic mobilization of mesenchymal stem cells (MSCs) and elevated stromal-cell derived factor (SDF-1) concentrations in the joint acutely. Biomarkers of cartilage breakdown and metabolism are elevated only slightly immediately after injury. In conclusion, while some studies may benefit from the more rapid onset of PTOA in the surgical ACL transection model, a noninvasive injury model avoids confounding biological factors and may be beneficial for future studies assessing pathology or potential treatment strategies.

AUTOBIOGRAPHICAL STATEMENT

I was born and raised in 1987 in a small town in southwestern Germany. The remains of old Roman buildings would be the front of the city flyer, but I spent most of my childhood riding my bike around the outskirts of the town amongst orchards and farms together with friends. My parents Birgit and Dietrich had lots of help from the grandparents and great-grandparents, and together with my sisters Julia and Jennifer, I got to spend lots of time with the elders of the family. My memories of elementary school mainly involve playing outside, learning the piano, assembling Legos, and defending myself against my sisters. At age 12, my father received an employment opportunity in Metro Detroit, and my family and I moved to the U.S with an unspecified return date. After acclimating in yet another small town, sports became the compass of daily activities. High school was spent with friends in the gym, on the soccer field, or in my Jeep Wrangler. The piano and classical music became close friends as well, and my parents took me to several music competitions throughout my high school years. A career focus began to emerge in the latter part of high school when I realized that I could combine my passion for engineering with my passion for sports, and the prospect for a biomedical engineering education was confirmed after choosing Lawrence Technological University for my undergraduate degree. I embraced the desk as my new companion, and many new friends were made during the standard extracurricular college activities. I received a full-time job offer from the Orthopaedic research laboratory at Beaumont hospital immediately after completing my Bachelor's degree, and my employment has continued there to date. I completed my Master's degree in biomedical engineering at Wayne State University while working at Beaumont, and the pursuit of the doctoral degree followed immediately. Having now completed my education, I will continue my career at Beaumont and look forward to the next steps in life.